Integration of a Liquid Hydrogen Fuel Tank into the Concept of the Flying-V

C.W.C. van Woensel

Technische Universiteit Delft

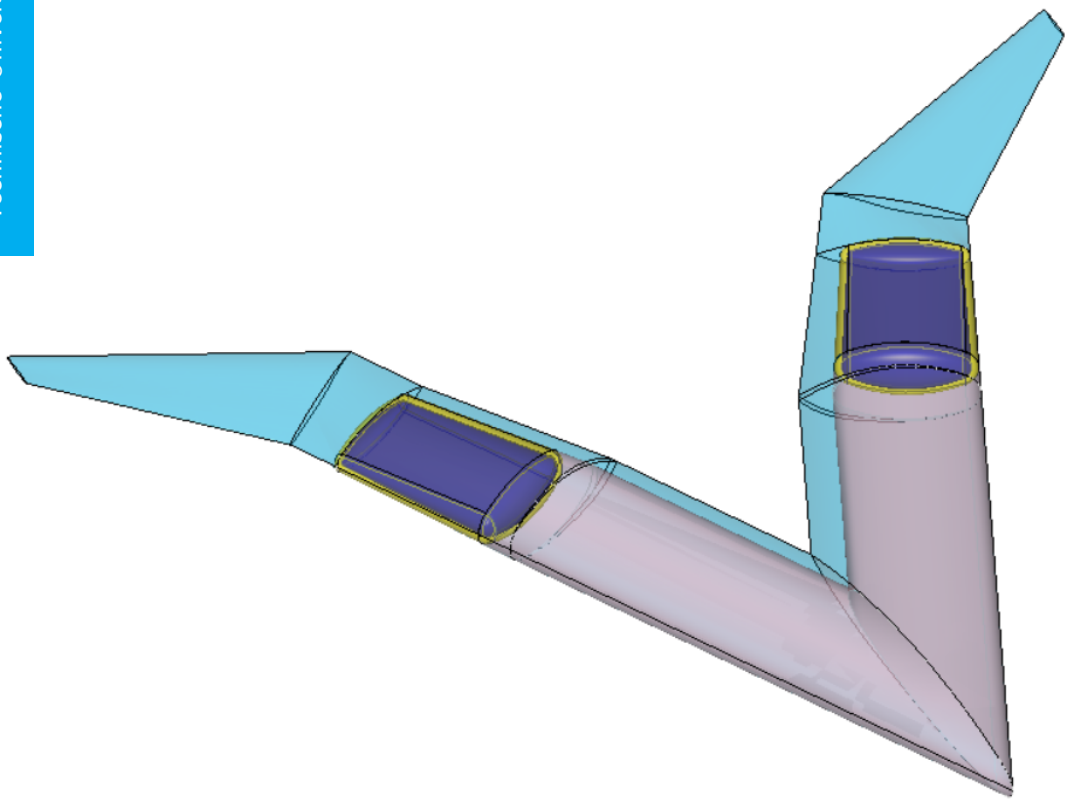

TU Delft Delft University of Technology

Challenge the future

Integration of a Liquid Hydrogen Fuel Tank into the Concept of the Flying-V

by

C.W.C. van Woensel

in partial fulfillment of the requirements for the degree of

Master of Science
in Aerospace Engineering

at the Delft University of Technology,
to be defended publicly on Monday June 21, 2021 at 02:00 PM.

Student number:	4305019	
Thesis committee:	Dr. Ir. R. Vos,	TU Delft, Supervisor
	Dr. Ir. G. La Rocca,	TU Delft
	Ir. B.T.C. Zandbergen,	TU Delft

TU Delft Delft University of Technology

ABSTRACT

The amount of emissions produced by aviation resulting from the use of kerosene is raising concerns. Therefore, a main point of developments and research in the aviation sector is regarding the reduction of its climate impact. The climate impact of aviation can be reduced by making use of alternative fuels, such as liquid hydrogen. A suitable candidate for the use of liquid hydrogen may be the Flying-V. The Flying-V is a flying wing aircraft with the fuselage sections inside the wings. The wing are swept back to form the shape of a V. The original concept of the Flying-V promised improvements in aerodynamic efficiency and a lower mass compared to its reference aircraft, an A350-900. The Flying-V is in further development at the TU Delft. A liquid hydrogen fuel tank is integrated into the concept of the Flying-V. The objective of the research is to contribute to the development of a Flying-V with liquid hydrogen, by making an assessment of the implications on the fuel system and the effect on mission performance resulting from the change of fuel.

A parametrization of the fuel tank is defined while keeping the outer mold line of the Flying-V constant. The fuel tank is located in the tapered part of the wing and is designed to be an integral fuel tank. The mechanical and thermal design of the tank is analyzed for a range of pressures and insulation thickness. Using a thermal resistance analogy the heat transfer rate of the ambient temperature to the liquid hydrogen is determined, resulting in the performance of the fuel tank. The main performance parameters of the fuel tank are the available fuel volume and the fuel tank weight. The influence of the integration of the fuel tank on the mission performance is analyzed and compared to the flight performance of a kerosene based Flying-V, the FV-900. The flight performance analysis uses fuel fractions and the Breguet range equation to determine the available cruise range from the available fuel volume.

The FV-900 is compared to two case studies each using three different configurations. The first case study consists of a retrofit case, where an existing Flying-V is retrofitted with a set of hydrogen fuel tanks. The second case study allows an iteration of the structure to take into account the portion of the maximum take-off weight that is not used due to the decrease in fuel weight when changing kerosene for liquid hydrogen. Regarding the different configurations, these include different combinations of fuel volume and cargo volume. Configuration 1 has the largest fuel volume with a minimal cargo volume. Configuration 2 ensures there is enough cargo volume for the luggage of 440 passengers in exchange for fuel volume. Configuration 3 increase the fuel volume slightly, compared to configuration 2, and has enough cargo volume for the luggage of the design number of 328 passengers.

It is concluded the available fuel volume is not enough for liquid hydrogen to have equivalent flight performance compared to a kerosene based Flying-V. In case of the retrofit the operating empty weight is increased up to 8.7%. All configurations have a lower range. Regarding the largest fuel volume, the range is 35%, 42% and 51% lower for 440, 328 and 250 passengers, respectively, compared to the FV-900. In case of the structure iteration the take-off weight is reduced by 32%, 37% and 37% for configuration 1 to 3, respectively. All the configurations have a lower range compared to the FV-900. Again, regarding the largest fuel volume, the range is 18%, 23% and 32% lower for 440, 328 and 250 passengers, respectively, compared to the FV-900. The configurations where the payload volume is sufficient have a significantly lower range. This research provides usable designs of a Flying-V using liquid hydrogen if one is willing to compromise on the range and available payload weight for no CO_2 emissions. However, keeping the payload weight up, the available volume left is not enough volume for liquid hydrogen to have equivalent flight performance.

PREFACE

This document is the final part of my Master degree in Aerospace Engineering at the Delft University of Technology. It will also be the final part of my student life in Delft. I would like to thank several people for their support all these years. First of all, I would like to thank my supervisor, Roelof Vos, for his guidance and support during this thesis project and for the very nice lectures in the Master program. Next, I would like to thank my friends for their company and support during all these years. A special thanks to the members of the 'Woens' for their "motivating" times. Lastly, I would like to thank my family for their love and support.

C.W.C. van Woensel
Delft, June 2021

CONTENTS

List of Figures

List of Tables

NOMENCLATURE

Roman Symbols

A	Surface area	[m^2]
a	Major axis ellipse	[m]
B	Boom area	[m^2]
b	Frame spacing	[m]
b	Minor axis ellipse	[m]
b	Span	[m]
C_L	Lift Coefficient	[-]
c_j	Specific fuel consumption	[kg/Ns]
c_p	Specific heat at constant pressure	[J/kg/K]
E	Endurance time	[min]
E	Young's Modulus	[Pa]
E_{miss}	Energy consumed during mission	[J]
e_w	Weld efficiency	[-]
F	Force	[N]
H_1	Oval crown height	[m]
H_2	Oval cabin height	[m]
H_3	Oval keel height	[m]
H_w	Oval height at input width	[m]
h	Heat of vaporization	[J/kg]
h	Specific enthalpy	[J/kg]
h	Convective heat transfer coefficient	[W/m^2 K]
j	Safety factor	[-]
k	Thermal conductivity	[W/m K]
L	Length	[m]
LHV	Lower Heating Value	[J/kg]
M_{ff}	Fuel fraction	[-]
$\dot{m}$	Mass Flow	[kg/s]
Nu	Nusselt number	[-]
P	Pressure	[Pa]
Pr	Prandtl number	[-]
Q	Heat leakage	[W]
q_{solar}	Solar irradiance	[W/m^2]
R	Radius	[m]
R	Range	[m]
R	Thermal resistance	[K/W]
Ra	Rayleigh number	[-]
Re	Reynolds number	[-]
S_w	Wetted surface area	[m^2]
T	Temperature	[K]
t	Thickness	[m]
u	Specific internal energy	[J/kg]

V	Tank volume	[m^3]
V	Velocity	[m/s]
W	Power input	[W]
W_f	Fuel weight	[kg]
W_{pl}	Payload weight	[kg]
W_{TO}	Take-off weight	[kg]
W_t	Tank weight	[kg]
w_H	Oval width at input height	[m]
x	Quality of fuel	[-]

Greek Symbols

α	Solar absorptance	[-]
β	Coefficient of thermal expansion	[1/K]
ϵ	emittance	[-]
η	Gravimetric storage density	[-]
λ	Latent heat of vaporization	[J/kg]
μ	Dynamic viscosity	[Pa s]
ρ	Density	[kg/m^3]
σ	Stefan Boltzmann constant	[$W/m^2/K^4$]
σ_f	Strength	[Pa]
σ_θ	Fatigue strength	[Pa]
ϕ	Energy derivative	[$Pa/J/m^3$]

Subscripts

01	Mid section fuel tank
1	Section 1, Crown arc
2	Section 2, Side arc
3	Section 3, Keel arc
alu	Aluminium
atm	Atmospheric
cond	Conduction
d	dome
ext	External
g	Gas
gh	Gaseous hydrogen
H2	Hydrogen
h	Horizontal
ins	Insulation
int	Internal
l	Liquid
lh	Liquid hydrogen
lower	Lower node
rad	Radiation
upper	Upper node
v	Vertical

1

INTRODUCTION

Aviation is growing at an estimated 3.5~5% per year [20–22] and the amount of emissions resulting from the use of kerosene and its corresponding climate impact is raising concerns. With this growth the amount of air traffic is expected to double in the next 15 years [23]. This means the emissions produced by aviation will increase as well if no further action is taken. At present aviation has approximately a 2% contribution to the global CO_2 emissions [22]. Taking other climate agents such as nitrogen oxides and water vapour into account, aviation has a contribution to climate change of approximately 5% [22]. To reduce the climate impact of aviation different developments and research are ongoing at universities, organisations and industry around the world.

One of the ways of reducing the climate impact of aviation is the use of alternative fuels, such as liquid hydrogen. The integration of these cryogenic fuels has been a point of research before. The first use of hydrogen was as a means of inflation of balloons. Following, is a well known hydrogen filled airship, the zeppelin. The first airplane that used hydrogen as a fuel was a B-57 of the U.S. Air Force in 1956 [6, 8]. The flight was part of an experiment to show the feasibility of using hydrogen in a turbojet engine. The flight of the B-57 using hydrogen took 21 minutes. During the 1970s several studies were performed by NASA Langley Research Center to study the use of liquid hydrogen as a fuel in commercial aviation [6, 14]. All of these studies integrated the hydrogen fuel tanks in the fuselages of the aircraft. The studies found that commercial aircraft with hydrogen fuel will have a lower fuel consumption per passenger-mile than aircraft fuelled by kerosene, synthetic fuel or methane [14]. An example of a more recent study is the CRYOPLANE project, a collaboration of 35 partners from all over Europe. The project consisted of a system analysis of a hydrogen fuelled aircraft, led by Airbus.

Another way of reducing the climate impact of aviation is to design alternative aircraft concepts with lower fuel consumption. An alternative configuration is the flying wing. In general a flying wing is tail-less aircraft with the fuselage integrated into the wing. An example of a flying wing is the Flying-V. The original concept of a Flying-V was defined by Justus Benad during his graduation assignment at Airbus GmbH in 2014 [24, 25]. The original concept of the Flying-V features two cylindrical pressurized fuselage sections inside the wing, along the leading edge. The wings are swept back to form the shape of a V. A preliminary aerodynamic analysis, mass evaluation and handling quality assessment have been carried out. Benad estimates a 10% higher lift-to-drag ratio and a 2% lower mass compared to its reference aircraft, the Airbus A350-900. The concept of the Flying-V is in further development at the TU Delft. An aerodynamic design optimization has been carried out to assess the aerodynamic performances of the Flying-V concept [26, 27]. Concurrently, further research focused on the analysis of a Flying-V structure concept [28]. During the research the cylindrical fuselages

from Benad's concept were deemed to have not enough design flexibility. Instead, the oval fuselage proposed by Vos et al. [29] is adopted. Engine integration studies have been performed [30, 31]. Models of the Flying-V have been tested in a windtunnel [32, 33] and a scale model has made its first flight test. At present the Flying-V is a concept for a long range transportation aircraft. The Flying-V is comparable to the Airbus A350 in its size and payload capacity. That is, the Flying-V has a span equal to 65 metres, can carry 314 passengers and 160 m^3 of cargo[1]. The increased aerodynamic performance and the lower weight compared to the Airbus A350 result in a decrease in fuel consumption of 20%[1]. The original concept by Benad and the concept by the TU Delft are depicted in Figure 1.1.

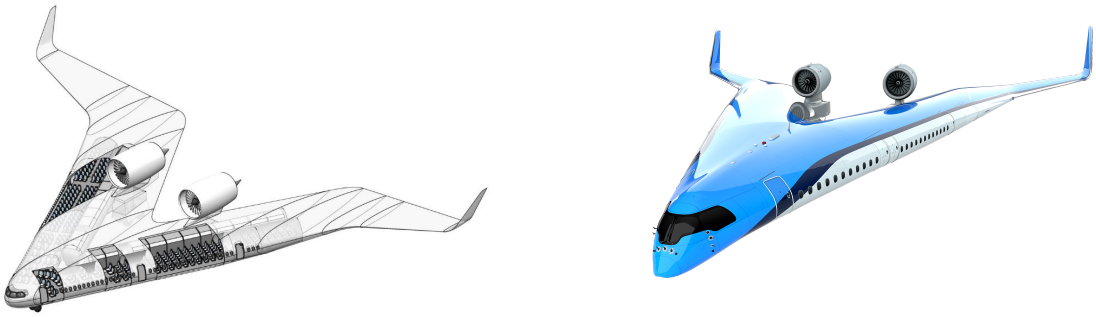

(a) Flying-V defined by Benad [24, 25]

(b) Flying-V defined by TU Delft[1]

Figure 1.1: Concepts of a Flying-V

1.1. RESEARCH OBJECTIVE

This thesis project proposes to integrate liquid hydrogen fuel into the concept of the Flying-V. The main objective of the research is to contribute to the development of a design of a Flying-V with alternative fuels, focusing on the cryogenic fuel liquid hydrogen, by making an assessment of the implications on the fuel system and the effect on the mission performance resulting from the change of fuel. The main research question to be answered is:

"How does a liquid hydrogen based Flying-V compare to a kerosene based Flying-V in terms of the fuel system and the mission performance?"

In order to answer the main question sub-questions are defined:

- "How is the parametrisation of the fuel tank in the Flying-V defined?"
- "What is the influence of the design of the fuel tank on the tank performance, i.e. boil-off rate, available fuel volume and tank weight?"
- "What is the influence of the integration of a liquid hydrogen fuel tank on the mission performance, i.e. range, cruise speed, cruise altitude and payload capacity?"

1.2. RESEARCH SCOPE

The research presented here encompasses the design of a cryogenic fuel tank integrated into the concept of the Flying-V. The parametrisation of the Flying-V by Hillen [5] and the family optimization by Oosterom [19] are used as a basis for the parametrisation and modelling of the fuel tank. The Outer Mold Line (OML) of the model is not changed during this research. The parametrization of

[1] Flying-V. Retrieved on March 29, 2020 from https://www.tudelft.nl/lr/flying-v/

the fuel tank is limited to the tapered part of the wing. The fuel tank is sized to handle pressurisation loads, to be able to estimated the material needed and therefore the resulting weight of the fuel tank. A more complete structural analysis and a structural weight optimization is not in the scope of this research. The thermodynamic analysis of the fuel tank assumes cruise flight conditions calculated using the International Standard Atmosphere. Furthermore the analysis is performed using steady state assumptions.

1.3. THESIS OUTLINE

Hydrogen as an aviation fuel is discussed in Chapter 2, giving background information on the use of hydrogen in aviation and liquid hydrogen properties. Next follows the fuel tank parametrization in Chapter 3. The fuel tank, including the tank design, material selection, sizing and flight performance analysis, is presented in Chapter 4. Verification and validation is discussed in Chapter 5. The results are presented and discussed in Chapter 6. Finally, the conclusions of the research and the recommendation for future work are presented in Chapter 7.

2

HYDROGEN AS AVIATION FUEL

At the moment almost all of aviation is using kerosene based fuels. However, the use of these kerosene based fuels is growing less popular. The amount of emissions resulting from the use of these fuels and its corresponding climate impact is raising concerns. Furthermore, the depletion of crude oil resources raises concerns as well for the future production of kerosene [34]. These reasons have made researchers look more intensively at alternative fuels for aviation. One of those alternatives can be hydrogen.
The use of hydrogen in aviation is discussed in Section 2.1 with the history of hydrogen in aviation and more recent hydrogen studies. Next follows the discussion of liquid hydrogen as fuel in Section 2.2. The safety issues are discussed in Section 2.3.

2.1. USE OF HYDROGEN IN AVIATION

The idea of an aircraft using hydrogen is not a new idea. The integration of hydrogen as a fuel has been a point of research before. There exist several different conceptual and working examples of the use of hydrogen in aviation. This section presents some of the history of hydrogen in aviation along with some of the more recent hydrogen studies.

2.1.1. HISTORY OF HYDROGEN IN AVIATION

The first aircraft to use hydrogen were balloons. However, the hydrogen was not used as a fuel but as a means of inflation. In 1783 two balloons filled with hydrogen were build and flown by Anne-Jean Robert, Nicolas-Louis Robert and Jacques Charles. The balloons were made of silk lined with rubber. In 1852 Henri Giffard flew a balloon filled with hydrogen and equipped with a steam engine for propulsion. One could call this one of the first airships. In 1872 Paul Haenlein flew an airship with an engine that was fueled by gaseous hydrogen [6]. A well known airship is of course the zeppelin, a hydrogen filled airship. The zeppelin was first made at the start of the 20th century. Several different types of zeppelins have flown during the years to follow with much success. However, the most well known zeppelin is the zeppelin that failed during flight, i.e. the Hindenburg. The crash happened in 1936. The Hindenburg carried 96 people, of which 35 lost their lives [6].
The first airplane that used liquid hydrogen was a B-57 of the U.S. Air Force in 1956 [6, 8]. The flight was part of an experimental program to show the feasibility of using hydrogen in a turbojet engine. The B-57 carried liquid hydrogen in a tank under its left wing to fuel its left engine and it used helium as a pressurant, which was carried under its right wing. The B-57 could operate on hydrogen for 21 minutes during cruise. Engine performance was concluded exceptionally smooth and no operational safety problems were found [6].
During the 1970s several studies were performed by NASA Langley Research Center to study the use

of liquid hydrogen as a fuel in commercial aviation [6, 14]. All of these studies integrated the hydrogen fuel tanks in the fuselages of the aircraft. The studies found that commercial aircraft with hydrogen fuel will have a lower fuel consumption per passenger-mile than aircraft fuelled by kerosene, synthetic fuel or methane [14]. These studies were purely conceptual and no flights were made.
In 1988 a Tupolev TU-155 flew for 21 minutes while using liquid hydrogen in one of its engines [6]. The TU-155 is a derivative of the TU-154, a commercial transport aircraft able to carry 164 passengers. The TU-155 had an tank installed in the aft section of the fuselage. Also in 1988 was the first flight entirely fueled by liquid hydrogen. A Grumman-American Cheetah was modified to carry a 40 gallon liquid hydrogen tank and a specially designed fuel injection system. The fuel volume should have been enough for a flight of approximately one hour [14]. According to Brewer it only flew for 36 seconds [6].

2.1.2. RECENT HYDROGEN STUDIES

The cases of the use of hydrogen in aviation mentioned in the section above are relatively dated. Furthermore, most cases were experiments without any further continued research or developments. This section presents more recent studies about the use of hydrogen in commercial aviation.

Cryoplane

In 2000 a project started called "CRYOPLANE". The project was a collaboration of 35 partners from all over Europe, that include industry, research institutes and universities. The project was coordinated by Airbus. Besides, the project was supported by the European Commission. The project goal was a system analysis of a liquid hydrogen fuelled aircraft and was planned to take 2 years [1]. The Cryoplane is depicted in Figure 2.1.

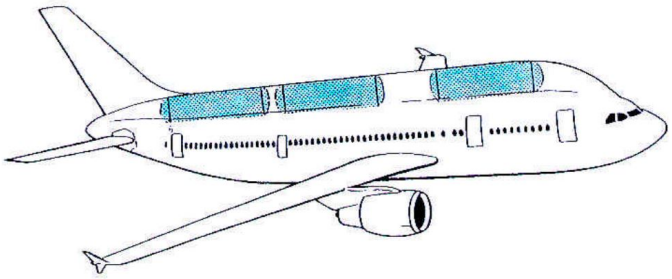

Figure 2.1: Design of the Cryoplane [1]

The projects starts to mention the fact that hydrogen has a higher energy content per weight than kerosene. However, they expect that this advantage will be diminished by the weight of the complex fuel system [35]. The project mentions fuel cells, such as the ones used to power cars. It is concluded that the high power requirements of an aircraft result in fuel cells that will be too heavy. The remaining option is to burn the hydrogen in turbofan engines.
Regarding the configuration of the aircraft, the main issue is the energy density of hydrogen. Hydrogen needs a storage volume that is 4 times as large as compared to kerosene. The project also concludes that the fuel tanks must be spherical or cylindrical to efficiently handle the pressurization loads [1]. Therefore, the configuration that is selected is a tube-and-wing aircraft with the tanks on top of the fuselage. It is thought that this is the best solution for large passenger airplanes. The fuel tanks on top of the fuselage require an additional fairing to cover the tanks. As this project is a "system analysis" the project does not mention any specifics. The report is limited to general claims and facts to take into account, i.e. the very low temperature of liquid hydrogen resulting in required insulation or changes needed to a turbofan engine to properly burn hydrogen.

Finally some estimations are made. First, it is expected that the energy consumption would increase by 9% to 14% due to the increase in wetted surface area. Second, the operational empty weight increases by 23% due to the tank structure. The maximum take-off weight may vary between an increase of 4.4% and a decrease of 14.8%. Finally it is expected for the operating cost to increase by 4% to 5%. [36]

LH2-400

In a study by Maniaci [14], the performance of a hydrogen fueled commercial aircraft has been compared to a conventional aircraft. For this purpose a hydrogen fueled aircraft is defined, named the LH2-400. The aircraft is a tube-and-wing aircraft with the fuel tanks placed on top of the fuselage. This can be compared to the design of the Cryoplane mentioned above. The base of the design is the Boeing 747-400. The hydrogen aircraft is designed to be mission equivalent, i.e. the same range, payload and basic operational parameters [14]. According to Maniaci, the aircraft have the same fuel energy efficiency, resulting in the same energy equivalent design as well. Maniaci concludes that the LH2-400 has a lower fuel weight than the Boeing, but this is offset by the weight of the cryogenic fuel tanks. The addition of these fuel tanks result in an increase in drag. Lowering the cruise Mach number increases the fuel burn efficiency to a maximum that is 10.5% higher than the maximum of the Boeing [14]. This leads to potential operating cost savings. According to Maniaci the LH2-400 is not an optimised design [14]. The fuel tanks placed on top of a tube-and-wing aircraft is not an efficient design. Furthermore, according to Maniaci, the hydrogen fuelled aircraft is sensitive to non-optimal design missions [14].

AHEAD Multi-Fuel Blended Wing Body

Advanced Hybrid Engines for Aircraft Development (AHEAD) proposes a new hybrid engine concept[1]. The engine concept is developed with the aim of using a cryogenic fuel in aviation. Together with the engine concept the AHEAD consortium designed a blended wing body using the engine concept. The climate impact of the AHEAD blended wing body is assessed by Grewe et al. [21].
The blended wing body is designed for 300 passengers, a cruise altitude of 13 km and a range of 14,000 km. The aircraft has a lift-to-drag ratio of 25. The blended wing body uses the new hybrid engine concept, that uses LH_2 or LNG in combination with a bio kerosene. The assessment of the blended wing body considered different configurations regarding the hydrogen version. That is, due to the possible drag and weight penalties resulting from liquid hydrogen storage, which were not examined in detail, two configurations were considered. One configuration where no changes were necessary and one configuration that required increased aircraft dimensions and an increase in weight [21]. The AHEAD technologies show an estimated reduction in climate impact of 10% to 25% compared to a B777 and B787 [21]. The schematic design of the blended wing body is depicted in Figure 2.2.

Figure 2.2: Design of the AHEAD Multi-Fuel BWB Aircraft [2]

[1]Advanced Hybrid Engines for Aircraft Development. Retrieved on March 2, 2020 from http://www.ahead-euproject.eu/

2.2. LIQUID HYDROGEN

Hydrogen is considered as a fuel because it has the highest energy content of any fuel by weight[2]. Hydrogen can be stored in several different states, that is in a gaseous state, a liquid state, a slosh state, a solid state or a subcooled liquid state [11].
Due to the relatively low density of hydrogen, storing hydrogen in its gaseous state would result in enormous tanks to meet the energy requirement. Such tanks would not only be impractical due to their volume but also due to the resulting weight. The storage of slosh or solid hydrogen requires a lot of energy to cool with no significant advantages in tank volume and weight. Furthermore, subcooled hydrogen leads to much higher pressure fluctuations in the tank, compared to liquid hydrogen, resulting in an increase in tank weight [11]. For aviation applications liquid hydrogen (LH_2) is the preferred option. In this case the hydrogen is stored as a saturated liquid where the vapor and the liquid are in equilibrium [3].

2.2.1. PROPERTIES

Hydrogen can be liquefied when it is stored below -252 $°C$ or 20.3 K at a pressure level of 1 atmosphere, i.e. Normal Boiling Point (NBP). The density of liquid hydrogen is 70.8 kg/m^3. This should be compared to a density of 0.084 kg/m^3 for gaseous hydrogen at room temperature and pressure (Normal Temperature and Pressure, NTP). The density of kerosene is 800 kg/m^3 [6]. As mentioned before, hydrogen has the highest energy content by weight. Liquid hydrogen has a calorific value of 120 MJ/kg, compared to a calorific value of 42,8 MJ/kg for kerosene, i.e. 2.8 times higher [1]. However, liquid hydrogen has the lowest energy content by volume. Liquid hydrogen has an energy density of 8 MJ/L, compared to an energy density of 32 MJ/L for kerosene[3], i.e. liquid hydrogen requires a volume that is four times larger than the volume required for kerosene for the same energy content.
To summarize, properties of liquid hydrogen are given by Table 2.1, including the properties of kerosene for comparison.

Table 2.1: Properties of hydrogen and kerosene [6, 16]

	Liquid Hydrogen	**Kerosene**
Normal Boiling Point (K)	20.3	440-539
Density at NBP (kg/m^3)	70.8	-
Density at NTP (kg/m^3)	0.084	811
Lower heating value (MJ/kg)	120	42.8
Energy density (MJ/L)	8.49	31.15
Specific heat (J/g·K)	9.69	1.98
Heat of vaporization (J/g)	445.59	360

2.2.2. HYDROGEN COMPOSITION

With the discussion of the properties of liquid hydrogen it is important to note that there are different types of hydrogen. Ordinary hydrogen can occur in two different isomers with difference in nuclear spin, that is ortho-hydrogen and para-hydrogen [3]. Hydrogen at normal temperature and pressure is composed of approximately 75% ortho-hydrogen and 25% para-hydrogen. This composition is called 'normal' hydrogen. At the Normal Boiling Point the composition of hydrogen is 0.2% ortho-hydrogen and 99.8% para-hydrogen [3].
To determine the effect of the ortho-para composition of hydrogen on the fuel tank design Verstraete

[2] Hydrogen basics. Retrieved on November 5, 2020 from https://hydrogeneurope.eu/hydrogen-basics-0
[3] Hydrogen storage. Retrieved on November 5, 2020 from https://www.energy.gov/eere/fuelcells/hydrogen-storage

[11] derived the energy derivative for para-hydrogen and 'normal' hydrogen. The energy derivative of para-hydrogen is depicted in the left hand side of Figure 2.3. The right hand side show the relative difference between the energy derivatives of para-hydrogen and 'normal' hydrogen, with 'normal' hydrogen as the reference. According to Verstraete, comparable difference can be found for the latent heat of vaporization. This parameter plays an important role in the thermodynamic design of the fuel tank.

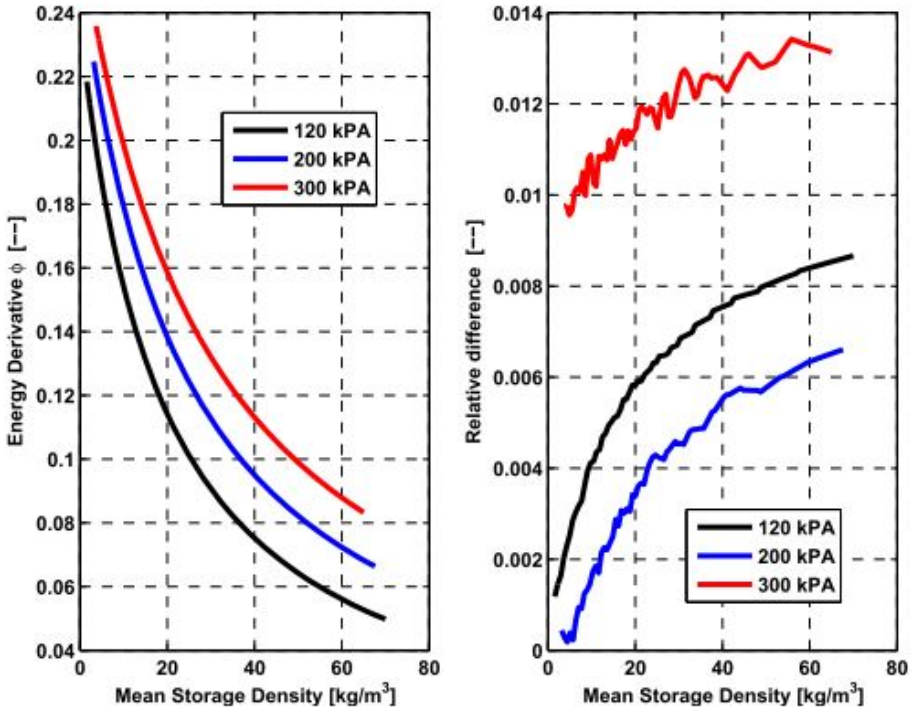

Figure 2.3: Energy derivatives of para-hydrogen (left), relative difference between energy derivatives of para-hydrogen and 'normal' hydrogen (right) [3]

From the figure it can be seen that the differences are small. As para-hydrogen results in slightly higher values and therefore in slightly higher influences in the fuel tank design, para-hydrogen is selected as the composition of hydrogen. This being a more conservative choice. From this point on when referring to liquid hydrogen in an analysis, the composition of 99.8% para-hydrogen is assumed.

2.3. SAFETY

As discussed in the sections above, hydrogen has often been considered as a fuel for aviation and will probably be an important fuel source for aviation in the future. Nevertheless there are certain 'high risks' associated with the use of hydrogen. Often the accident with the Hindenburg is brought up. However, compared to other fuels, in many instances hydrogen is the safest fuel [4]. During the CRYOPLANE project a safety analysis was performed as well. The conclusion was that the overall safety level of hydrogen will not be lower than the safety level corresponding to the use of kerosene [37].

Regarding the risks of a fuel leak and the flammability of hydrogen an experiment has been conducted by the University of Miami [4]. A hydrogen fuel leak and a kerosene fuel leak were ignited after giving the fuel some time to spread. The experiment is depicted in Figure 2.4. It can be seen that the hydrogen leak burned in a composed fashion and the kerosene leak destroyed the vehicle.

When cryogenic or liquid hydrogen is released into the atmosphere it will turn into gas and rise and dissipate into the air. However, kerosene being a liquid and staying a liquid, will collect at the space around the leak. Therefore, regarding a fuel leak, hydrogen is considered to be a safe fuel.

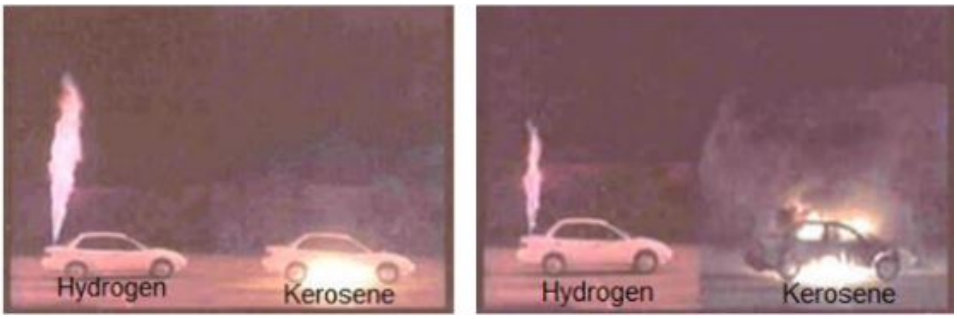

Figure 2.4: Hydrogen and kerosene fuel leak experiment by University of Miami [4]

The use of hydrogen as a fuel does possess a significant risk when the hydrogen is mixed with oxygen in closed systems. With the correct ratio of hydrogen to oxygen the mixture can be very explosive. Regarding the fuel tank design one should ensure air does not enter the tank. That is, the minimum pressure of the fuel tank needs to be higher than atmospheric pressure. Therefore the filling pressure is selected to be 1.2 bar.
Furthermore, the fuel system requires to be purged before filling and after emptying the fuel tank to prevent air and hydrogen, respectively, staying in the system. Purging of such a system is usually done by using nitrogen.

3

Fuel Tank Parametrisation

The design and analysis of the cryogenic fuel tank requires the dealing with geometry. The fairly complex geometry is to be used for some of the inputs in the fuel tank analysis. Therefore a parametrisation of the Flying-V fuel tank is created. The geometry is modelled using ParaPy, a Python based Knowledge Based Engineering (KBE) system. Preceding studies on the Flying-V have been using ParaPy as well. Object Oriented Programming (OOP) is used in this process. This chapter presents the geometric model, starting with an overview of the model structure followed by descriptions of the different parts of the model.

3.1. Class Diagram of the Fuel Tank Geometry

The geometry of the fuel tank is modelled in ParaPy, using the work of Hillen [5] and Oosterom [19] as a basis. Hillen created a parametrisation of the Flying-V OML, with the main components being the fuselage and the wing. The fuel tank is added to these components. An overview of the model structure is depicted by the class diagram is Figure 3.1.

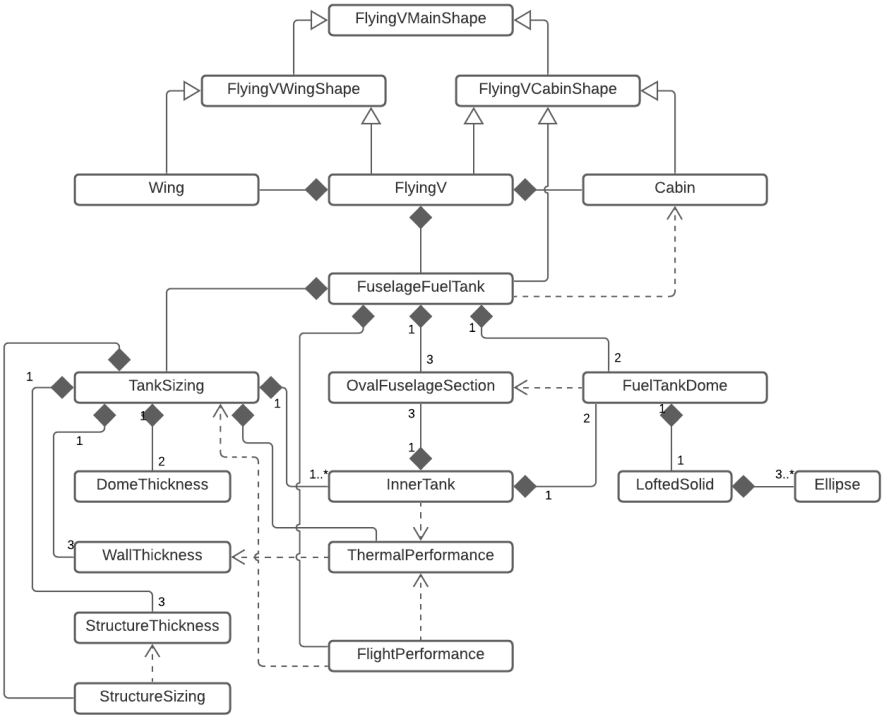

Figure 3.1: UML class diagram of the Flying-V fuel tank

The start of the diagram is the same as for Hillen. That is, the class "FlyingVWingShape" and the class "FlyingVCabinShape" inheriting from the class "FlyingVMainShape". Following is the class "FlyingV" with its parts, the wing and the cabin. Hillen elaborates on the these parts with subsequent children classes and parts. For clarity these are omitted in this diagram. For this research the focus lies on the third part of the "FlyingV" class, i.e. the class "FuselageFuelTank". This class is the starting point for the modelling of the cryogenic fuel tank of the Flying-V. The fuel tank is placed inside the wing and in parts of the cabin. It is therefore indicated that the fuel tank depends on the cabin to perform its operations.
The fuel tank itself is made out of different lofts between oval fuselage sections and domes on either end of the tank. An inner tank is created to take into account the metal and insulation layer. Furthermore, a class related to the sizing of the tank and a class related to the analysis of the flight performance are included. The oval fuel tank sections, the fuel tank domes and the inner fuel tank are discussed in the section below. The tank sizing, thermal performance and the flight performance analyses are discussed in the following chapter.

3.2. FUEL TANK GEOMETRY

From the start of the research is was decided to use the oval cross-section for the fuel tank as well and to locate the fuel tank in the tapered part of the wing, i.e. using part of the cargo volume to store fuel. The starting point of the fuel tank is the end of the cabin solid, section 3, as created by Hillen. Regarding the cabin and the wing, the part of the Flying-V between section 2 and section 3 consists of a single loft. Using these linear relations of the loft between sections 2 and 3, the dimensions of an oval in this part of the wing can be determined as a function of a given length. In this way a loft between the cabin end and a section with a varying location can be made. The wing sections and a fuel tank with variable *Length01* is depicted in Figure 3.2.

A certain *offset* is created to make the starting point of the fuel tank variable as well. This offset is defined from the cabin end in the direction of the nose of the aircraft. This way the fuel tank can be shortened at the back to allow for different configurations and combinations with the cargo compartments for example. This offset is also depicted by Figure 3.2.

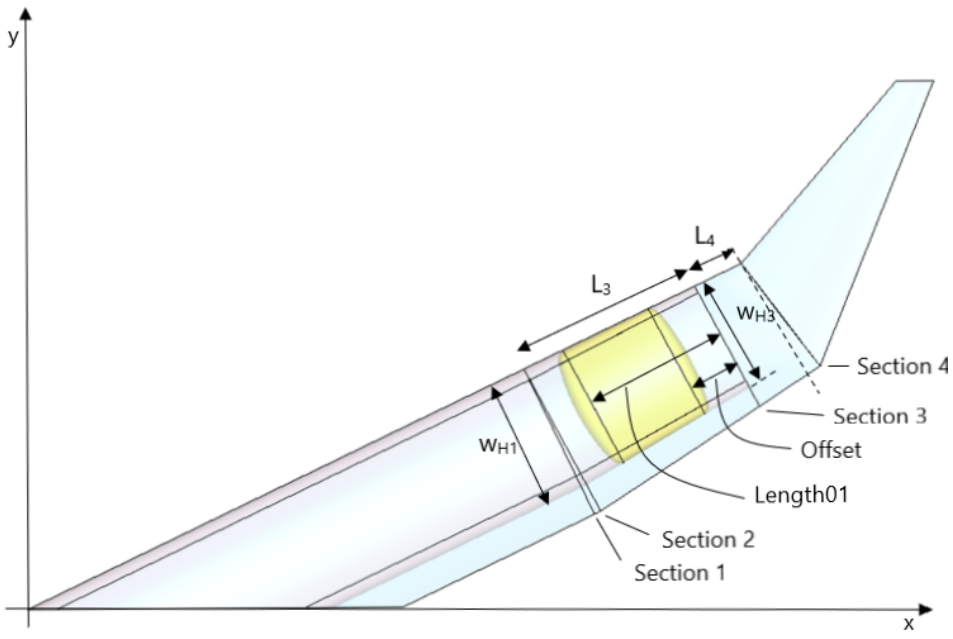

Figure 3.2: Schematic of the wing planform with fuel tank (yellow)

3.2.1. FUEL TANK CROSS-SECTION

The cabin of the Flying-V is constructed from oval sections, with the wing formed around the cabin. These ovals are used for the fuel tank as well. The oval cross-section was originally introduced by Hoogreef [7]. The oval design replaced the original circular fuselage design by Benad [24], providing more design flexibility and more volume efficiency. Hillen [5] slightly changed the oval cross-section in the parametrisation that is currently used. The oval cross-section defined by Hillen can be seen in the class diagram above as the class "OvalFuselageSection".

The oval cross-section is defined by several parameters, i.e. the crown height H_1, the cabin height H_2, the keel height H_3, the cabin width at arm-rest height W_H and the arm-rest height H_W [5]. These parameters define the trapezoid structure of the oval cross-section. Furthermore, the oval cross-section consists of four arcs, i.e. the crown arc, two side arcs and the keel arc. These arcs are connected at the corners of the trapezoid structure, at which the arc connections are tangent. The oval cross-section is depicted in Figure 3.3.

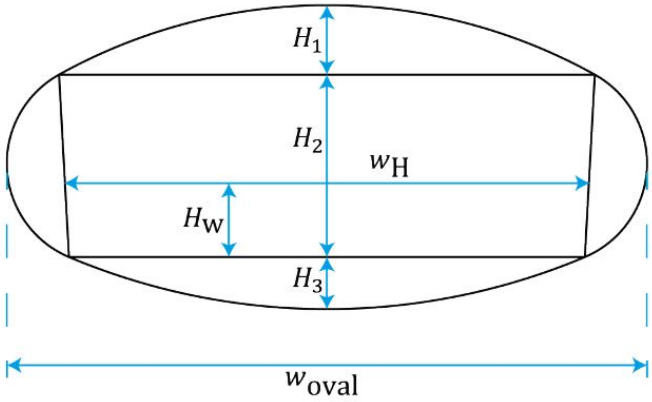

Figure 3.3: Oval cross-section parametrisation [5]

A loft between these oval cross-sections form the middle section of the fuel tank. As the fuel tank is located in the tapered part of the wing, the fuel tank is tapered as well and has a variable cross-section along its length.

3.2.2. FUEL TANK DOMES

The fuel tank is closed on either end by a dome. These domes can have different shapes. The question of which shape it should be was also asked in a study documented by Brewer [6]. The study looked into "what shape of end closure offered the best combination of light weight and minimum length, thereby leading to minimum Direct Operating Cost (DOC) for the aircraft operator" [6]. The different dome shapes considered were a hemisphere, ellipsoidal and torispherical, depicted in Figure 3.4. The tank weight, internal volume and surface area of each dome were analysed for a tank with a specified volume. The elliptical and the torispherical domes were found most and equally efficient. The torispherical dome is a more complex structure, so the elliptical dome was selected. The elliptical dome with the lowest DOC had a ratio of the major over minor axis equal to $(a/b) = 1.6$ [6].

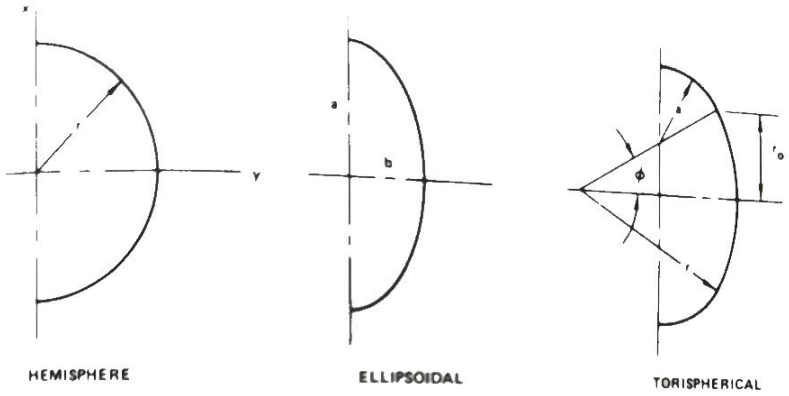

Figure 3.4: Dome shape configurations [6]

The elliptical dome configuration with an ellipse ratio of 1.6 is used to define the fuel tank domes. To construct the domes the oval cross-section of the fuel tank ends are required. Along this oval several different ellipses are constructed, placed parallel to the vertical axis of the oval and connecting between points on the upper and lower half of the oval. The ellipses are depicted in Figure 3.5.

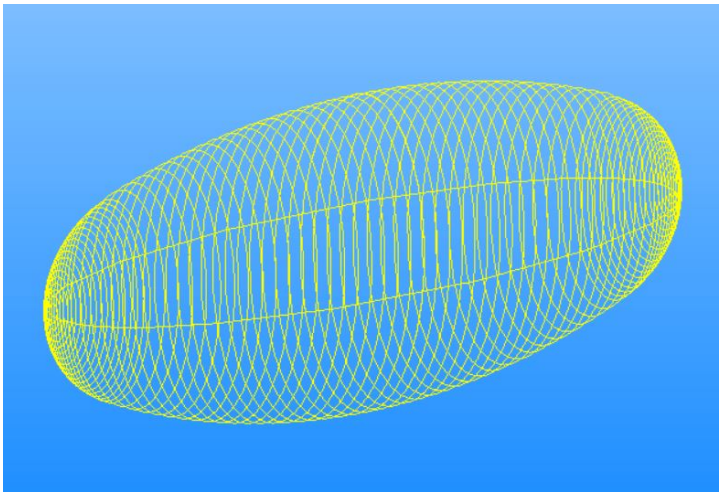

Figure 3.5: Ellipses used to construct a fuel tank dome

These ellipses are used to construct a lofted solid, resulting in an ellipsoid. This ellipsoid is split in half, leading to a dome end of the fuel tank. An example of a complete fuel tank is depicted in Figure 3.6.

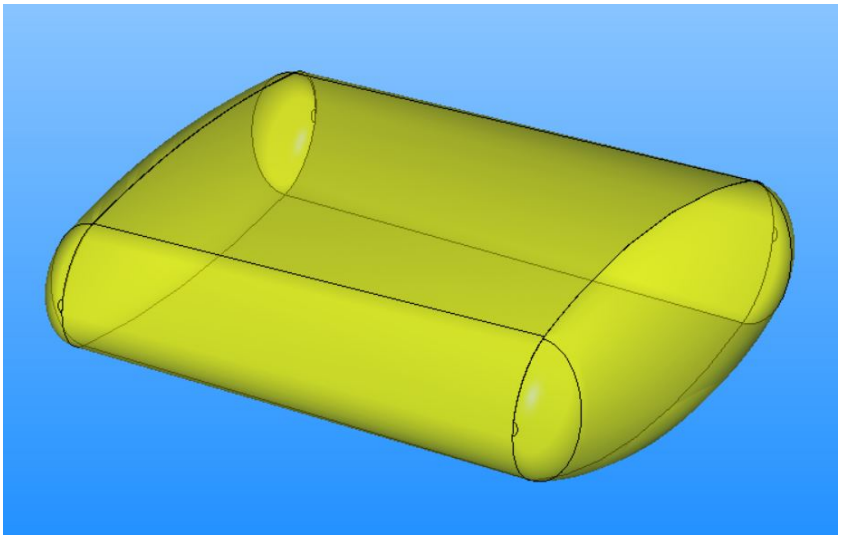

Figure 3.6: Complete fuel tank with mid section and dome ends

3.2.3. INNER TANK

To protect the hydrogen fuel from heat leaking into the tank, the fuel tank is insulated. However, a certain amount of heat will leak into the tank causing the fuel to boil. This results in a rise in pressure. The sizing of the tank to take into account this pressure result in a certain tank wall thickness. To take into account the thickness of the tank wall and the thickness of the insulation an inner tank is defined. Certain parameters of this inner tank are provided to the thermal analysis.

The construction of the inner fuel tank follows the same procedure as the outer fuel tank. That is, it is made from oval sections and two tank domes as well. To take into account the thickness of the metal and insulation layer the oval needs to be adjusted. The corners of the trapezoid are moved inward along a line perpendicular to the arcs connecting at the node. This is depicted in Figure 3.7 as the dashed red line for the lower node. This results in the change in height of the cross-section given by Equation (3.1) and the change in width of the cross-section given by Equation (3.2).

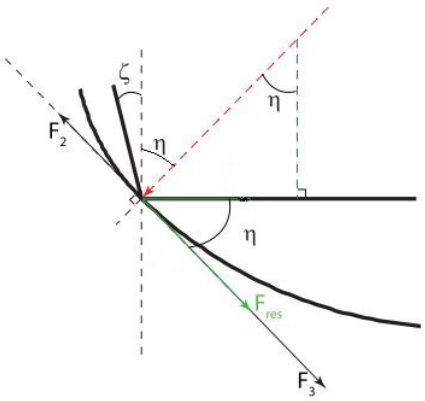

Figure 3.7: Free body diagram of the lower node of the oval cross-section [7]

$$\Delta H = \cos(\eta) \cdot \Delta t \tag{3.1}$$

$$\Delta W_H = \sin(\eta) \cdot \Delta t \tag{3.2}$$

Where Δt is the thickness of the metal plus insulation layer. These changes in height and width happen for the upper and lower node and are subtracted from the cabin height and cabin width, respectively. The height of the arm rest is adjusted accordingly to the change in cabin height. Finally the location of inner fuel tank oval section is adjusted so that the section is centered in the section of the outer tank. An example of an inner tank is depicted in Figure 3.8.

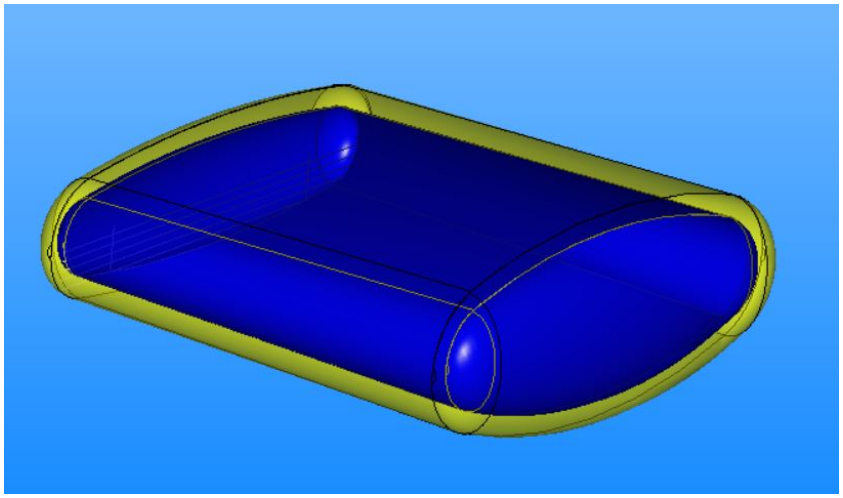

Figure 3.8: Outer and inner fuel tank

4

Cryogenic Fuel Tank

A major component of a cryogenic fuel system is the fuel tank. The fuel tank is required to contain the fuel. Regarding cryogenic fuel, the fuel tank is also required to keep the fuel below its boiling point to prevent over-pressurisation or the loss of fuel. This results in an additional insulation system to protect the fuel tank. Furthermore, the density and energy content of cryogenic fuels, i.e. the volume that is required, complicate the system even more. That is, the feasibility of a lightweight and insulated cryogenic fuel tank is a key technical issue for liquid hydrogen flights [11].

4.1. Fuel Tank Configuration

For a fuel tank design there are two options, i.e. an integral tank or a non-integral tank. A non-integral tank basically only carries the fuel. Therefore, the loads to be taken into account are resulting from the containment of fuel, i.e. pressurization, fuel dynamic and thermal loads [6]. A non-integral tank is then mounted and supported by the structure of the aircraft.

An integral tank is part of the structure and therefore also has to carry the loads experienced by the structure, such as axial, bending and shear loads [6]. Verstraete et al. [11] mention an integral tank has a higher volume efficiency. They are using a tank fitted in the fuselage. Due to this volume efficiency the fuselage will be smaller, have lower drag and less weight compared to a fuselage with a non-integral tank of the same fuel volume. Furthermore they say the integral tank, the fuselage and the insulation are more readily accessible for inspections and repairs. Brewer [6] documents several studies performed by NASA regarding integral or non-integral tank designs. Structural concepts for a fuel tank in the aft section of a fuselage are compared. The results show a higher volume efficiency for the integral tank and a higher fuel weight fraction for the integral tank. Brewer mentions an integral tank is better accessible as well.

In case of the integration of a cryogenic fuel system into the concept of the Flying-V in this study, where the outer mold lines are kept constant, the integral tank would be the most volume efficient. This additional volume, with respect to a non-integral fuel tank design, is very much needed to contain liquid hydrogen. Therefore an integral tank design is selected for this study.

4.2. Fuel Tank Construction

With the decision made on the fuel tank configuration the next choice is regarding the fuel tank construction. Basically there are two options, i.e. internal insulation or external insulation.
With internal insulation the insulation layer is located on the inside of the fuel tank, being in contact with the hydrogen. In this case the insulation protects the fuel tank wall of the cryogenic conditions.

One can assume the fuel tank wall to be at ambient conditions. This minimizes the thermal expansion of the fuel tank wall. The insulation experiences cryogenic conditions. Therefore the insulation needs to impermeable to or protected from hydrogen. Permeation of hydrogen is the process where hydrogen breaks down into hydrogen ions, diffuses through the material and reforms back into hydrogen molecules[1]. This process is disadvantageous for the exposed material, whose properties are affected and will deteriorate. It also results in the loss of hydrogen. One cannot completely eliminate the permeation of hydrogen, but only reduce the rate of diffusion. Material with a high rate of permeation can be protected with an impermeable liner. In this case, one should take into account the thermal expansion coefficients of the used materials. A discrepancy between these coefficients can lead to damage to the liner or even separation of the liner from the tank [8].
With external insulation the insulation layer is located on the outside of the fuel tank. In this case the wall material will be in contact with the hydrogen and experience cryogenic conditions. This results in thermal expansions of the wall structure due to the continuously changing volume of hydrogen. The insulation on the outside of the tank needs to be impermeable to air to prevent cryopumping [3]. The outside of the insulation experiences ambient conditions, while the inside of the insulation is in contact with the wall layer that experiences cryogenic conditions. If air permeates to this point it will significantly decrease the insulation effectiveness, as it is basically filled with higher conductive air.

For this research it has been decided to keep the fuel tank wall aligned with the skin of the aircraft, i.e. internal insulation. The fuel tank wall material, insulation material and liner material will be discussed in the next section.

4.3. MATERIAL SELECTION

A significant part of the fuel tank design is the selection of the materials to be used. As a cryogenic fuel tank is a more complex system than a kerosene fuel tank, there are more requirements to be fulfilled during the design process. Several of these requirements are with regard of the material selection. As mentioned above, the fuel tank will be featuring internal insulation. The materials to be used for the fuel tank wall, the internal insulation and the liner material are discussed in the following sections.

4.3.1. WALL MATERIAL

The fuel tank wall material needs to be selected with several requirements in mind. The material needs to have high strength and a high stiffness. These are required to handle the loads resulting from pressurization as well as parts of the axial, bending and shear loads. The material density should of course be low to be able to design a lightweight fuel tank.
In this study the fuel tank wall is designed to be on the outside of the fuel tank and should under normal circumstances not be in contact with the hydrogen. In case this does happen due to a fault in the insulation, one should take into account the fracture toughness of the material. A high fracture toughness is required regarding the cryogenic temperatures of the hydrogen. The temperature of liquid hydrogen is 20.3 K. At this temperature many materials become brittle. Material embrittlement can result in failure below the expected yield stresses [8]. In case the wall material does come in contact with hydrogen the selected material should also have a low rate of permeation of hydrogen. As mentioned above, permeation of hydrogen results in the deterioration of material performance and in the loss of hydrogen.
Mital et al. [8] defined performance indices associated with these material properties to assist in the selection of the available materials. These performance indices are given by Table 4.1. Maximizing

[1] Hydrogen Permeation. Retrieved on November 26, 2020 from https://www.yokogawa.com/us/library/resources/application-notes/hydrogen-permeation/

the ratio of strength over density results in a strength-limiting design with minimized mass. Maximizing the stiffness results in a deformation-limiting design with minimized mass. For a damage-tolerant design the fracture toughness needs to be maximized. These performance indices for different materials are depicted in Figures 4.1 to 4.3. Looking at these figures and using the performance indices from Table 4.1 some materials stand out. Figure 4.1 presents strength versus density for various materials. In this case materials from the upper left corner are preferred. One can see composites to have a relatively high strength and a relatively low density. In case of pressure vessels an important material property is yield-before-break K_{Ic}/σ_f [8], which makes sure the critical stress is higher than the yield stress. This property is depicted in Figure 4.2. Again, materials from the upper left corner are preferred. One can see metals perform well in this case. Figure 4.3 depicts material stiffness versus density. According to Mital et al. not a primary design variable, although it is desirable to minimize the deformation under loads while minimizing mass [8]. That is, materials from the upper left corner are preferred again. One can see that composites offer relatively high stiffness and lower density compared to metals. Finally there is the requirement of low permeation of LH_2. Metals have a lower rate of permeation than non-metallic materials [8].

Table 4.1: Performance indices for mechanical components of cryogenic storage tank [8]

Function and constraints	**Performance indices, maximize**
Strength-limiting design with minimum mass	σ_f/ρ
Deformation-limiting design with minimum mass	E/ρ
Damage-tolerant design with minimum mass	K_{Ic}/ρ

Where ρ is the density, σ_f is the strength, K_{Ic} is the fracture toughness and E is the Young's modulus.

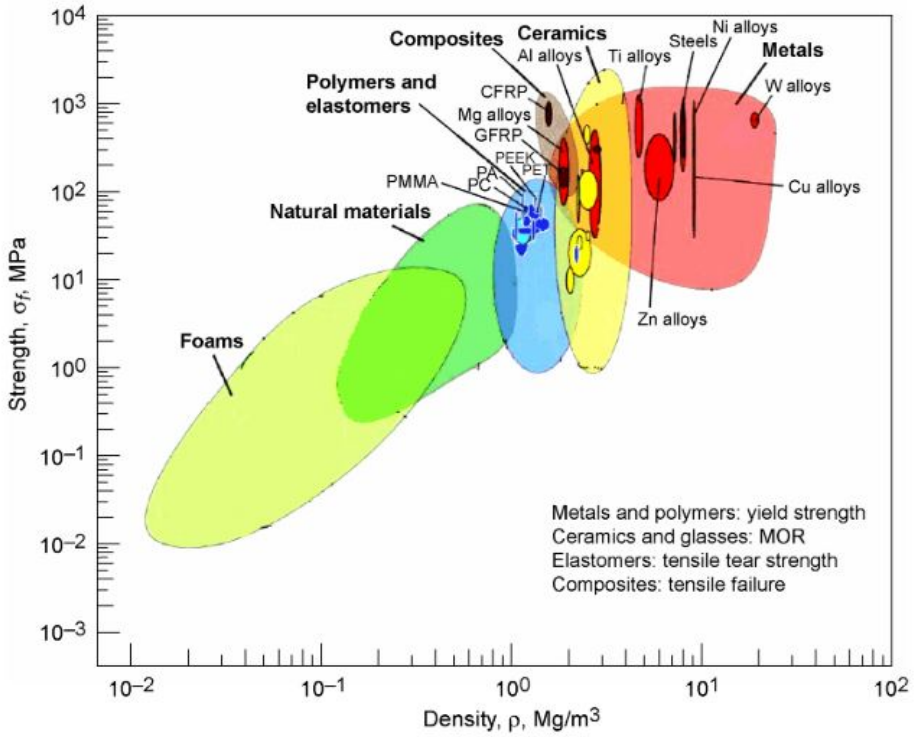

Figure 4.1: Strength versus density for various materials [8]

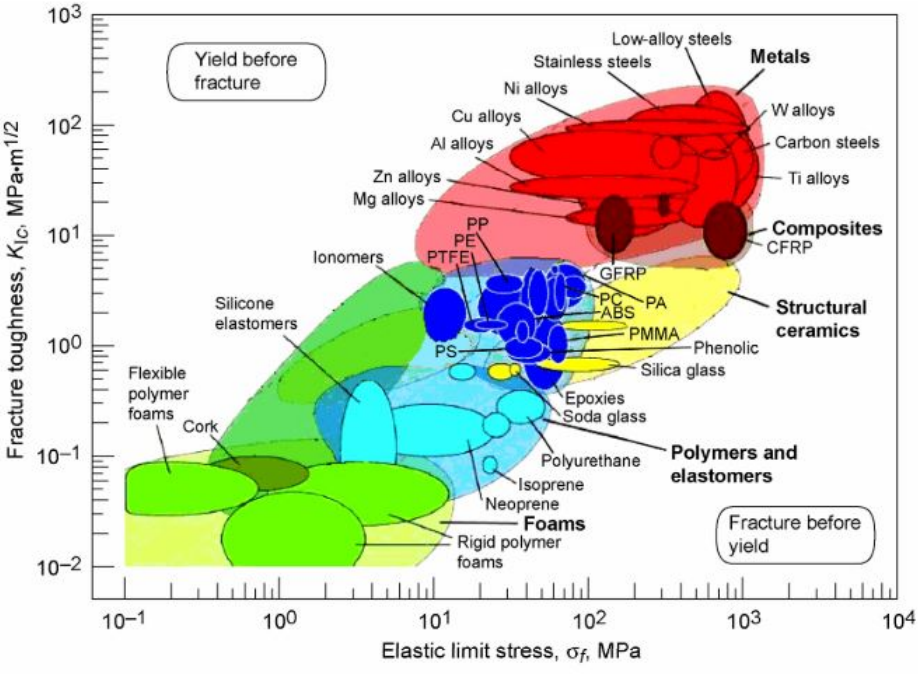

Figure 4.2: Fracture toughness versus strength for various materials [8]

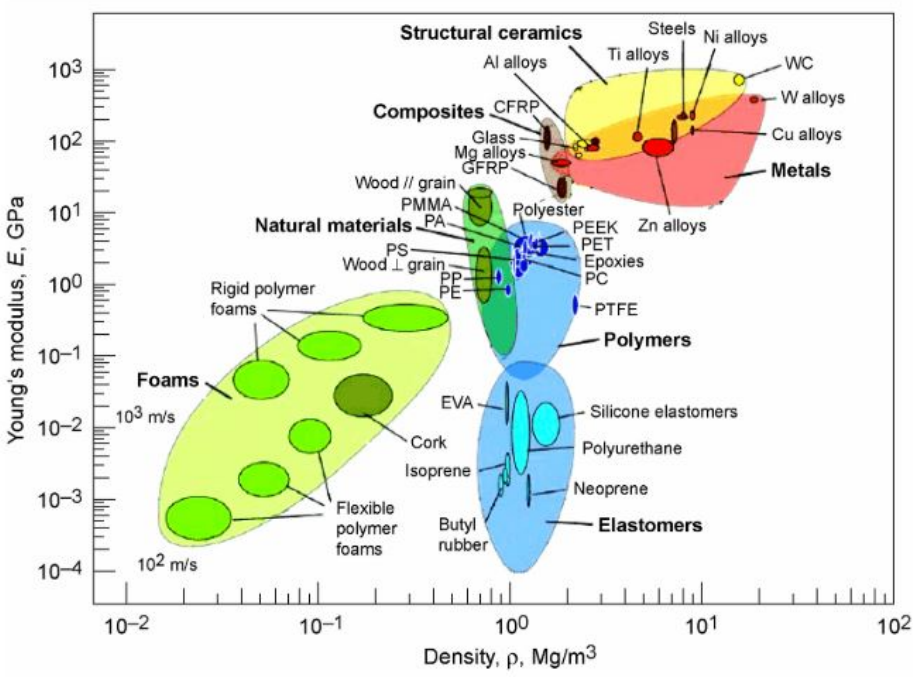

Figure 4.3: Young's modulus versus density for various materials [8]

In this study the material selected for the fuel tank wall is a aluminium alloy. Aluminium alloys have relatively high strength and high stiffness with a density that is not exorbitant. Aluminium alloys are widely used in aviation. Furthermore, aluminium alloys show a low rate of permeation to hydrogen. Aluminium alloys also show an increase in strength with a decrease in temperature.
To be more specific on the selected alloy, it is the aluminium alloy 7075-T6. This alloy is preferred over other alloys due to its high yield strength.

As discussed in Chapter 3, the oval fuel tank needs an internal trapezoid structure to handle the pressurization loads. This structure is connected to the outside tank wall, but goes through the insulation and is exposed to the hydrogen inside the fuel tank. Therefore, the trapezoid material is selected to be aluminium 7075-T6 as well.

From the figures shown above, one can see that carbon fiber reinforced composite materials perform well under the mentioned requirements. According to Verstraete et al. [11] the use of composites can even lead to a potential tank wall weight saving of 25%.
In this study composites are not chosen because of the relatively new application of composites with hydrogen. Not all opinions are aligned about the performance of composites when in contact with hydrogen, whereas the use of metallic alloys are widely accepted. One could decide to use composites for the external tank wall and still use aluminium for the internal trapezoid structure, as this is always in contact with hydrogen. The problem here is the uncertainty about the connection of the aluminium to the composite and the different coefficients of thermal expansion. This could possibly lead to local stresses at the connection points. This problem is found to be out of the scope of this study and is recommenced for future studies. For now the more conservative choice of an aluminium fuel tank is used.

4.3.2. INSULATION MATERIAL

One of the biggest challenges of using liquid hydrogen or liquefied natural gas as a fuel is working with the cryogenic temperatures. As mentioned before, the liquid fuels need to be kept below their boiling point to prevent boil-off of the fuel. To keep the fuels at their cryogenic temperatures and reduce the amount of boil-off the fuel tank needs to be insulated. The thickness of the insulation layer will have an effect on the available fuel volume. Therefore, for an insulation system to be efficient it needs to have a low thermal conductivity, a low thermal diffusivity and a low density [8]. Minimizing the thermal conductivity minimizes the steady-state heat flux, i.e. the heat flow rate through the insulation is minimized. Minimizing the thermal diffusivity minimizes the temperature rise per unit of time, i.e. the time for thermal energy to reach the fuel is maximized. Meanwhile, minimizing the density of the material will result in a light weight solution. Next to these requirements one can define several others. Mital et al. [8] have defined several of these requirements, or performance indices, to assist in the selection of the available insulation materials. These performance indices are given by Table 4.2. These performance indices for different materials are depicted in Figures 4.4 to 4.6. Looking at these figures and using the performance indices from Table 4.2 some materials stand out. From Figure 4.4 one can see polymer foams and aerogels have low thermal conductivity. Taking into account thermal diffusivity in Figure 4.5, one arrives at aerogels and rigid polymer foams. According to Mital et al. [8] a multi-layer insulation (MLI) system offers a thermal diffusivity that is comparable to metals, but has a thermal conductivity two orders lower than polymer foams (MLI consists of alternating layers of low conductivity spacer and low emissivity foil; a vacuum is required to minimize the heat transfer by residual gas conduction [11]). From Figure 4.6 one can see that most materials with a low thermal conductivity show large thermal distortion.

Table 4.2: Performance indices for thermal components of cryogenic storage tank [8]

Function and constraints	**Performance indices, maximize**
Minimum heat flux at steady-state	$1/k$
Minimum temperature rise in specified time	$1/a$
Maximum energy stored for given temperature rise and time	$k/\sqrt{a}$
Minimum thermal distortion	k/α

Where k is the thermal conductivity, a is the thermal diffusivity, ρ is the density and α is the thermal

expansion coefficient.

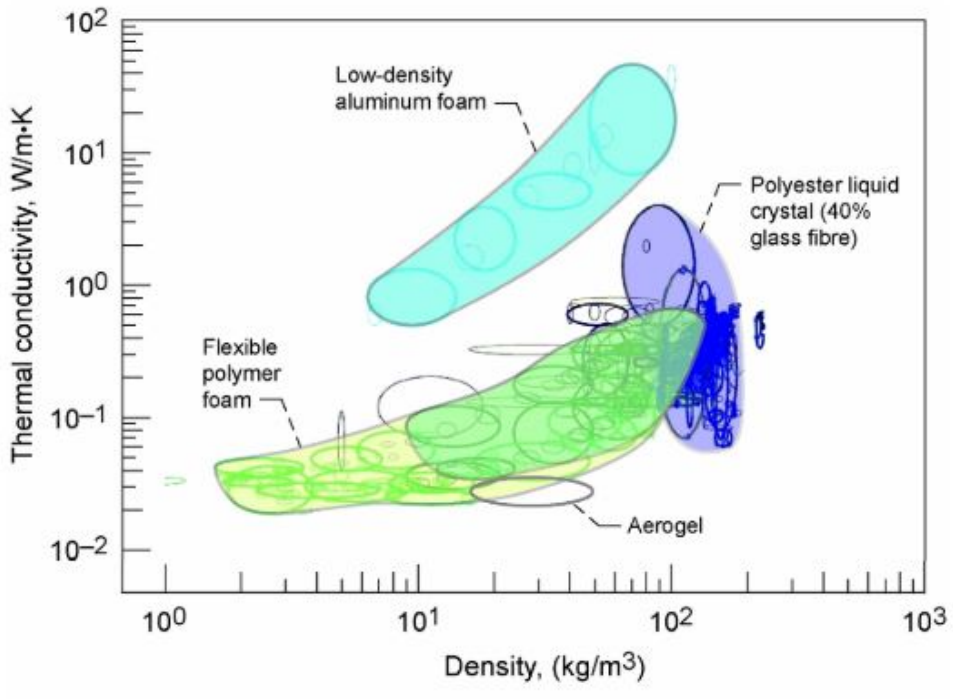

Figure 4.4: Thermal conductivity versus density for various materials [8]

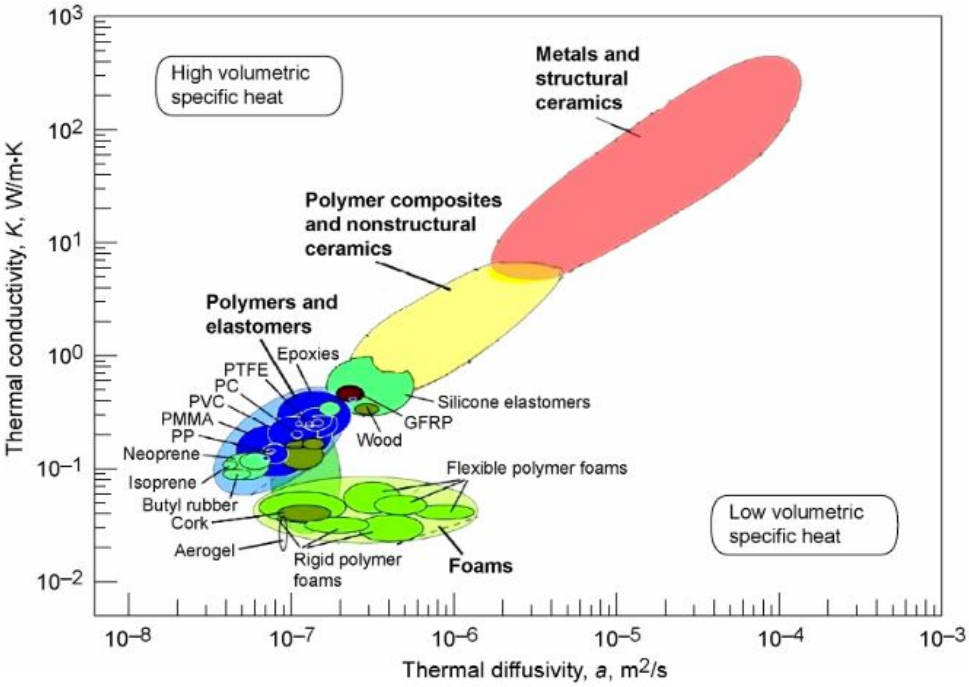

Figure 4.5: Thermal conductivity versus thermal diffusivity for various materials [8]

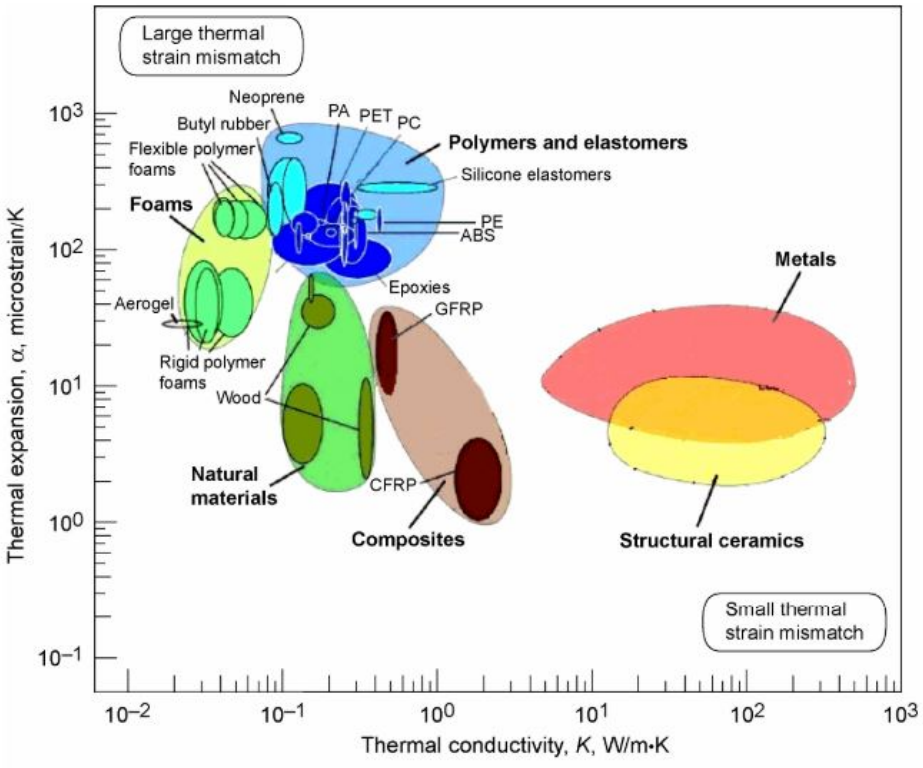

Figure 4.6: Thermal expansion versus thermal conductivity of various materials [8]

In this study three different types of insulation are considered, i.e. polymer foam, multi-layer insulation (MLI) and aerogels. From these options polymer foam, more specifically polyurethane, is selected as the material to be used. Although polyurethane foam has the highest thermal conductivity, the risk associated with the use of polyurethane foam is significantly lower and the use is relatively straight forward. That is, the required vacuum by the MLI results in a more complex and heavier insulation. Furthermore, a loss of this vacuum results in the immediate loss of insulating performance which can lead to catastrophic failures for the aircraft. Subsequently, aerogels, having great insulating qualities, are very brittle and fragile. This results in a less straightforward use. Therefore polyurethane seems as the safest and most conservative choice.

4.3.3. LINER MATERIAL

To protect the insulation from the hydrogen a liner material is preferred. A liner will prevent contact between the insulation and the hydrogen which prolongs the lifetime of the insulation. Mital et al. [8] mention polymer and elastomer films as a permeation barrier, such as fluoropolymers, polysulfide, polyeurathene, nitrile and butile. These films can be cured-in-place or can be sprayed on the insulation. However, the data on these films used with hydrogen is limited.

Fischer [38] presents a cryogenic insulation that can be applied inside of the hydrogen tank, called Inner Wetted Thermal Insultation (IWTI). This is a cryogenic insulation concept based on polyurethane foam developed for low cryogenic conditions. To protect the foam Fischer mentions two liner options, i.e aluminium foil glued to the foam and a spray-on polymeric liner [38]. The feasibility of both options has been shown.

For this study the polymeric liner is selected as the preferred option. The liner shows good compatibility to the polyurethane foam, can be applied with a spraying process and is low mass due to the insignificant thickness required [38]. This liner is selected to work together with the polyurethane foam selected in the section above. The liner is a very small component and is assumed to have a

negligible influence on thermal analysis.

4.4. TANK SIZING

To determine the available fuel volume of the cryogenic fuel tank of the Flying-V the fuel tank needs to be sized. The sizing method needs to take into account mechanical and thermal requirements corresponding to a particular operation. The result is a lightweight and insulated cryogenic fuel tank, where a trade-off is made between the insulation thickness and the internal tank pressure.

The method used to size the structure of the tank related to the tank pressure is discussed in Section 4.4.1. Following is the method used for the thermodynamic design of the fuel tank in Section 4.4.2.

4.4.1. MECHANICAL DESIGN

The mechanical design of the fuel tank begins with the so-called design strategy. That is, the fuel tank can be designed for different operating pressures during flight.

The first option is to design the fuel tank to operate at a constant gauge pressure. Constant gauge pressure is used for kerosene fuel [3]. In case of using hydrogen, constant gauge pressure will lead to a decrease in pressure during climb resulting in a superheated liquid [3]. The boil-off rate of the hydrogen will increase and the boiled off fuel has to be vented. During the descend the pressure in the tank needs to be increased again by letting air into the tank. The mixture of hydrogen and air results in an explosive mixture and the moisture in the air can freeze which can cause obstructions of the fuel pump and fuel lines.

The second option is to design the fuel tank to operate at a constant absolute pressure. Constant absolute pressure will lead to an increase in internal pressure when the atmospheric pressure decreases. During these phases of the flight the fuel will need to be vented. When the atmospheric pressure increases the internal pressure decreases again. In these cases the fuel needs to be heated to keep the internal pressure above the filling pressure. According to Verstraete et al. [11] this option result in a relatively light tank structure, due to a relatively low design pressure. However, a lot of fuel needs to be vented during flight, increasing the operating cost.

The third option is to design the fuel tank to operate with a fluctuating pressure during flight. The tank pressure is allowed to fluctuate between the fill pressure and the venting pressure [11]. The fuel tank insulation is required to keep the tank pressure lower than the venting pressure, minimizing the venting of fuel. This third option is selected for this research.

PRESSURE FLUCTUATIONS

During the flight fuel is withdrawn and heat is leaking into the tank. This results in changes to the temperature and pressure equilibrium of the fuel. These changes in pressure are required to determine the design venting pressure of the fuel tank, i.e. the maximum allowable pressure inside the fuel tank. To determine the pressure fluctuation Equation (4.1) is used [39].

$$\frac{\mathrm{d}P}{\mathrm{d}t} = \frac{\phi}{V}\left(Q + W + \dot{m}_i\left[h_i - h - \rho\left(\frac{\partial h}{\partial \rho}\right)_P\right] - \dot{m}_o\left[h_o - h - \rho\left(\frac{\partial h}{\partial \rho}\right)_P\right] + \rho^2\left(\frac{\partial h}{\partial \rho}\right)_P \frac{\mathrm{d}V}{\mathrm{d}t}\right) \tag{4.1}$$

The equation uses the first law of thermodynamics and conservation of mass to a control volume that holds the fuel. The control volume is assumed to be inelastic and the fuel is assumed to be in a homogeneous state. The specific fluid enthalpy is given by Equation (4.2) and the energy derivative by Equation (4.3) [39].

$$h = u + \frac{P}{\rho} \tag{4.2}$$

$$\phi = \frac{1}{\rho\left(\frac{\partial u}{\partial P}\right)_\rho} \tag{4.3}$$

Where ϕ is the energy derivative, V is the tank volume, Q is the heat leaking into the tank, W is the power input in the tank, $\dot{m}$ is the mass flow rate, h is the specific enthalpy of the mass flow and u is the specific internal energy of the fluid.

Assuming the tank is inelastic, there is no mass flow entering the tank and there is no power input in the tank Equation (4.1) can be simplified into Equation (4.4), which can be rearranged into Equation (4.5) [39].

$$\frac{\mathrm{d}P}{\mathrm{d}t} = \frac{\phi}{V}\left(Q - \dot{m}_o\left[h_o - h - \rho\left(\frac{\partial h}{\partial \rho}\right)_P\right]\right) \tag{4.4}$$

$$\frac{\mathrm{d}P}{\mathrm{d}t} = \frac{\phi}{V}\left(Q - \dot{m}_o \cdot h_{lg} \cdot \left[x \cdot \frac{\rho_\mathrm{g}}{\rho_\mathrm{l} - \rho_\mathrm{g}}\right]\right) \tag{4.5}$$

Where h_{lg} is the heat of vaporization, x is the quality of the fuel ($x = 1$ for saturated vapor only and $x = 0$ for saturated liquid only) and ρ_l and ρ_g are the density of the liquid and gas, respectively.

As mentioned in Section 2.2.2, the hydrogen used is assumed to be mainly para-hydrogen. The energy derivative of para-hydrogen is determined by Verstraete [3] and compared to data from Allidieris & Janin [40] and Lin et al. [39] as well. The energy derivative is depicted in Figure 4.7.

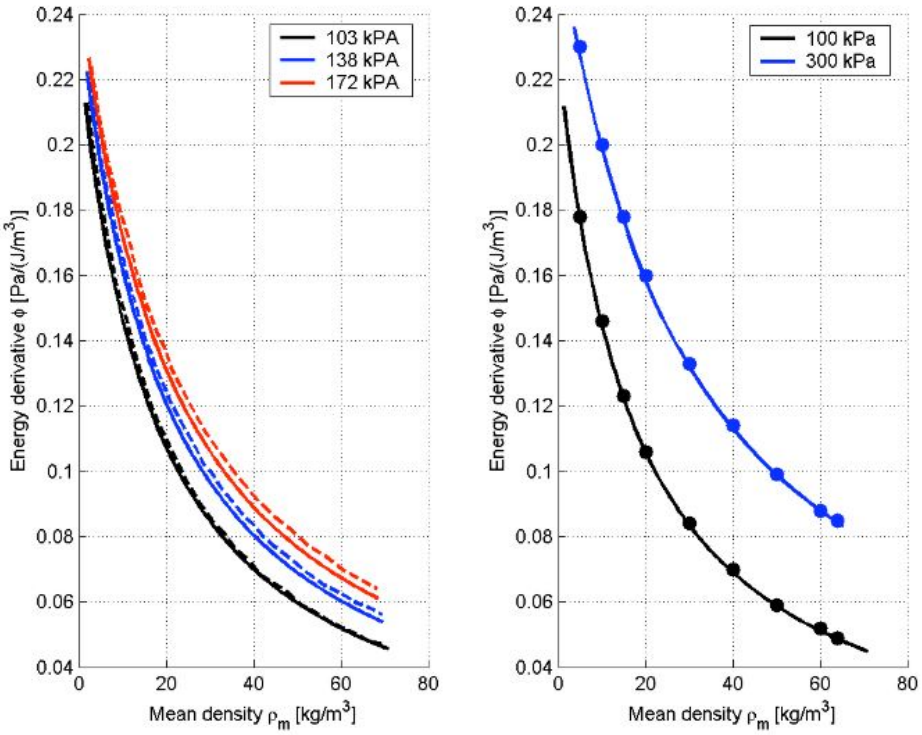

Figure 4.7: Energy derivatives of para-hydrogen compared to Allidieris & Janin (dots right) and Lin et al. (dashed lines left) [3]

Using the method described above one should note that the fuel is assumed to be homogeneously mixed. However, this will not be the case and a certain amount of stratification exists which effects

the pressure rise in the tank. To account for stratification effects Lin et al. [39] use twice the pressure rise rate for aircraft fuel tanks.

WALL THICKNESS

The fuel tank walls are sized using a pressure vessel calculation. Although an integral fuel tank is selected, which also takes into account axial, bending and shear loads next to the pressurization loads, a finite element analysis is out of the scope of this research. In this preliminary design phase the fuel tank will be sized for pressurization loads.

The pressurization load is determined by the selected venting pressure. The mechanical design is a function of the venting pressure. Pressurization of the fuel tank causes hoop-stresses and longitudinal stresses. The hoop-stresses are twice as large as the longitudinal stresses. Therefore, for a simple pressure vessel calculation only the hoop-stresses are taken into account. As the oval cross-section is made from three different circular arcs, the hoop-stress is taken into account for each arc separately. The wall thickness of each arc is determined by Equation (4.6) [7]. The wall thickness of the elliptical tank domes is determined by Equation (4.7) [3].

$$t_i = \frac{\Delta P \cdot R_i \cdot j}{\sigma_{\theta_i}} \tag{4.6}$$

Where ΔP is the pressure difference, R is the arc radius, j is the safety factor of 1.5, σ_θ is the fatigue strength of the wall material at 10^5 cycles.

$$t_d = \frac{\Delta P \cdot R_a \cdot K}{\sigma_\theta \cdot e_w + \Delta P \cdot (K - 0.1)} \tag{4.7}$$

$$K = \frac{1}{6}\left[2 + \frac{R_a}{R_b}\right] \tag{4.8}$$

Where R_a and R_b are the radii of the major and minor axis of the ellipse, respectively, and e_w is the weld efficiency.

TRAPEZOID STRUCTURE THICKNESS

To prevent the oval from becoming a circle due to pressurization a trapezoid structure is present that connects to the nodes between the circular arcs and takes in the pressurization loads.
To determine the required thickness of the walls, floor and ceiling of the trapezoid structure the first step is to determine the resultant forces in the nodes. Hoogreef [7] has decomposed the resultant forces due to pressurization into the horizontal and vertical components at the nodes. These forces are given by Equation (4.9) and Equation (4.10) for the upper node and by Equation (4.11) and Equation (4.12) for the lower node.

$$F_{h_{upper}} = \Delta P \cdot \Delta l \cdot (R_1 - R_2) \cdot (\cos(\beta) + \sin(\beta) \cdot \tan(\zeta)) \tag{4.9}$$

$$F_{v_{upper}} = \Delta P \cdot \Delta l \cdot (R_1 - R_2) \cdot \sin(\beta) \cdot \frac{1}{\cos(\zeta)} \tag{4.10}$$

$$F_{h_{lower}} = \Delta P \cdot \Delta l \cdot (R_3 - R_2) \cdot (\cos(\eta) - \sin(\eta) \cdot \tan(\zeta)) \tag{4.11}$$

$$F_{v_{lower}} = \Delta P \cdot \Delta l \cdot (R_3 - R_2) \cdot \sin(\eta) \cdot \frac{1}{\cos(\zeta)} \tag{4.12}$$

Where R_1 to R_3 are the radii of the crown arc, the side arc and the keel arc, respectively. Δl is the unit tank length. The angles β, ζ and η are depicted in Figure 4.8.

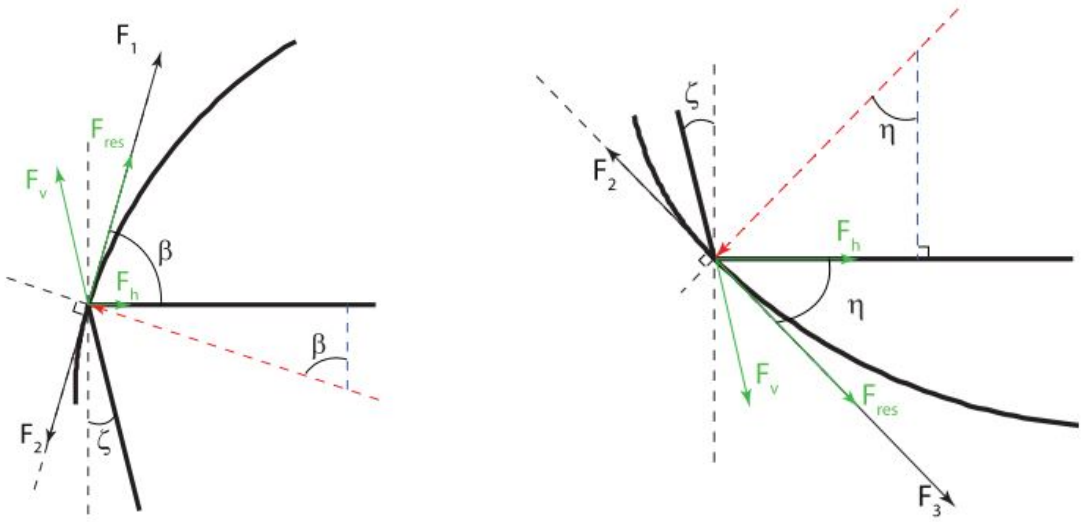

(a) Upper node

(b) Lower node

Figure 4.8: Free body diagram for pressurization [7]

With the resultant forces known one can determine the required thicknesses at the upper and lower nodes. The required thickness for the tension in the walls is determined using Equation (4.13) [7].

$$t_{wall} = \frac{j \cdot F_v}{\sigma_\theta \cdot \Delta l} \tag{4.13}$$

The floor/ceiling are assumed to be buckling critical. The critical force for the first buckling mode is given by Equation (4.14). The resulting thickness for the floor/ceiling is given by Equation (4.15) [7].

$$F_{\text{crit}} = \frac{\pi^2 \cdot EI}{L^2} = \frac{\pi^2 \cdot E \cdot \frac{1}{12} \cdot \Delta l \cdot t^3}{L^2} \tag{4.14}$$

$$t = \sqrt[3]{\frac{F_h \cdot L^2}{\pi^2 \cdot E \cdot \frac{1}{12} \cdot \Delta l}} \tag{4.15}$$

The resulting thicknesses are per unit length, i.e. over the length of the fuel tank this would result in a panel from end to end. This would be very heavy and of course not realistic. The use of separated frames is conventional. Therefore idealization of a panel is adopted to idealize the wall, floor and ceiling panels into a combination of direct stress carrying booms. The direct stress distribution in the actual panel in analyzed as extreme stresses at each boom. The loading producing the stresses in the actual and the idealized panel is the same, therefore for the idealized panel moments for each boom need to be equated [9]. From theses moment expressions can be obtained for the boom areas. Idealization of a panel is depicted in Figure 4.9. The moment about the right-hand edge of each panel is given by Equation (4.16) [9].

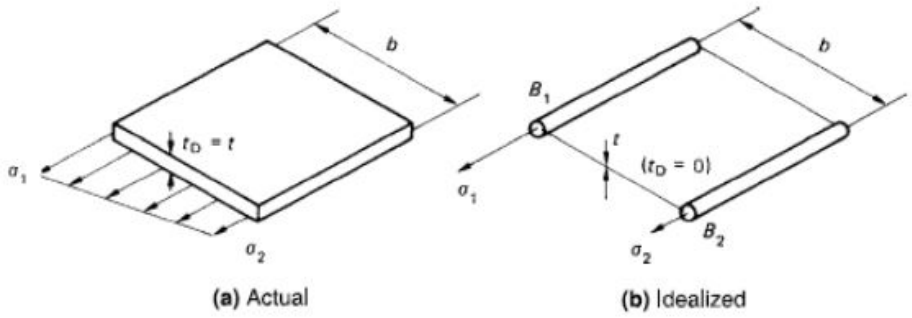

Figure 4.9: Idealization of a panel [9]

$$\sigma_2 \cdot t_D \cdot \frac{b^2}{2} + \frac{1}{2} \cdot (\sigma_1 - \sigma_2) \cdot t_D \cdot b \cdot \frac{2}{3} \cdot b = \sigma_1 \cdot B_1 \cdot b \tag{4.16}$$

The area of boom 1, B_1, follows depicted by Equation (4.17). The same can be done for the other boom resulting in the area of boom 2, B_2, depicted by Equation (4.18).

$$B_1 = \frac{t_D b}{6} \cdot \left(2 + \frac{\sigma_2}{\sigma_1}\right) \tag{4.17}$$

$$B_2 = \frac{t_D b}{6} \cdot \left(2 + \frac{\sigma_2}{\sigma_1}\right) \tag{4.18}$$

This method is expanded to a system with multiple booms next to each other, where every boom is effected by the boom left and right from it. B gives the surface area of the boom and b is the frame separation. In this work the frame separation is set to a conventional 62.5 cm.

During the sizing process each boom is modelled as a supported boom. This is to increase the buckling resistance. The number of supports selected is equal to 5. These supports are not taken into account as the area between the floor and the keel arc or the ceiling and the crown arc is filled with a plate, like a rib plate in a wingbox. The plate will act as an anti-slosh plate, which will decrease the boil-off due to sloshing [11]. At the same time the plate will support the beam to increase the buckling resistance just as the supports would. There is a difference between supporting a beam with individual supports columns or with plates, but that structural problem is out of the scope of this research. The 5 supports are used to determine the buckling load on the boom and determine the boom area. The weight of the anti-slosh plates is used in the weight of the structure. Therefore the resulting weight will be a conservative estimation.

4.4.2. THERMAL DESIGN

The thermal design focuses on the insulation of the fuel tank. As mentioned before, the fuel tank is designed with a layer of polyurethane foam on the inside of the fuel tank. A significant insulation layer is needed to prevent heat leaking into the tank and causing the fuel to boil-off. However, with keeping the outer mold lines constant, the insulation layer will also consume the available fuel volume and it adds to the weight of the fuel tank. Therefore a trade-off between the boil-off rate, fuel volume and tank weight needs to be conducted. To determine these parameters with the corresponding insulation thickness a thermal model analyses the thermal performance of the fuel tank as a function of the insulation thickness.

The thermal analysis is assumed to be steady-state. During flight heat will be leaking into the fuel tank promoting the evaporation of the hydrogen fuel. This changes the fuel quality, which changes

the internal convective heat transfer coefficient and as a result the heat transfer rate. Therefore the problem is actually inherently transient. However, with a certain insulation thickness it can be demonstrated that the boil-off rate of the hydrogen is insignificant during the flight and the fuel quality is approximately constant. Therefore the steady-state analysis is assumed to hold in first approximation.

The thermal model uses an electrical resistance analogy where the thermal resistances of the different heat transfers are placed in series. The total thermal resistance of the system is the sum of the individual resistances. The thermal resistance network of the fuel tank is depicted in Figure 4.10. The network consists of forced convection on the external surface, pure conduction through the tank wall and insulation layer and natural convection on the internal surface. At the same time the external wall is influenced by the solar radiation and re-radiation of the skin.

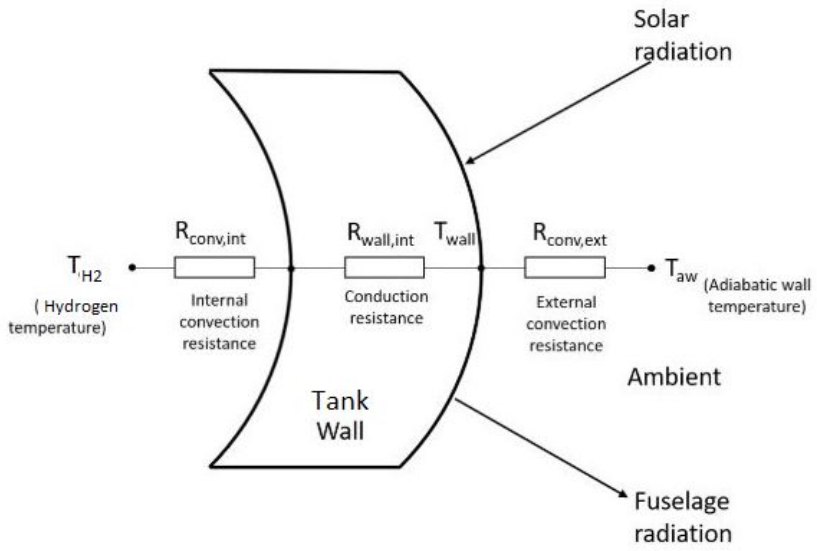

Figure 4.10: Thermal resistance network [10]

FORCED CONVECTION OF THE EXTERNAL SURFACE

The external surface of the aircraft is affected by the airflow during flight. This causes a heat transfer due to convection. For the forced convection over the surface of the wing a flat plate correlation is used, given by Equation (4.19) [3].

$$Nu_L = 0.03625 \cdot Pr^{0.43} \cdot Re_L^{0.8} \tag{4.19}$$

Where

$$Nu = \frac{h_{\text{ext}} \cdot L}{k_{\text{air}}} \qquad Pr = \frac{\mu_{\text{air}} \cdot c_p}{k_{\text{air}}} \qquad Re_L = \frac{\rho \cdot V \cdot L}{\mu_{\text{air}}} \tag{4.20}$$

The Nusselt number and the Reynolds number are based on the length L of the object in question, in this case the mean chord of the wing where the fuel tank is located. As the wing is swept the flow velocity over the wing is affected. Therefore the effective Mach number and the effective Reynolds number are determined and used. h_{ext} is the external convective heat transfer coefficient, k_{air} is the thermal conductivity of the air, μ_{air} is the dynamic viscosity of the air, ρ is the air density and c_p is the specific heat at constant pressure.
Using the equation depicted above the external convective heat transfer coefficient can be determined. This leads to the thermal resistance for external convection, given by Equation (4.21) [12].

$$R_{\text{ext}} = \frac{1}{2\pi \cdot r_{\text{tank}} \cdot L_{\text{tank}}} \cdot \frac{1}{h_{\text{ext}}} \tag{4.21}$$

Where $2\pi \cdot r_{\text{tank}} \cdot L_{\text{tank}}$ is equal to the fuel tank surface area, which is taken from the ParaPy model.

CONDUCTION OF THE TANK MATERIAL

The fuel tank consists of an aluminium tank wall with an polyurethane foam layer on the inside. For the heat to leak through these layers, heat transfer via conduction has to happen. In this case it is assumed to be pure conduction. That is, it is assumed that the materials are completely solid with no imperfections such as air pockets in the material or between the layers of material. Even the foam, which inherently consists of gas bubbles, is modelled as a solid material.

To determine the thermal resistance for pure conduction heat transfer Equation (4.22) [12] is used. This equation uses cylindrical coordinates. As no such equation exists for an oval shaped cylinder, the oval-shaped fuel tank is modelled as a cylinder and Equation (4.22) is used. The fuel tank is modelled as a cylinder with the same length and the same volume. The result is an "effective radius" that the cylinder would have with this length and volume. This radius is used in further calculation.

$$R_{\text{cond}} = \frac{1}{2\pi \cdot L_{\text{tank}}} \cdot \frac{ln\left(\frac{r_o}{r_i}\right)}{k} \tag{4.22}$$

Where r_o and r_i are the outer and inner radii of the layer of material in question and k is the thermal conductivity.

Equation (4.22) is used to determine the thermal resistance of the aluminium layer and of the foam layer. These resistances are is series and therefore summed to form the conduction thermal resistance.
In case of the foam layer the process is a bit more detailed. That is, the thermal conductivity of polyurethane foam is significantly influenced by the temperature. This is depicted in Figure 4.11. Therefore the foam layer is divided into 11 layers with its own thermal conductivity through which the temperature is assumed to vary linearly between the fuel temperature and the external skin temperature. Finally the thermal resistances of these layers are summed to form the thermal resistance of the foam.

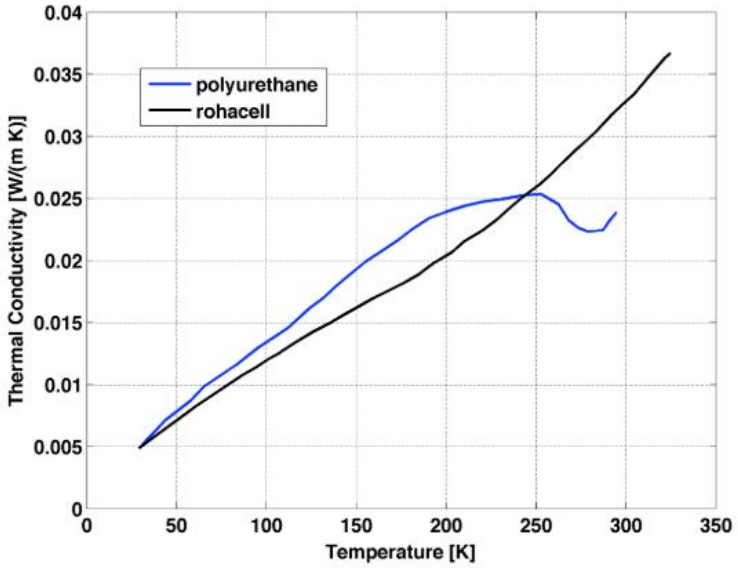

Figure 4.11: Thermal conductivity as a function of temperature of polyurethane and rohacell foam, derived from Brewer [6] by Verstraete [3]

NATURAL CONVECTION OF THE INTERNAL SURFACE

On the inside of the fuel tank heat transfers from the ambient into the fuel by natural convection. The natural convection occurs for the liquid fuel and for the fuel vapours. These parts have a different heat transfer rate and a different thermal resistance. Regarding the electrical resistance analogy these resistances are placed parallel to each other.

To determine the internal convection of the liquid phase the correlation of Equation (4.23) is used [3].

$$Nu_h = 0.0605 \cdot Ra_h^{1/3} \tag{4.23}$$

Where

$$Ra_h = \frac{g \cdot \beta \cdot \Delta T \cdot h^3 \cdot Pr \cdot \rho}{\mu_{\text{lh}}} \qquad Pr = \frac{\mu_{\text{lh}} \cdot c_p}{k_{\text{lh}}} \tag{4.24}$$

The Nusselt number and the Rayleigh number are based on the liquid height h in the tank. g is the gravitational acceleration, β is the coefficient of thermal expansion (CTE) of the liquid, ΔT is the temperature difference and μ_{lh} is the dynamic viscosity of the liquid hydrogen. Just as for the forced convection case, the internal convective heat transfer coefficient h_{int} is determined using Equation (4.25).

$$Nu_h = \frac{h_{\text{int}_{\text{lh}}} \cdot h}{k_{\text{lh}}} \tag{4.25}$$

In case of the gaseous phase only minimal data can be found and the correlation for the Nusselt number is set to 17 [6].
The internal convective heat transfer coefficients of the liquid and gaseous phase are finally combined into an internal convection thermal resistance. In this case the resistances are in parallel, so they can not be summed. The wetted areas by the liquid and by the gaseous phase need to be taken into account. The resulting thermal resistance is given by Equation (4.26) [3].

$$R_{\text{int}} = \frac{1}{2\pi \cdot r_i \cdot L} \cdot \frac{S_{w_{\text{tot}}}}{h_{\text{int}_{\text{lh}}} \cdot S_{w_{\text{lh}}} + h_{\text{int}_{\text{gh}}} \cdot S_{w_{\text{gh}}}} \tag{4.26}$$

Where $2\pi \cdot r_i \cdot L$ is equal to the fuel tank internal surface area, which is taken from the ParaPy model. $h_{\text{int}_{\text{lh}}}$ and $h_{\text{int}_{\text{gh}}}$ are the internal convective heat transfer coefficients for the liquid and gaseous hydrogen, respectively. $S_{w_{\text{tot}}}$ is the wetted surface area and $S_{w_{\text{lh}}}$ and $S_{w_{\text{gh}}}$ are the wetted surface area by the liquid and gaseous hydrogen, respectively. To determine the liquid and gaseous fuel height and the wetted areas the liquid volume fraction is used. The liquid volume fraction is a function of the pressure inside the tank and the fill pressure of 1.2 bar. This is depicted by Figure 4.12 [11].

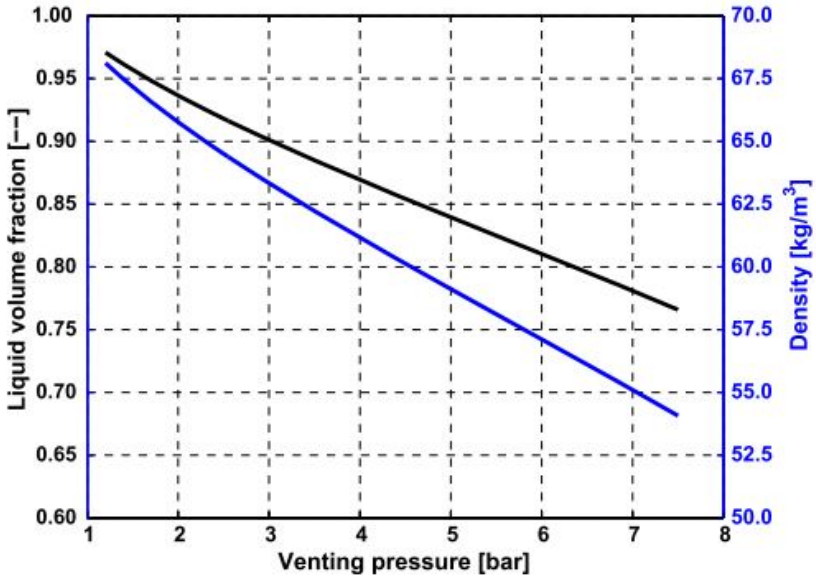

Figure 4.12: Liquid volume fraction and density of hydrogen as function of the venting pressure [11]

RADIATION ON THE EXTERNAL SURFACE

The external surface of the wing is also influenced by radiation. The sun radiates on the wing surface and the wing itself re-radiates back to the ambient. To determine the heat transfer by radiation the temperature of the skin is required. However this is unknown. Using the thermal resistances discussed above and assuming that the wing external skin is in a steady state thermal equilibrium, the skin temperature can be determined [10].

By assuming the steady state thermal equilibrium and using $\dot{Q}_{\text{Intloss}} = \dot{Q}_{\text{Extloss}}$ the skin temperature T_{skin} can be solved for. $\dot{Q}_{\text{Intloss}}$ is the heat loss from the internal tank to the external surface and $\dot{Q}_{\text{Extloss}}$ is the heat loss from the external surface to the ambient [10]. Note, as the system is actually transferring heat from the ambient into the tank, both of these losses are actually gains and are therefore both negative. $\dot{Q}_{\text{Intloss}}$ and $\dot{Q}_{\text{Extloss}}$ are given by Equation (4.27) and Equation (4.28), respectively [10].

$$\dot{Q}_{\text{Intloss}} = \frac{T_{\text{H2}} - T_{\text{skin}}}{R_{\text{int}} + R_{\text{cond}_{\text{alu}}} + R_{\text{cond}_{\text{ins}}}} \tag{4.27}$$

Where T_{H2} is the temperature of the hydrogen and R_{int}, $R_{\text{cond}_{\text{alu}}}$ and $R_{\text{cond}_{\text{ins}}}$ are the thermal resistances for the internal convection, conduction through the aluminium and conduction through the insulation, respectively.

$$\dot{Q}_{\text{Extloss}} = \frac{T_{\text{skin}} - T_{\text{atm}}}{R_{\text{ext}}} + \epsilon \cdot \sigma \cdot \left(T_{\text{skin}}^4 - T_{\text{sky}}^4\right) \cdot A - \alpha \cdot q_{\text{solar}} \cdot \frac{1}{2} A \tag{4.28}$$

Where T_{atm} is the atmospheric temperature and R_{ext} is the thermal resistance for the external convection. The next part on the right hand side represents the re-radiation of the skin to the ambient, where ϵ is the infrared emittance of the skin, σ is the Stefan Boltzmann constant, T_{sky} is the sky temperature given by Equation (4.29) [41] and A is the surface area of the tank. The last part on the right hand side represents the radiation of the sun onto the skin, where α is the solar absorptance of the skin, q_{solar} is the solar irradiance and $\frac{1}{2}A$ is half of the surface area of the tank, i.e. the irradiated area. Regarding the infrared emittance and the solar absorptance, the surface is assumed to be painted white with the corresponding value given by Lienhard [41]. The solar irradiance q_{solar} is

given by Thekaekara et al. [42], who measured the solar irradiance with a research aircraft at several different zenith angles during different flights.

$$T_{sky} = T_{atm}\left[0.711 + 0.0056 \cdot T_{dp} + 7.3 \cdot 10^{-5} \cdot T_{dp}^2 + 0.013 \cdot \cos\left(\frac{2\pi t}{24}\right)\right] \tag{4.29}$$

Where T_{dp} is the dew-point temperature given in $°C$ instead of Kelvin and t is the hour past midnight. This equation is applicable from dew-point temperatures between $-20°C$ to $30°C$ [41].

Equating Equation (4.27) to Equation (4.28) one can solve for the skin temperature. The skin temperature is then required to determine the thermal resistance of the external surface regarding the heat transfer by radiation. To determine the radiative heat transfer an equivalent convective coefficient is used, given by Equation (4.30) [41]. This equation can be used when the temperature difference between the body and the ambient are small.

$$h_{rad} = 4 \cdot \sigma \cdot T_m^3 \cdot \epsilon \qquad for \qquad \left(\frac{\Delta T}{T_m}\right)^2 / 4 \ll 1 \tag{4.30}$$

Where

$$\Delta T = T_{atm} - T_{skin} \qquad T_m = \frac{T_{atm} + T_{skin}}{2} \tag{4.31}$$

The radiation thermal resistance is given by Equation (4.32).

$$R_{rad} = \frac{1}{2\pi \cdot r_{tank} \cdot L_{tank}} \cdot \frac{1}{h_{rad}} \tag{4.32}$$

Where $2\pi \cdot r_{tank} \cdot L_{tank}$ is equal to the fuel tank surface area, which is taken from the ParaPy model.

TOTAL THERMAL RESISTANCE, HEAT TRANSFER RATE & BOIL-OFF RATE

The total thermal resistance is the sum of the different thermal resistances placed in series, i.e. Equation (4.33).

$$R_{tot} = R_{ext} + R_{rad} + R_{cond_{alu}} + R_{cond_{ins}} + R_{int} \tag{4.33}$$

The resulting heat transfer rate is given by Equation (4.34). A 30% margin is included to take into account the additional heat flow into the tank through the piping, support structure and other equipment [3]. The boil-off rate of the hydrogen is given by Equation (4.35), where the heat transfer rate is divided by the latent heat of vaporization.

$$Q = 1.3 \cdot \frac{T_{atm} - T_{H2}}{R_{tot}} \tag{4.34}$$

$$\dot{m}_{boil\text{-}off} = \frac{Q}{\lambda} \tag{4.35}$$

4.5. FUEL TANK VOLUME AND WEIGHT

The sizing of the fuel tank and the analysis of the thermal model lead to the available fuel tank volume and the resulting fuel tank weight as a function of the venting pressure and the insulation thickness. The tank volume and the tank weight are discussed in this section.

4.5.1. TANK VOLUME

The volume of the "inner tank" modelled in ParaPy can be easily acquired. However, this volume is not equal to the available fuel volume. Regarding the available fuel volume one should take into account space required for gas ullage. With a fuel tank filled with liquid hydrogen, a certain amount of stratification will be present. One should even ensure there is a certain amount of stratification present. That is, according to Allidieris & Janin [40], the pressure rise will be much higher for a fully saturated liquid than for a two-phase mixture and more insulation is needed to prevent heat leaking into the tank which increases the internal pressure. Therefore a certain amount of volume is left available for the gas parts of a two-phase mixture. In the Cryoplane study by Allidieris & Janin a 3% gas ullage allowance is adopted. This is used in this study as well.
The 3% gas ullage is required at the venting pressure. Therefore, the mean density of the hydrogen depends on the selected venting pressure [3]. This can be seen in Figure 4.12. The density in this figure is the mean density of the hydrogen with the corresponding liquid volume fraction. As the 3% gas ullage is required at the venting pressure, one should already allow a higher fraction of gas at the filling pressure. This is to make sure, when the pressure inside the tank reaches the venting pressure, one is venting hydrogen gas and there is still hydrogen gas left inside the tank when the venting stops to ensure there is a two-phase mixture. For example, if the venting pressure is selected to be 4 bar, with a fill pressure of 1.2 bar, the maximum fill level for liquid hydrogen is 87% of the tank volume to ensure 3% of the volume is gas at the venting pressure.

Next to the gas ullage allowance certain allowances are required for the expansion and contraction of the structure due to temperature changes, internal equipment, trapped fuel and gas space for the exit pipe. Table 4.3 show the different volume allowances adopted by in a NASA study documented by Brewer [6].

Table 4.3: Additional volume allowances as adopted by Brewer [6]

Allowance	[%]
Tank expansion and contraction	0.9
Internal equipment	0.6
Trapped fuel	0.3
Gas space for exit pipe	1.0
Total	1.8

Finally, to determine the available fuel volume the liquid volume fraction, corresponding to the selected venting pressure, minus the additional volume allowances of 1.8% is multiplied with the volume of the internal fuel tank.

4.5.2. TANK WEIGHT

The weight of the fuel tank is a combination of the external wall weight, the insulation weight, the internal structure weight minus the "structure that is already there" weight.
The volumes of the external wall, the insulation layer and the internal structure can be acquired using ParaPy. For the external wall an inner tank without insulation is created. The outer tank volume minus this inner tank results in the volume of the external wall. For the insulation volume the same is done, but with an inner tank with a layer of insulation. The outer tank volume minus the external wall volume minus the inner tank volume results in the insulation layer volume. The volume of the internal structure follows from the idealization of a panel as discussed in Section 4.4.1. Multiplying these volumes with the respectable densities results in the weights of these components.

In case there is no fuel tank there will be a wing structure. In order to not take this weight into account twice the part of the cabin where the fuel tank would be is sized, this is labeled as "structure

that is already there" weight. This sizing uses the cabin pressure at cruise altitude. This cabin pressure is normally equivalent to a cabin altitude[2] of 8000 ft . In this way the weight of the structure that is already there is determined. This weight is subtracted from the weights mentioned above.

Next the fuel weight is determined from the available fuel volume. The filled tank weight is the sum of the tank weight and the fuel weight. With the fuel weight and the filled tank weight the gravimetric storage density is determined. This density is given by Equation (4.36) and represents the fraction of liquid hydrogen in the overall fuel tank mass [11]. The gravimetric storage density is used as a figure of merit for the fuel tank design.

$$\eta = \frac{W_f}{W_f + W_t} \tag{4.36}$$

Where W_f is the available fuel mass and W_t is the tank mass.

4.6. WEIGHT ESTIMATION

To determine the flight performance of a liquid hydrogen Flying-V the weight of the aircraft needs to be estimated. The first step is to determine the empty weight of the aircraft. For this estimation weight fractions from Roskam [18] are used. Roskam divides the empty weight into the structure weight W_{struc}, the power plant weight W_{pwr} and the fixed equipment weight W_{feq}. For these weight groups Roskam presents weight fraction data relative to the gross weight for various jet transport aircraft. These fractions can be found in Appendix B. For the power plant weight fraction and the fixed equipment weight fraction the average is taken. In case of the structure weight fraction the weight estimation of the Flying-V by Claeys [17] is used. This is preferred over Roskam as the structure of a Flying-V is significantly different compared to a tube-and-wing transport aircraft, whereas the power plant and the fixed equipment are more comparable. The weight fractions are depicted in Table 4.4. For the empty weight the fractions are summed and multiplied with the MTOW and added to two times the tank weight. The empty weight is given by Equation (4.37). The MTOW is adopted from Oosterom [19] corresponding to the parametrization that is used.

Table 4.4: Component weight fractions. W_{struc} adopted from Claeys [17], W_{pwr} and W_{feq} adopted from Roskam [18]

Weight group (/MTOW)	**Fraction**
W_{struc}	0.2728
W_{pwr}	0.0809
W_{feq}	0.1325

$$W_{empty} = \left(W_{struc} + W_{pwr} + W_{feq}\right) \cdot MTOW + 2 \cdot W_t \tag{4.37}$$

Following are the crew weight W_{crew} and the payload weight W_{pl}. Adding the crew weight to the empty weight one arrives at the operating empty weight (OEW). Using the operating empty weight and adding the payload weight and the total fuel weight the result is the take-off weight W_{TO}.

4.6.1. CASE STUDIES

For the flight performance two case studies are analyzed. The first case study is regarding a retrofit of an existing Flying-V with a set of hydrogen fuel tanks. As the fuel weight of liquid hydrogen is lower compared to the fuel weight of kerosene there is a significant portion of the MTOW that is not used. Therefore, in case of this retrofit the theoretical maximum payload weight is determined. In theory this weight is still available due to the decrease in fuel weight when changing kerosene

[2]Cabin altitude. Retrieved on October 13, 2020 from https://www.skybrary.aero/index.php/Cabin_Altitude

for liquid hydrogen. The maximum payload weight is determined by Equation (4.38). This payload weight will also be found on the payload-range diagram.

$$W_{\text{pl}_{\text{max}}} = MTOW - W_{\text{empty}} - W_{\text{crew}} - 2 \cdot W_{\text{f}} \tag{4.38}$$

The second case study is regarding an iteration of the structure to take into account the aforementioned portion of the MTOW that is not used. It is important to note that the OML of the aircraft stay constant. The iteration uses the weight estimation discussed in this section. It starts with the MTOW from Oosterom to determine the take-off weight. This take-off weight is then used as the new MTOW to perform the estimation again. This process is repeated until the difference between subsequent take-off weights relative to the take-off weight of the previous iteration drops below a certain convergence requirement. Regarding the weight fractions the fixed equipment weight is not changed as the fraction is always multiplied with the starting MTOW. A change in take-off weight changes the wing loading and the required power. This changes the weight of the structure and the weight of the power plant, respectively. With the OML constant it is thought the fixed equipment stays constant as well.
Finally, when the iteration is converged, the take-off weight is used in the flight performance analysis of this case study.

4.7. FLIGHT PERFORMANCE

With the available fuel and the weight of the aircraft determined, the available range can be determined. To determine the range the Breguet range equation is used in combination with a regular design mission. This mission is depicted in Figure 4.13. This mission takes into account a reserve including a certain amount of diversion and a certain amount of loitering. For the non fuel-intensive phases of the mission fuel fractions are used, which are given by Table 4.5.

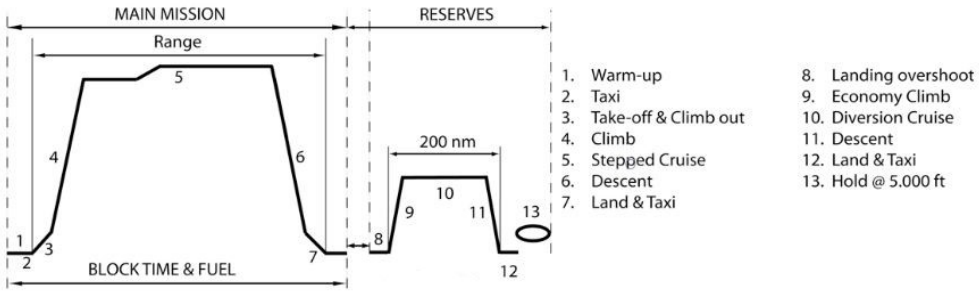

Figure 4.13: Mission profile [3]

Table 4.5: Fuel Fractions as presented by [3] from Roskam

Flight Phase	$\mathbf{M_{ff}}$
Warm-up	0.995
Taxi	0.99
Take-off	0.995
Climb	0.98
Descent	0.99
Land & Taxi	0.992
Overshoot	0.992
Reserve Climb	0.98

To make the fuel fractions valid for the use of hydrogen the fuel fractions for kerosene need to be adjusted. To perform a certain phase a certain amount of energy is required. This is the same for every fuel. However the amount of fuel needed to reach this amount of energy is different. A calorific equivalent fuel use for hydrogen with respect to kerosene is derived in Equation (4.39).

$$\begin{aligned} [J]_{\mathrm{K}} &= [J]_{\mathrm{H2}} \\ \frac{[J]}{[kg]}_{\mathrm{K}} \cdot [kg]_{\mathrm{K}} &= \frac{[J]}{[kg]}_{\mathrm{H2}} \cdot [kg]_{\mathrm{H2}} \\ \Rightarrow LHV_{\mathrm{K}} \cdot \Delta m_{\mathrm{K}} &= LHV_{\mathrm{H2}} \cdot \Delta m_{\mathrm{H2}} \\ \Rightarrow \Delta m_{\mathrm{H2}} &= \frac{LHV_{\mathrm{K}}}{LHV_{\mathrm{H2}}} \cdot \Delta m_{\mathrm{K}} \end{aligned} \tag{4.39}$$

Where LHV is the lower heating value and Δm is the fuel use. From the fuel fraction method follows Equation (4.40).

$$\begin{aligned} \Delta m = M_{\mathrm{used}} \cdot W_{\mathrm{TO}} &= (1 - M_{\mathrm{ff}}) \cdot W_{\mathrm{TO}} \\ \Rightarrow (1 - M_{\mathrm{ff_{H2}}}) \cdot W_{\mathrm{TO_{H2}}} &= \frac{LHV_{\mathrm{K}}}{LHV_{\mathrm{H2}}} \cdot (1 - M_{\mathrm{ff_K}}) \cdot W_{\mathrm{TO_K}} \\ M_{\mathrm{ff_{H2}}} &= 1 - \frac{LHV_{\mathrm{K}}}{LHV_{\mathrm{H2}}} \cdot (1 - M_{\mathrm{ff_K}}) \cdot \frac{W_{\mathrm{TO_K}}}{W_{\mathrm{TO_{H2}}}} \end{aligned} \tag{4.40}$$

Where M_{ff} is the fuel fraction and W_{TO} is the take-off weight.

Using the final relation from Equation (4.40) works for the non fuel-intensive flight phases. In case of the diversion and the loiter phase the Breguet range and endurance equations are used, given by Equation (4.41) and Equation (4.42), respectively.

$$R = \frac{V}{g \cdot c_{\mathrm{j}}} \cdot \frac{L}{D} \cdot \ln\left(\frac{W_{\mathrm{start}}}{W_{\mathrm{end}}}\right) \tag{4.41}$$

$$E = \frac{1}{g \cdot c_{\mathrm{j}}} \cdot \frac{L}{D} \cdot \ln\left(\frac{W_{\mathrm{start}}}{W_{\mathrm{end}}}\right) \tag{4.42}$$

Where R is the range, E is the endurance time, V is the velocity, L/D is the lift to drag ratio, c_{j} is the specific fuel consumption and W_{start} and W_{end} are the weight at the start and the end of the phase, respectively.

With the fuel fractions of the non fuel-intensive phases and the fuel fractions of the diversion and loiter phases determined, the remaining phase of interest is the main cruise phase. For the main cruise phase one is interested in the fuel fraction W_4/W_5. The weight at the start of the cruise W_4 over the weight at the end of the cruise W_5. W_4 is found by multiplying the fuel fractions of the first four phases with the take-off weight, i.e. Equation (4.43).

$$W_4 = \prod_{i=1}^{i=4} M_{\mathrm{ff}_i} \cdot W_{\mathrm{TO}} \tag{4.43}$$

In case of the weight at the end of the cruise phase, W_5, the fuel weight used in cruise is required. This requires the fuel fraction of the entire mission without the cruise. This is a product of all the fuel fractions except for the one for cruise. The weight of the fuel used during cruise is then given by Equation (4.44). Finally, the weight at the end of the cruise phase is given by Equation (4.45).

$$W_{f_{cruise}} = W_f - \left(1 - \prod_{i=1}^{i=n} M_{ff_{i\neq 5}}\right) \cdot W_{TO} \tag{4.44}$$

$$W_5 = W_4 - W_{f_{cruise}} \tag{4.45}$$

The available range is then given by the Breguet range equation in Equation (4.46).

$$R = \frac{V}{g \cdot c_j} \cdot \frac{L}{D} \cdot \ln\left(\frac{W_4}{W_5}\right) \tag{4.46}$$

To compare the payload-range performance the Payload Range Energy Efficiency (PREE) is used. The PREE is given by Equation (4.47). This parameter depicts the work required to move a unit of payload over a unit of distance per unit of energy consumed by the system [43].

$$PREE = \frac{W_{PL} \cdot R}{E_{miss}} \tag{4.47}$$

Where W_{PL} is the payload weight in N, R is the range and E_{miss} is the total energy consumed during the mission, excluding reserves.

In case of the second case study, where the take-off weight will be lower compared to a kerosene based Flying-V, the wing loading is reduced. To be able to fly at the same cruise speed and lift-to-drag ratio the cruise altitude needs to be increased. According to Equation (4.48) the decrease in mid-cruise weight needs to be compensated by a decrease in density, i.e. altitude. The flight performance analysis will then be performed for this altitude.

$$V_{cruise} = \sqrt{\frac{W}{S} \cdot \frac{2}{\rho} \cdot \frac{1}{C_L}} \tag{4.48}$$

5

VERIFICATION AND VALIDATION

This chapter presents the verification and the validation of the thermodynamic model and the flight performance analysis discussed before. The verification and the validation of the thermal model will be discussed first, followed by the validation of the flight performance analysis. The structural model of the oval cross-section has been validated by Schmidt [44] using FEM analysis.

5.1. THERMODYNAMIC MODEL

This section presents the verification and validation of the thermodynamic model. One should note that not every part of the thermal model is included in the verification and validation process, as experimental data on these subjects is very scarce. The verification of the thermal model uses an example from a textbook regarding heat and mass transfer called "Fundamentals of Heat and Mass Transfer" [12]. The validation uses the data of an experiment performed by Sass et al. [13].

5.1.1. VERIFICATION

For the verification of the thermodynamic model example 3.6 of the book "Fundamentals of Heat and Mass Transfer" is used. The example presents a spherical, thin-walled metallic container to store liquid nitrogen. The nitrogen is at a temperature of 77 K. The container has a diameter of 0.5 m and is insulated with an evacuated, reflective insulation composed of silica powder. This insulation is 25 mm thick and the outer surface is exposed to ambient air at 300 K. [12] A schematic of the container is depicted in Figure 5.1.

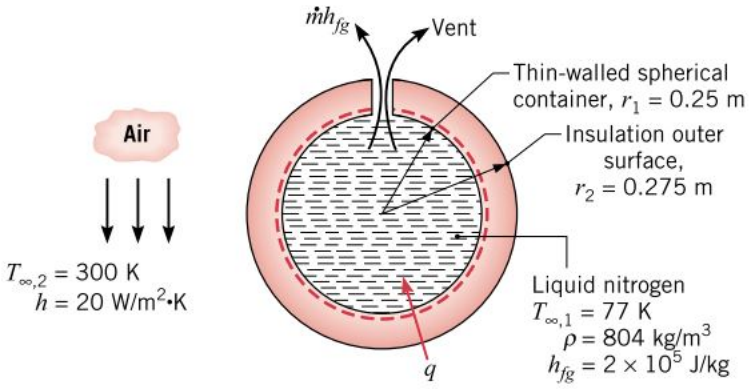

Figure 5.1: Schematic of the nitrogen container [12]

The convection coefficient is given to be 20 $W/m^2 \cdot K$, the latent heat of vaporization of nitrogen is $2 \cdot 10^5$ J/kg and the density of liquid nitrogen is 804 kg/m^3.

The parameters of the nitrogen container are used as inputs for the thermodynamic model. Next to the parameters given by the example the model requires several other parameters, i.e. the surface area of the inner sphere, the thermal conductivity of the silica powder [12] and the thermal conductivity, the dynamic viscosity, the specific heat at constant pressure and the coefficient of thermal expansion of the liquid nitrogen[1]. An overview of all the parameters used is given by Table 5.1.

Table 5.1: Overview of the parameters used for verification

Parameter	**Value**	**Unit**
Inner Diameter	0.5	m
Outer Diameter	0.55	m
Inner Surface Area	0.785	m^2
Ambient Temperature	300	K
Inner Temperature	77	K
Convection Coefficient	20	$W/m^2 \cdot K$
Thermal Conductivity Silica	0.0017	$W/m \cdot K$
Thermal Conductivity Nitrogen	0.1455	$w/m \cdot K$
Dynamic viscosity Nitrogen	$163.75 \cdot 10^{-6}$	$Pa \cdot s$
Specific Heat at constant Pressure	2037	$J/kg \cdot K$
Coefficient of Thermal Expansion	0.012987	1/K
Latent Heat of Vaporization	$2 \cdot 10^5$	J/kg
Density Nitrogen	804	kg/m^3

In the example it is assumed that the conditions are steady-state, the transfer is one-dimensional in radial direction and the properties are constant. This corresponds to the assumptions made in the thermodynamic model used in this research. Furthermore, the example assumes the resistance to heat transfer through the container wall and from the container to the nitrogen to be negligible. Finally, the radiation exchange between the outer surface and the surroundings is assumed to be negligible as well. In the thermodynamic model used in the research the influence of the tank wall, the internal convection and radiation are normally taken into account. In case of this example there is no information on the tank wall other than it being thin-walled, i.e. in this case its impact is assumed to be negligible as well.

With all the required parameters collected and assumptions made, the rate of heat transfer to the nitrogen and the boil-off of the nitrogen are calculated. The results are compared to the results of the example in Table 5.2.

Table 5.2: Heat transfer rate and boil-off rate of nitrogen container

	Example	**Model**	**Difference**
Heat trasfer rate [W]	13.06	12.90	-1.2%
Boil-off rate [kg/s]	$6.53 \cdot 10^{-5}$	$6.45 \cdot 10^{-5}$	

As can be seen from the table above, there is a slight difference between the results. This can be explained by the assumptions made by the example. The example ignores the influence of the radiation and the internal convection on the total thermal resistance of the container. In the model

[1] Nitrogen Properties. Retrieved on March 18, 2021 from https://www.engineeringtoolbox.com/nitrogen-d_1421.html

the thermal resistance due to the internal convection adds to the total thermal resistance and the thermal resistance due to the radiation slightly decrease the total thermal resistance. The combined impact of these processes on the total thermal resistance comes down to 1.2 %. Thus it is concluded that the model does what is should in case of this simple example.

5.1.2. VALIDATION

For the validation of the thermodynamic model the experiment conducted by Sass et al. [13] is used. Sass et al. cunducted a technology demonstration test project at the Cryogenics Test Laboratory at the Kennedy Space Center. The test was aimed to provide thermal performance data for glass microspheres and perlite insulation systems for liquid hydrogen tanks applications [13]. The tests were performed using two spherical liquid hydrogen tanks, custom designed for this experiment. The tanks were fitted with a range of sensors, among which temperature sensors and liquid level sensors. Mass flow meters and weight scales are used to measure the evaporative boil-off rate of the cryogenic fluid [13]. The heat transfer rate follows from the boil-off rate using the heat of vaporization.
The spherical tanks have a capacity of 1000 liters and an outer diameter of 1.524 m. The thickness of the insulation layer is 0.135 m. The ambient temperature was approximately 295 K and the internal temperature was 77 K and 20 K for liquid nitrogen and liquid hydrogen, respectively. The spherical tanks are depicted in Figure 5.2.

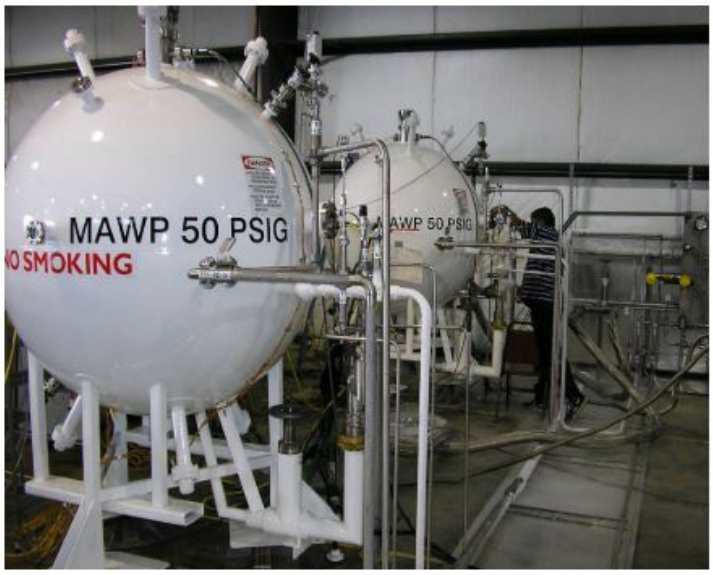

Figure 5.2: Tank used for the thermal performance testing by Sass et al. [13]

The same as before, the parameters of the storage tanks are used as inputs for the thermodynamic model. Besides the dimensions of the tank and the temperatures of the ambient and the fuel, the average fill level and the average vacuum level are given as well. The fill level influences the internal convection process and the vacuum level is relevant for the performance of the insulation materials. The insulation is located in an annulus where a near vacuum is created. The thermal conductivity of these insulation materials is reported by Scholtens et al. [45], where the performance depends on the operating pressure. Next to these parameters the model requires the surface area of the inner sphere and the thermal conductivity, the dynamic viscosity, the specific heat at constant pressure and the coefficient of thermal expansion of the liquid hydrogen. An overview of all the parameters used is given by Table 5.3.
In case of the convection coefficient no information is given. The convection coefficient is a func-

tion of the tank diameter. It is therefore scaled by ratio using the coefficient and the diameter of the previously discussed example problem. The result is a convection coefficient of 14.4 $W/m^2 \cdot K$.

Table 5.3: Overview of the parameters used for validation

Parameter	Value	Unit
Inner Diameter	1.254	m
Outer Diameter	1.524	m
Inner Surface Area	4.94	m^2
Ambient Temperature	295	K
Inner Temperature	20	K
Average Tank level (Perlite)	81	%
Average Tank level (Glass)	82	%
Average Vacuum level	< 0.13	Pa
Convection Coefficient	14.4	$W/m^2 \cdot K$
Thermal Conductivity Perlite	0.001	$W/m \cdot K$
Thermal Conductivity Glass	0.00071	$W/m \cdot K$
Thermal Conductivity Liquid Hydrogen	0.103	$w/m \cdot K$
Thermal Conductivity Gaseous Hydrogen	0.1897	$w/m \cdot K$
Dynamic viscosity Liquid Hydrogen	$1.3 \cdot 10^{-5}$	$Pa \cdot s$
Specific Heat at constant Pressure	969	$J/kg \cdot K$
Coefficient of Thermal Expansion	0.01658	1/K
Latent Heat of Vaporization	$4.4559 \cdot 10^5$	J/kg

With all the required parameters collected, the rate of heat transfer to the hydrogen and the boil-off of the hydrogen are calculated for both insulation materials. The results are compared to the results of the experiment in Table 5.4.

Table 5.4: Heat transfer rate and boil-off rate of hydrogen for perlite and glass microsphere insulation

	Material	Experiment	Model	Difference
Heat trasfer rate [W]	Perlite	12.6	12.215	-3.1%
Boil-off rate [kg/s]		$2.83 \cdot 10^{-5}$	$2.74 \cdot 10^{-5}$	
Heat trasfer rate [W]	Glass	8.3	8.673	+4.4%
Boil-off rate [kg/s]		$1.86 \cdot 10^{-5}$	$1.95 \cdot 10^{-5}$	

As can be seen from the table above, there is a slight difference between the results. As the external convection coefficient is unknown, this may be part of the slight difference. Furthermore, the tanks in the experiment have additional pipes, lines and sensors attached to the tank and going through the insulation. This will result in additional heat leaked into the tank and is not taken into account in the model in this case. In case of the Flying-V fuel tank a 30% margin is included to take into account the additional heat flow into the tank through the piping, support and other equipment, as advised by Verstraete [3]. All in all, the differences are deemed low enough and it is concluded the model is valid.

5.2. FLIGHT PERFORMANCE ANALYSIS

This section presents the validation of the flight performance analysis. The validation uses payload-range data of a Boeing 747-400 as reported by Maniaci [14].

Maniaci discusses the relative performance of a commercial transport aircraft fuelled by liquid hydrogen, called the LH2-400. The performance is relative to an energy equivalent Boeing 747-400. To

analyse the mission performance of the LH2-400 and compare it to the mission performance of a Boeing 747-400 Maniaci first validates his performance analysis of the Boeing 747-400 with payload-range data of the Boeing 747-400. The payload-range diagram of a Boeing 747-400 is depicted by Figure 5.3. The 'x' marks represent the values calculated by Maniaci [14].

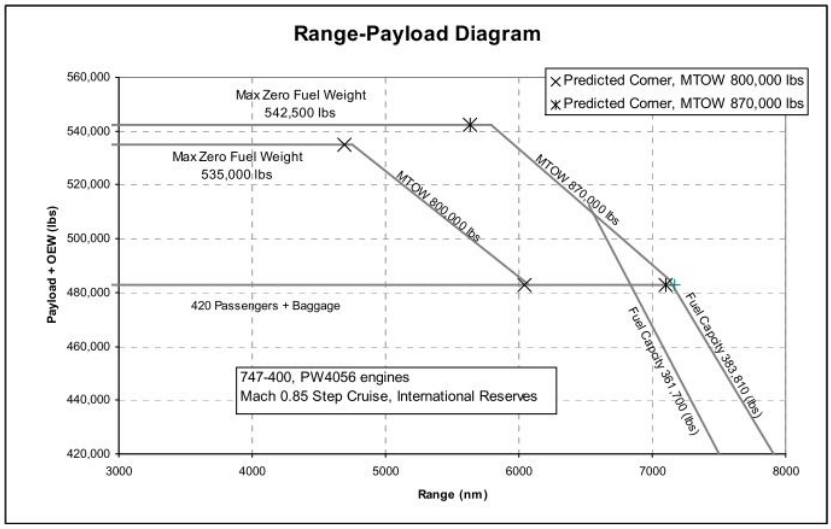

Figure 5.3: Payload-Range diagram for Boeing 747-400 [14]

According to Maniaci the bottom left marker, i.e. 800,000 lbs maximum take-off weight and 420 passenger plus baggage payload, is the main point of interest. For this point, the prediction made by Maniaci has a difference of 0.6% in range to the range given by the data. Therefore it is concluded by Maniaci that the mission performance analysis is acceptable.

The parameters used by Maniaci to arrive at the point mentioned above are used as inputs to the flight performance analysis of this research. That is, using a different model than Maniaci, but with the same input parameters to see if it arrives at the same point.

5.2.1. INTERNATIONAL STANDARD RESERVES

Before comparing to the Boeing payload-range data a couple of unknowns have to be sorted out. The first unknown is regarding the reserve fuel. The fuel carried by the Boeing 747-400 takes into account a reserve for a possible diversion and loiter phase. According to Maniaci, the reserve fuel required is based on the Standard International Reserves which are presented by Torenbeek [46]. The Standard International Reserves for diversion and loiter for this type of aircraft are 200 nautical miles and 30 minutes, respectively. These values are used for the flight performance analysis of this research as well.

5.2.2. RANGE OF CLIMB AND DESCENT PHASES

The second unknown is regarding the climb and descent phases. The range presented by the Boeing payload-range data is a sum of the climb, cruise and descent phases of the mission. The analysis in this research only presents the range of the cruise phase and the actual ranges of the climb and descent phases are not given by Maniaci.

An assumption is made regarding the contribution of the climb and descent phases to the total range by using aircraft performance parameters presented by Sun et al. [15]. Sun et al. present WRAP: An open-source kinematic aircraft performance model. The model uses data mining methods as well as maximum likelihood estimations on open access flight data from Automatic Depen-

dent Surveillance-Broadcast (ADS-B) to extract accurate aircraft performance parameters. More than thirty parameters from seven different flight phases are obtained for several different commercial aircraft. [15] An example of the performance parameters is depicted in Figure 5.4. In case of this example the data is of an Airbus A320.

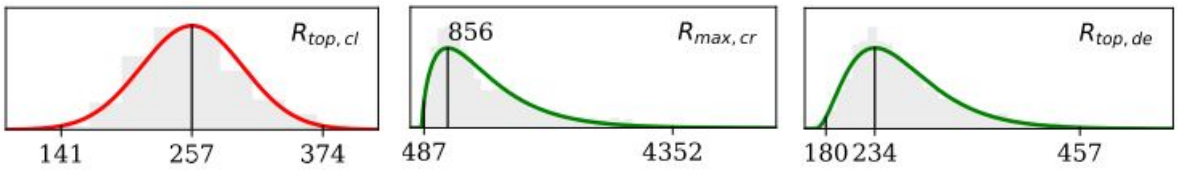

(a) Climb range (km) (b) Cruise range (km) (c) Descent range (km)

Figure 5.4: Examples of the performance parameters (A320) as presented by Sun et al. [15]

The aircraft treated by Sun et al. also included the Boeing 747-400. As can be seen by the example presented above, the collected data behaves like distributions. Therefore Sun et al. present the minimum (min), optimum (opt) and maximum (max) values of the different parameters in accompanying open access data files. The optimum and the maximum climb and descent ranges for the Boeing 747-400 are presented in Table 5.5. These ranges are added to the cruise range resulting from the flight performance analysis to get the total range used in this validation process.

Table 5.5: Climb and descent ranges Boeing 747-400 [15]

Range	**Climb**	**Descent**
Optimum	223 km	262 km
Maximum	374 km	510 km

5.2.3. PRELIMINARY RESULTS

With the assumptions made regarding the fuel reserves and the climb and descent ranges, the parameters used by Maniaci are used as inputs for the flight performance analysis. An overview of all the parameters used and the resulting range is given in Table 5.6. The ranges is given as an "optimum" and a "maximum". This corresponds to the climb and descent ranges from table 5.5 that are added to the cruise range calculated by the model.

Table 5.6: Preliminary flight performance results Boeing 747-400

Parameter	**Value**	
Take-off weight	363 ton	
Operating empty weight	179 ton	
Payload weight	40 ton	
Fuel weight	144 ton	
L/D	19.0	
SFC	$1.65 \cdot 10^{-5}$ kg/sN	
Ranges	**B747-400**	**Model**
Optimum	6077 nm	5505.45 nm (-9.4%)
Maximum	6077 nm	5720.9 nm (-5.9%)

One can see there is a difference of 9.4% and 5.9% when using the optimum climb and descent ranges or the maximum climb and descent ranges, respectively. The main assumptions made in the flight performance analysis of the model is the use of fuel fractions. It is concluded the differences

are significant and the fuel fractions used are not the right ones for this these types of long range aircraft. Therefore the fuel fractions will be adjusted to better represent the fuel used during non intensive phases compared to the intensive phases.

5.2.4. ADJUSTING FUEL FRACTIONS

With the ranges of long range aircraft increasing over the years, it is deemed necessary to adjust the fuel fractions as defined by Roskam all those years ago. This is because the part of the fuel burned during the non intensive phases relative to the fuel burned during cruise is decreasing. Therefore the fuel fractions given by Table 4.5 are adjusted slightly. Furthermore, the overshoot phase is deemed unnecessary and unconventional, i.e. the overshoot phase is no longer used. The new fuel fractions are given by Table 5.7.

Table 5.7: Adjusted fuel fractions

Flight Phase	$\mathbf{M}_{ff}$	**New** $\mathbf{M}_{ff}$
Warm-up	0.995	0.997
Taxi	0.99	0.992
Take-off	0.995	0.995
Climb	0.98	0.98
Descent	0.99	0.99
Land & Taxi	0.992	0.994
Reserve Climb	0.98	0.99

With the adjusted fuel fractions the ranges of the Boeing 747-400 are calculated again and are presented in Table 5.8. One can see the differences are lower. It is concluded the model is now accurate enough and is deemed valid.

Table 5.8: Flight performance results Boeing 747-400 after adjusting fuel fractions

Ranges	**B747-400**	**Model**
Optimum	6077 nm	6089.4 nm (+0.2%)
Maximum	6077 nm	6304.86 nm (+3.6%)

6

Results and Discussion

This chapter presents the results of the liquid hydrogen fuel tank design for the Flying-V. First, the fuel tank performance is presented and the influence of the design of the fuel tank on its performance is discussed. Next, three different configurations of the Flying-V are presented. With these configurations the fuel volume and cargo volume are varied. For each of these configurations two case studies are discussed. One where the integration of a cryogenic fuel tank is treated as a retrofit and one where the structure is iterated to take into account the lower fuel weight. Finally, a liquid hydrogen based Flying-V is compared to a kerosene based Flying-V in terms of mission performance. All the inputs used to produce the results presented in this chapter can be found in Appendix A.

6.1. Hydrogen Fuel Tank Performance

This section presents the resulting parameters of the mechanical and thermal design of a liquid hydrogen fuel tank for the Flying-V. With these parameters the influence on the performance of the fuel tank is assessed. The parameters include the boil-off rate of the liquid hydrogen, available fuel volume, empty tank weight, full tank weight, gravimetric storage density and the pressure rise during cruise. These parameters are given as a function of the venting pressure and the insulation thickness by Figure 6.1 to Figure 6.8. The effects of the venting pressure and the insulation thickness are of interest here. These figures are an example of a possible fuel tank design, in this case labeled as "Configuration 1". The tank is depicted in Figure 6.17, using the optimized parametrization by Oosterom [19] for the OML. One should note that these parameters (except for the range) are for a single fuel tank, i.e only one side of the Flying-V.

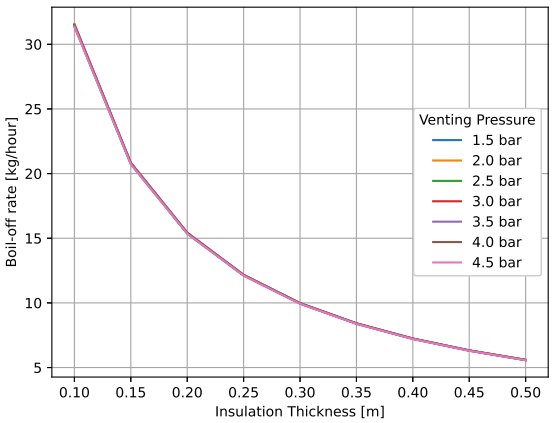

Figure 6.1: Boil-off rate

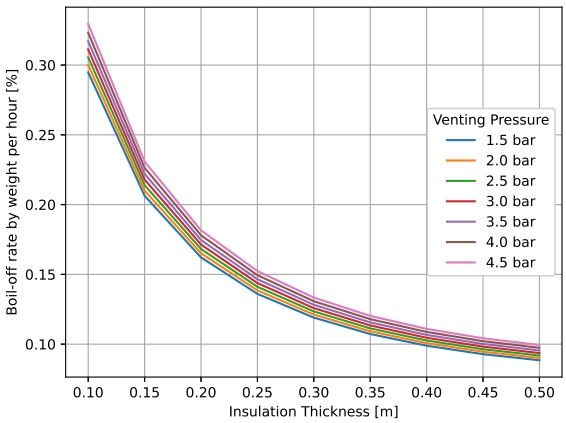

Figure 6.2: Boil-off rate by weight per hour

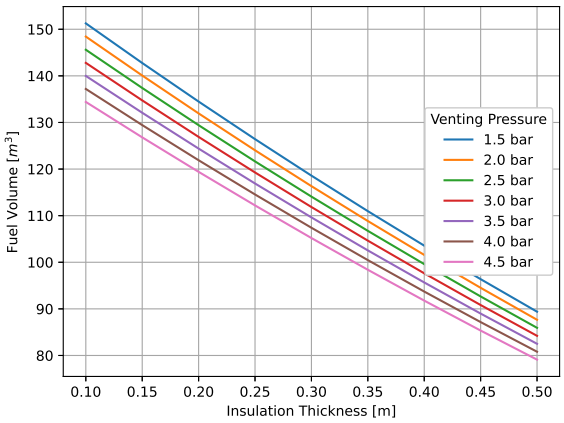

Figure 6.3: Available fuel volume

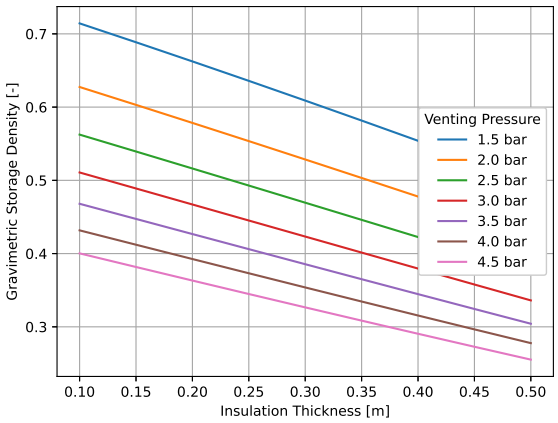

Figure 6.6: Gravimetric storage density

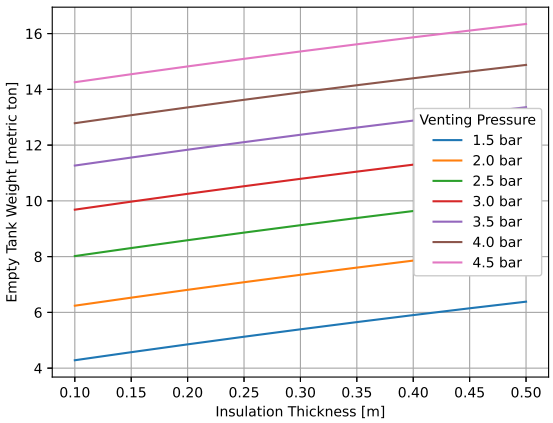

Figure 6.4: Empty tank weight

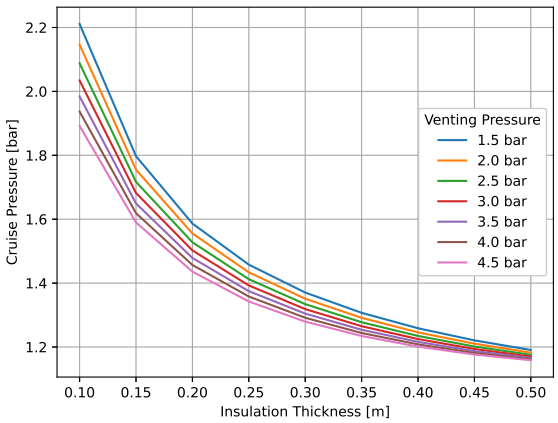

Figure 6.7: Tank pressure end of cruise phase

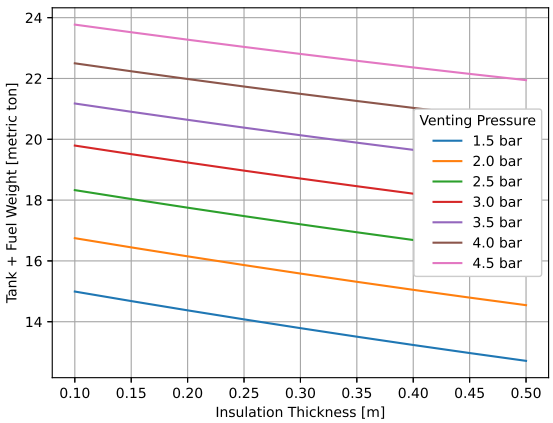

Figure 6.5: Filled tank weight

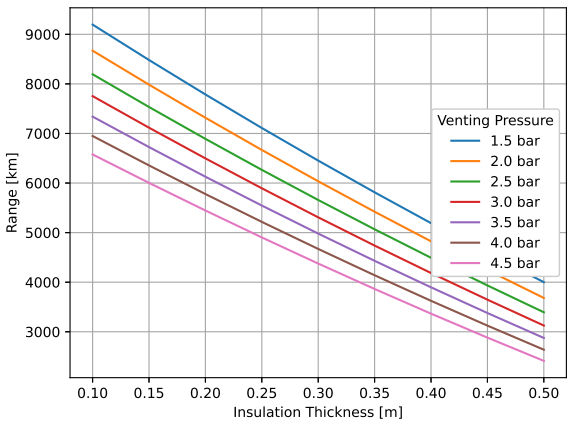

Figure 6.8: Cruise range

To start, there is the boil-off rate of the liquid hydrogen in kilogram per hour and the boil-off rate by weight per hour depicted by Figures 6.1 and 6.2. One can see that the boil-off rate slightly decreases with increasing venting pressure. The main influence of the venting pressure is on the tank wall thickness. As the thermal conductivity of the wall is insignificant the effect is insignificant. The venting pressure also has an effect on the liquid volume fraction, which decreases with increasing venting pressure. As it is easier for liquid to take up heat the thermal resistance of the liquid/gas mixture increases. This leads to a slightly lower heat transfer rate and a slightly lower boil-off rate. The boil-off rate decreases with increasing insulation as the insulation prevent heat leaking into the tank. Looking at the boil-off rate by weight, there is a bigger difference between the venting pressures. That is, due to the decreasing liquid volume fraction the average density of the fuel decreases. Therefore, with almost the same absolute boil-off and a lower weight, the boil-off rate by weight increases.
The available fuel volume is depicted by Figure 6.3. This is the volume of the fuel tank available for the liquid hydrogen fuel after taking into account the gas ullage and the additional volume allowances for expansion and contraction, trapped fuel etc. One can see that with increasing venting pressure and increasing insulation thickness the available fuel volume decreases. An increase in venting pressure decreases the liquid volume fraction of the tank that is allowed and an increase in insulation thickness decreases the actual internal volume. Taking into account that the OML of the Flying-V is kept constant, every increase in insulation thickness is on the inside of the fuel tank limiting the available volume.
Figures 6.4 and 6.5 depict the weight of the fuel tank structure and the weight of the tank filled with liquid hydrogen, respectively. It can be seen that the insulation has a small influence on the tank weight as the density of the insulation is low. The influence of the venting pressure is more significant. It is interesting to note that the empty tank weight increases with increasing insulation thickness, but the filled tank weight decreases slightly with increasing insulation thickness. This is due to the fuel volume drastically decreasing with increasing insulation thickness and the weight of the fuel itself being relatively low.
Figure 6.6 depicts the gravimetric storage density of the fuel tank. The gravimetric storage density, as given by Equation (4.36), is used as a figure of merit for the fuel tank design. With increasing venting pressure and increasing insulation thickness the gravimetric storage density decreases, as the tank weight increases and the available fuel volume decreases.
Finally, there are the pressure rise during cruise and the cruise range, depicted by Figure 6.7 and Figure 6.8, respectively. Regarding the pressure rise during cruise, first the pressure rise rate as given by Equation (4.5) is determined. Second, the cruise range is converted to the resulting cruise time using cruise speed and multiplied with the pressure rise rate. The resulting pressure rise or decline is added to the fill pressure of 1.2 bar. It can be seen that the pressure rise significantly decreases with increasing insulation thickness, as the fuel is better protected from heat leakage. Regarding the venting pressure, the pressure rise is lower due to the weight of the system increasing with increasing venting pressure. The available fuel volume is slightly decreased as well. The increase in weight and the decrease in available fuel leads to a lower range and therefore less time for the pressure to build. The range depicted by Figure 6.8 is the range with a minimum number of passengers, i.e. 250 passengers in triple class configuration.

The tank of "Configuration 1" presented above has a surface-to-volume ratio of 1.162. Figure 6.18 depicts a different tank design, labeled "Configuration 2". This tank is shorter and shifted forward into the thicker part of the wing to accommodate more cargo space. The surface-to-volume ratio of this tank is 1.133. Figure 6.9 to Figure 6.16 depict the same parameters as discussed above for this fuel tank design. The parameters for configuration 3 can be found in Appendix C

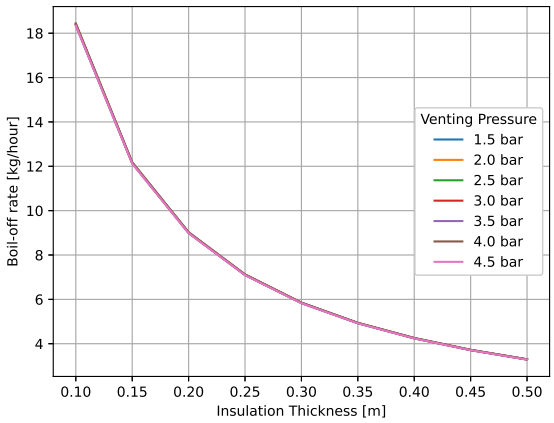

Figure 6.9: Boil-off rate

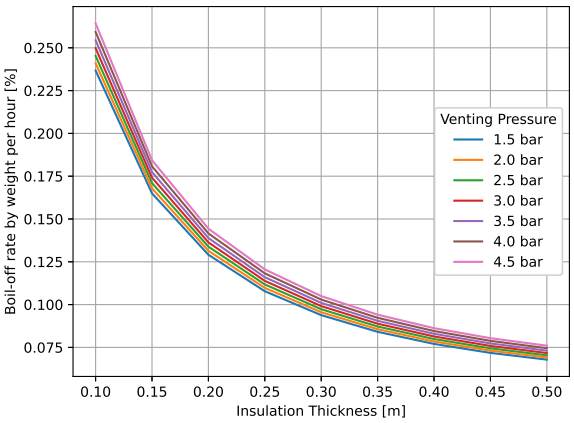

Figure 6.12: Boil-off rate by weight per hour

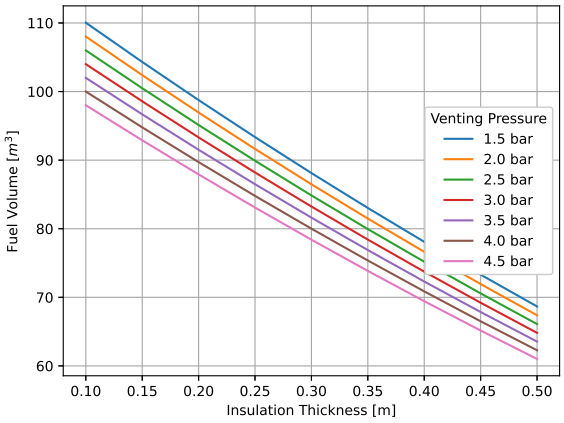

Figure 6.10: Available fuel volume

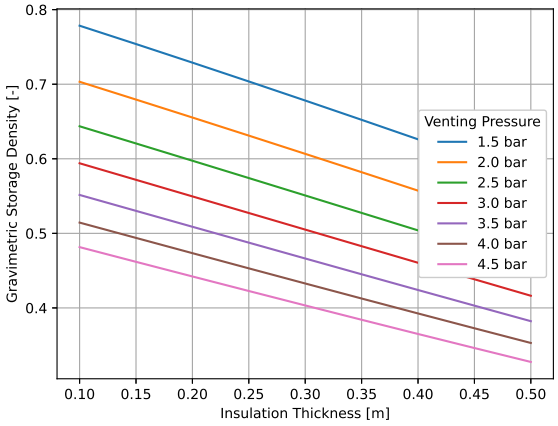

Figure 6.13: Gravimetric storage density

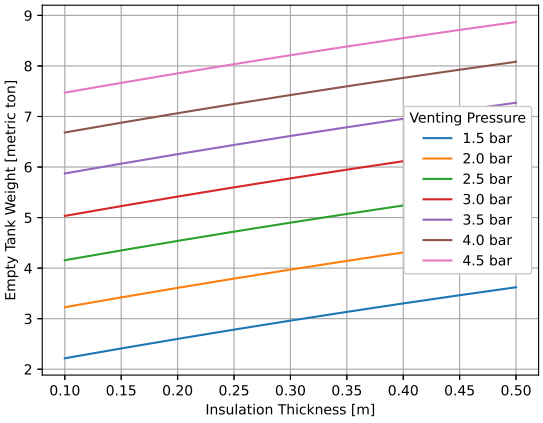

Figure 6.11: Empty tank weight

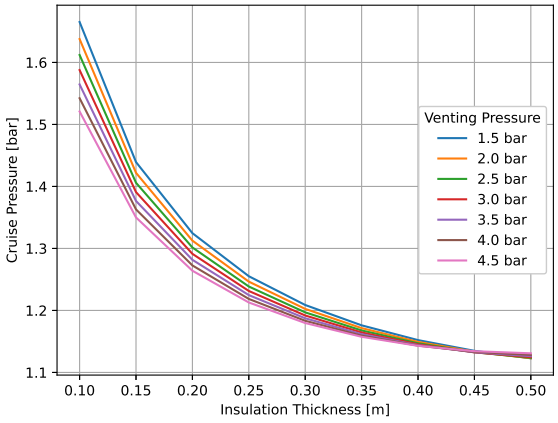

Figure 6.14: Tank pressure end of cruise phase

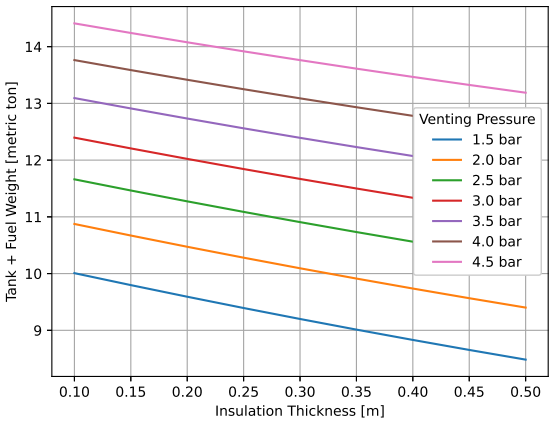

Figure 6.15: Filled tank weight

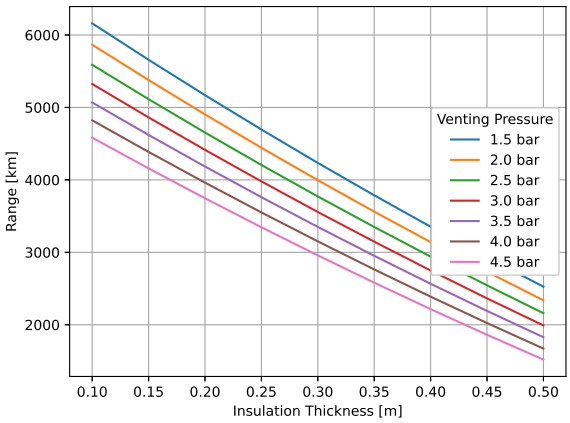

Figure 6.16: Cruise range

As expected the available fuel volume and the weight of the fuel tank are lower as the tank is smaller. The resulting range is lower due to the lower amount of fuel and the pressure rise is therefore lower as well. However, with a lower surface-to-volume ratio the surface area per unit of volume is lower leading to a more thermal efficient design. This is depicted by a lower boil-off rate and a lower boil-off rate by weight per hour. The gravimetric storage density is higher for this configuration. That is, regarding the weight of the system, this configuration has a higher figure of merit. It can be concluded that using the tapered part of the wing with a lower thickness is not the most efficient for a liquid hydrogen fuel tank.

6.2. CONFIGURATION AND CASE STUDIES

For this research different configurations of a liquid hydrogen Flying-V are analyzed. Next to different configurations two different case studies are analyzed. The case studies, discussed in Section 4.6.1, consider a retrofit design and an iteration of the structure. The configurations are presented in this section.

Three different configurations are analyzed, each with a different combination of fuel and cargo volume. The configurations take into account different number of passengers. The maximum number of passengers is set equal to 440 seated in a single economy class. This number is based on the Flying-V having 8 type A doors, allowing 440 passengers. The design number of passengers is adopted from Oosterom [19], which is 328 passengers divided over business class and economy class. The minimum number of passengers is set to 250 seated in a triple class configuration. This number of passengers follows from the available floor area and a passenger density ratio (PDR) for a triple class configuration (0.91 pax/m^2) taken from Baan [47]. This will be discussed in more detail in the subsection of configuration 1.

BASELINE KEROSENE FLYING-V

As a baseline a kerosene based Flying-V is used to compare with the performance of the liquid hydrogen based Flying-V. The input parameters for the parametrization used in this research are from the optimized FV-900 from Oosterom [19]. The baseline kerosene based Flying-V used is therefore the same optimized Flying-V. More specifically, the family optimisation with commonality constraints of the FV-900, the FV-900 FO-F, is used. The main design parameters and key characteristics of the FV-900 FO-F are given by Table 6.1. The complete set of input parameters for the FV-900 FO-F can be found in Appendix A. The following configurations all use the same input parameters.

Table 6.1: Main design parameters and key charactersitics FV-900 FO-F [19]

Parameter	Unit	FV-900 FO-F
L_1	m	24.0
L_3	m	11.0
b_{outer}	m	14.75
b_{total}	m	60.7
W_{H_1}	m	6.2
W_{H_3}	m	5.8
$MTOW$	t	234
L/D	-	21.6

CONFIGURATION 1

Configuration 1 is designed to have a large fuel tank and a minimal cargo volume. The fuel tank fills almost the entire tapered section of the wing. The cargo space is moved in front of the fuel tank into the cabin area. Configuration 1 is depicted in Figure 6.17. The cargo containers selected for this configuration are two LD-9s and two LD-3s, split over the two sides of the aircraft. The floor area of the constant cross-section part of the Flying-V is determined and the cargo area is subtracted. Using a PDR for a single class results in 446 passengers, i.e. the aforementioned 440 passengers fit and are selected. Following, the cargo volume is determined to determine the luggage weight. From this follows the available luggage weight per passenger. This is done for the case with 328 passengers and for the case with 250 passengers as well. One should note the luggage weight per passenger is capped at 40 lbs, as this is a conventionally used estimation, even if there is more volume available. Details about the passengers and the luggage is given by Table 6.2.

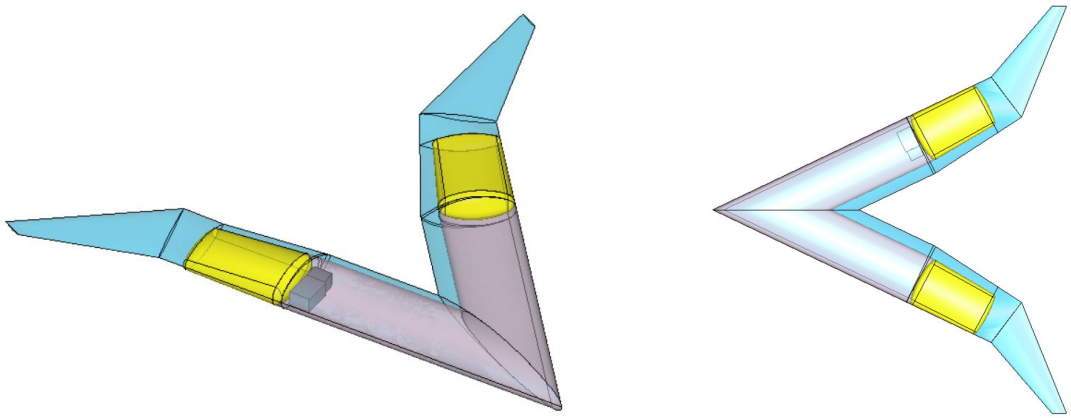

(a) Isometric view (b) Top view

Figure 6.17: Liquid hydrogen Flying-V configuration 1

Table 6.2: Available passenger area and available luggage capacity per passenger

Parameter	Value
Floor area cabin	296 m^2
Area passenger cabin	275.66 m^2
Cargo volume	33.08 m^3
Luggage density	161 kg/m^3
Luggage 440 pax.	26 lbs/pax.
Luggage 328 pax.	35 lbs/pax
Luggage 250 pax.	40 lbs/pax

Next the case studies are performed. For this configuration the fuel tank venting pressure selected is 1.75 bar. The insulation thickness is set at 0.16 m. The tank performance is presented in Table 6.6. The results of the flight performance analysis for both case studies is presented in Table 6.7 and Table 6.8.

CONFIGURATION 2

Configuration 2 is designed to have a cargo volume sufficient for the maximum number of passengers and their luggage. The fuel tank is smaller compared to configuration 1 and is moved forward into the thicker part of the wing. The cargo space is moved behind the fuel tank into the narrower part of the wing. Configuration 2 is depicted in Figure 6.18. The cargo containers selected for this configuration are eight LD-4-45s and four LD-4s, split over the two sides of the aircraft. The LD-4-45 is a LD-4 container but with a reduced height to 45 inches. These container were introduced in the research of Oosterom [19]. The floor area of the passenger cabin is larger than that of configuration 1, as the cargo area is moved. Therefore 440 passengers are assumed to fit. Following, the cargo volume is determined to determine the luggage weight. From this follows the available luggage weight per passenger. This is done for the case with 328 passengers and for the case with 250 passengers as well. Again, the luggage weight per passenger is capped at 40 lbs. Details about the passengers and the luggage is given by Table 6.3.

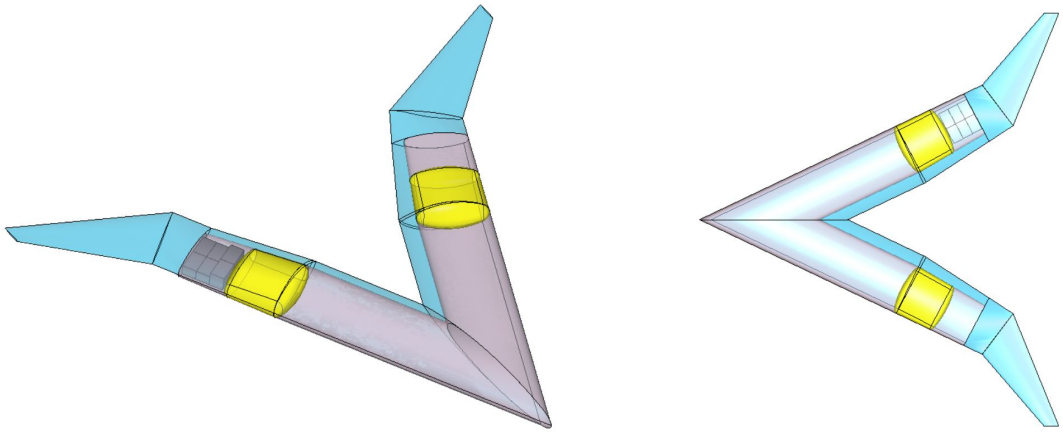

(a) Isometric view (b) Top view

Figure 6.18: Liquid hydrogen Flying-V configuration 2

Table 6.3: Available passenger area and available luggage capacity per passenger

Parameter	**Value**
Area passenger cabin	287 m^2
Cargo volume	58.36 m^3
Luggage density	161 kg/m^3
Luggage 440 pax.	40 lbs/pax.
Luggage 328 pax.	40 lbs/pax
Luggage 250 pax.	40 lbs/pax

Next the case studies are performed. For this configuration the fuel tank venting pressure selected is 1.75 bar. The insulation thickness is set at 0.13 m. The tank performance is presented in Table 6.6. The results of the flight performance analysis for both case studies is presented in Table 6.7 and Table 6.8.

CONFIGURATION 3

Configuration 3 is designed to have a cargo volume sufficient for the design number of passengers and their luggage. The fuel tank is larger compared to configuration 2. The cargo space is moved behind the fuel tank into the narrower part of the wing. Configuration 3 is depicted in Figure 6.19. The cargo containers selected for this configuration are ten LD-4-45s, split over the two sides of the aircraft. The floor area of the passenger cabin is larger than that of configuration 1, as the cargo area is moved. Therefore 440 passengers are assumed to fit. Following, the cargo volume is determined to determine the luggage weight. From this follows the available luggage weight per passenger. This is done for the case with 328 passengers and for the case with 250 passengers as well. Again, the luggage weight per passenger is capped at 40 lbs. Details about the passengers and the luggage is given by Table 6.4.

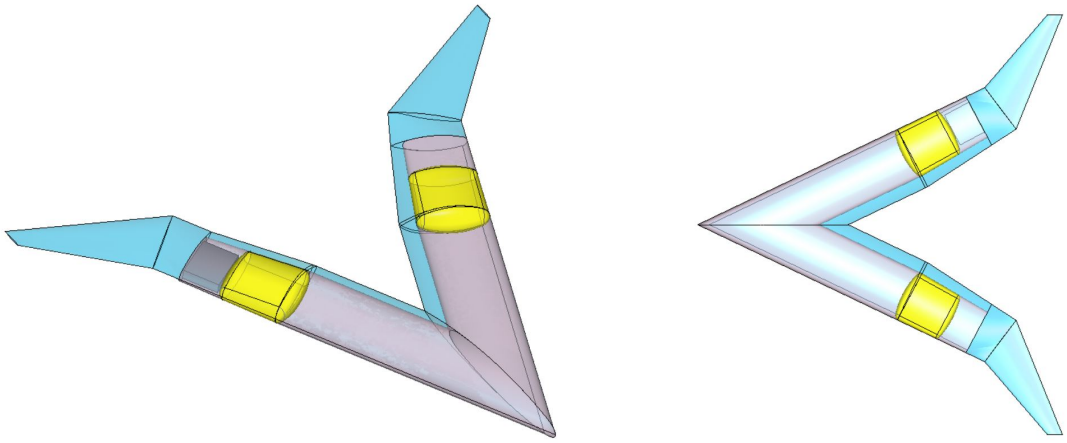

(a) Isometric view

(b) Top view

Figure 6.19: Liquid hydrogen Flying-V configuration 3

Table 6.4: Available passenger area and available luggage capacity per passenger

Parameter	**Value**
Area passenger cabin	287 m^2
Cargo volume	42.6 m^3
Luggage density	161 kg/m^3
Luggage 440 pax.	34 lbs/pax.
Luggage 328 pax.	40 lbs/pax
Luggage 250 pax.	40 lbs/pax

Next the case studies are performed. For this configuration the fuel tank venting pressure selected is 1.75 bar. The insulation thickness is set at 0.13 m. The tank performance is presented in Table 6.6. The results of the flight performance analysis for both case studies is presented in Table 6.7 and Table 6.8.

6.2.1. INTERNAL VOLUME USAGE

The baseline Flying-V and the liquid hydrogen configurations have the same OML and therefore the same internal volume of 1900 m^3. However, the internal volume is used differently by the different configurations. The hydrogen configurations require a relatively large volume for the fuel tanks, usually at the expense of the cargo volume and a portion of the passenger cabin. For the baseline the fuel volume is distributed next to the cabin near the TE and in the outer wing. This does not

take up volume of the passenger cabin or the cargo space. The internal volume distributions of the different configurations and the baseline Flying-V are depicted by Figure 6.20.

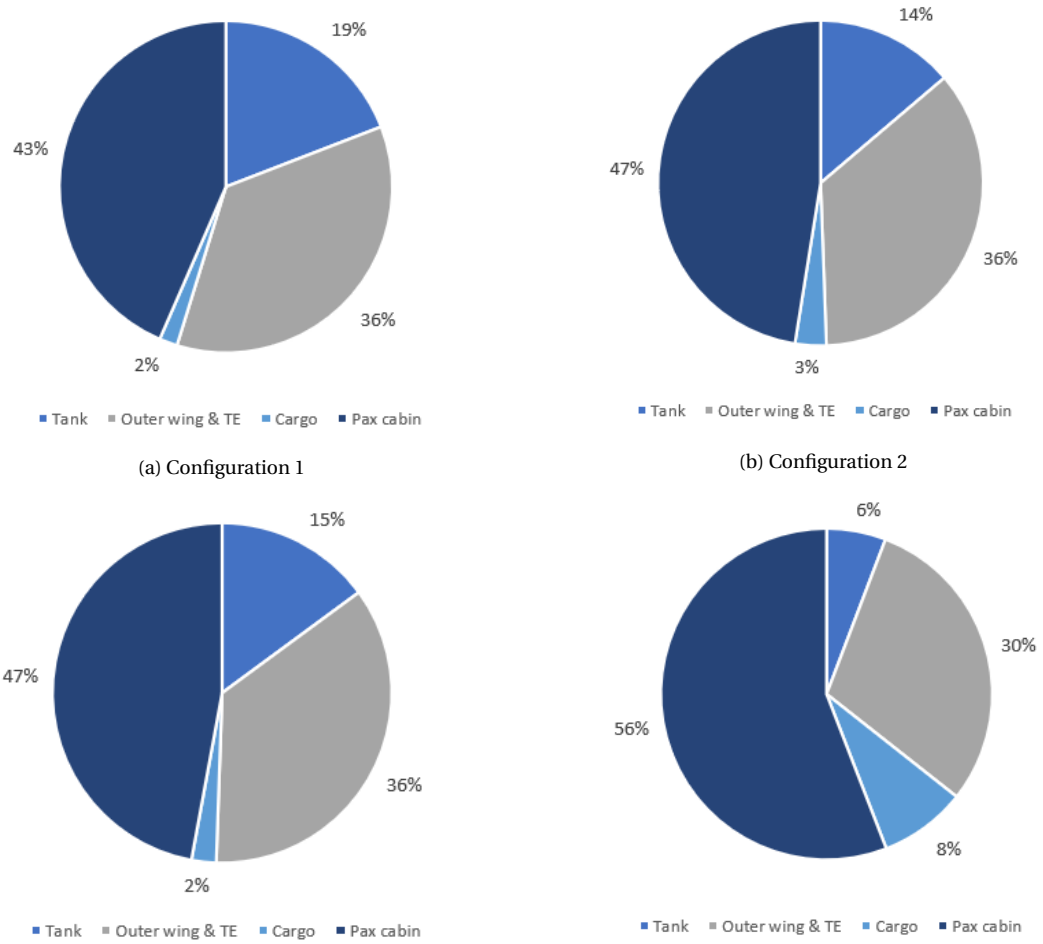

(a) Configuration 1

(b) Configuration 2

(c) Configuration 3

(d) Baseline FV-900 FO-F

Figure 6.20: Internal volume distributions of the different configurations and the baseline Flying-V

Regarding the floor space available for the passengers one could compare the PDR of the different configurations. These PDR are given by Table 6.5. From these ratios it can also be seen that the hydrogen configuration result in less space for the passengers as there are more passengers per square meter.

Table 6.5: PDR of the hydrogen configurations and baseline Flying-V

	Conf. 1	**Conf. 2**	**Conf. 3**	**FV-900 FO-F**
Floor area [m^2]	276	287	287	296
PDR [pax/m^2] with n_{pax}				
440 pax	1.6	1.53	1.53	1.49
328 pax	1.19	1.14	1.14	1.11
250 pax	0.91	0.87	0.87	0.84

6.2.2. FLIGHT PERFORMANCE BASELINE FLYING-V

The results of the flight performance analysis are compared to the flight performance results by Oosterom in Figure 6.21.

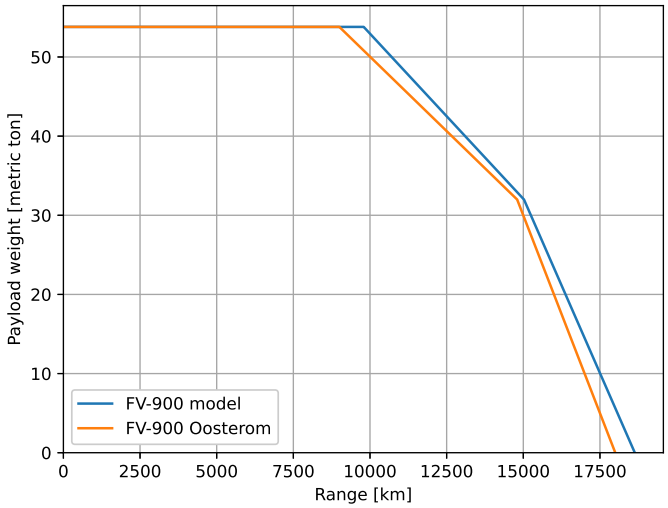

Figure 6.21: Payload-range diagram for the FV-900 FO-F

It can be seen that there is a slight overestimation by the model of this research. This difference is mainly caused by a difference in the fuel fractions. As discussed in Section 5.2.4, the fuel fractions used in this research were adjusted to better fit the Boeing payload-range data. All the fuel fractions used by Oosterom are lower compared to the fuel fractions used in this research.

The flight performance analysis by Oosterom takes into account a 5% fuel reserve [19]. The flight performance analysis in this research takes into account a fuel reserve for a 200 nm diversion and 30 minutes of loiter. To be able to compare the payload-range data of the kerosene based Flying-V to the payload-range data of the liquid hydrogen based Flying-V the international reserves for diversion and loiter are used. Furthermore, all the passengers are able to carry 40 lbs of luggage. The payload-range diagram of the FV-900 FO-F taking into account reserves for diversion and loiter is depicted in Figure 6.22.

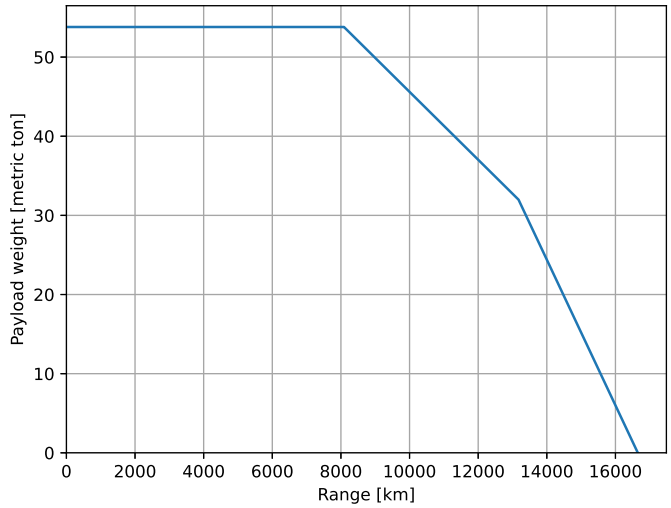

Figure 6.22: Payload-range diagram for the FV-900 FO-F taking into account diversion and loiter

6.3. COMPARISON OF RESULTS

This section presents the results of the different configuration and case study analysis. First the fuel tank performance is presented in Table 6.6. Next, the flight performance analysis results for case 1 are presented in Table 6.7 followed by the payload-range diagrams. Finally, the flight performance analysis results for case 2 are presented in Table 6.8 followed by the payload-range diagrams.

The fuel tank performance in the previous section is presented for a range of venting pressures and insulation thicknesses. The results for the different configurations are for one combination of venting pressure and insulation thickness. To determine the combination of venting pressure and insulation thickness the boil-off rate by weight per hour and the pressure rise during cruise of the fuel tank are examined. As a top level requirement the tank design should aim for a boil-off rate of 0.2% by weight per hour. Furthermore, the fuel volume should be maximized and the fuel system weight should be minimized. Therefore the lowest possible venting pressure and the lowest possible insulation thickness are selected. The minimum insulation thickness follows from the boil-off rate by weight per hour equal to 0.2%. This gives a combination of venting pressure and insulation thickness. This combination is cross-referenced with the pressure at the end of the cruise phase. This pressure should be higher than the selected venting pressure to prevent venting of fuel. If not, the combination of venting pressure and insulation thickness is changed, while respecting the boil-off rate of 0.2% by weight per hour and is checked again with the pressure rise. This process is repeated until a suitable combination of venting pressure and insulation thickness is found. The fuel tank performance for the different configurations is presented in Table 6.6.

Table 6.6: Overview of the tank performance for the different configurations

Parameter	**Conf.1**	**Conf. 2**	**Conf. 3**
Offset [m]	0	5.6	4.9
Length01 [m]	10.0	11.0	11.0
Surface/Volume [m^2/m^3]	1.162	1.133	1.124
Venting pressure [bar]	1.75	1.75	1.75
Insulation thickness [m]	0.16	0.13	0.13
Boil-off rate [kg/hr]	39.0	28.2	31.6
Tank weight [t]	11.2	5.7	6.4
Fuel weight [t]	19.8	15.0	16.2
Fuel volume [m^3]	280	211	228
Total weight [t]	31.1	20.7	22.6
Gravimetric storage density [-]	0.64	0.72	0.72

The fuel tanks of the different configurations presented in the table above all have the same selected venting pressure and almost the same insulation thickness. The main difference in the design are the dimensions of the tanks. It can be seen that there are significant differences in the fuel volume and the weight. The largest tank, configuration 1, does not seem to be the most efficient tank design. The absolute heat leak is the largest, but this is to be expected with the largest surface area for heat to transfer. Furthermore, the gravimetric storage density is the lowest and increases with decreasing volume.

In this research the tank is increased in volume by expanding the fuel tank into the tapered part of the wing. This increases the tank volume, but also increase the tank structure weight even more, due to the larger curvature. This is detrimental for the gravimetric storage density.

FLIGHT PERFORMANCE CASE 1: RETROFIT

Table 6.7: Flight performance analysis results for case 1: Retrofit, plus the kerosene based FV-900

	Conf. 1	**Conf. 2**	**Conf. 3**	**FV-900**
MTOW [t]	234	234	234	234
OEW [t]	126	120	121	115
Max payload [t]	89	99	97	53.8
Max payload range [km]	4800	2700	3200	7600
Range [km] with n_{pax} (PREE [-])				
440 pax	7000 (1.41)	4700 (1.42)	5400 (1.42)	10800 (1.31)
328 pax	7600 (1.18)	5200 (1.16)	5900 (1.18)	13200 (1.16)
250 pax	8100 (0.95)	5700 (0.94)	6400 (0.97)	16700 (0.98)

The first case study is regarding a retrofit of an existing Flying-V with a set of hydrogen fuel tanks. The first aspect to notice is the increase in operating empty weight compared to the FV-900. The operating empty weight is increased up to 8.7% for configuration 1. As it is a retrofit, the only difference is the fuel system, which is heavier for liquid hydrogen. This is as expected. On the other hand, the fuel weight of liquid hydrogen is significantly lower compared to kerosene. This can be seen by looking at the maximum payload weight. As shown by Equation (4.38), the maximum payload weight is the weight theoretically still available due to the decrease in fuel weight when changing kerosene for liquid hydrogen. One should note that for the hydrogen configurations this is still with a full fuel tank. The maximum payload given for the FV-900 is a design maximum payload weight, selected by Oosterom, with a reduced fuel load.

Looking at the range for comparison there are a few options. Making sure every number of passengers can carry the conventional luggage weight, the FV-900 should be compared to configuration 2. In this case the range of configuration 2 is significantly lower than the FV-900. That is, 56%, 61% and 66% lower for 440, 328 and 250 passengers, respectively. However, the PREE are more or less the same, i.e. the work done per unit of energy consumed is the same. For the design number of passengers, 328, Configuration 3 has enough cargo space to carry the normal luggage load. In this case the range is increased a bit, but still a difference of 55% compared to the FV-900. In case of the largest hydrogen fuel volume, configuration 1, the ranges are of course the closest to the FV-900. Comparing configuration 1 to the other configurations the range is increased significantly, but it is still less than the FV-900. That is, 35%, 42% and 51% lower for 440, 328 and 250 passengers, respectively. In terms of the PREE, these are higher. This is mainly explained by the fact that the passengers in configuration 1 cannot carry the normal luggage weight, i.e. the payload weight is lower.

The payload-range diagrams for configuration 1 to 3 are depicted in the following figures. The payload-range diagram of the FV-900 FO-F is imposed as well. Here one can again see the significant difference in range between the hydrogen and the kerosene aircraft.

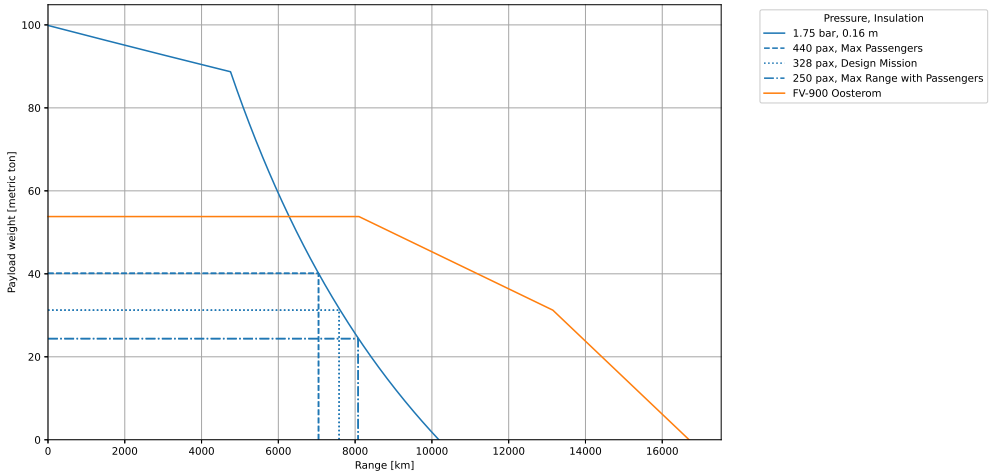

Figure 6.23: Payload-range diagram case 1, configuration 1

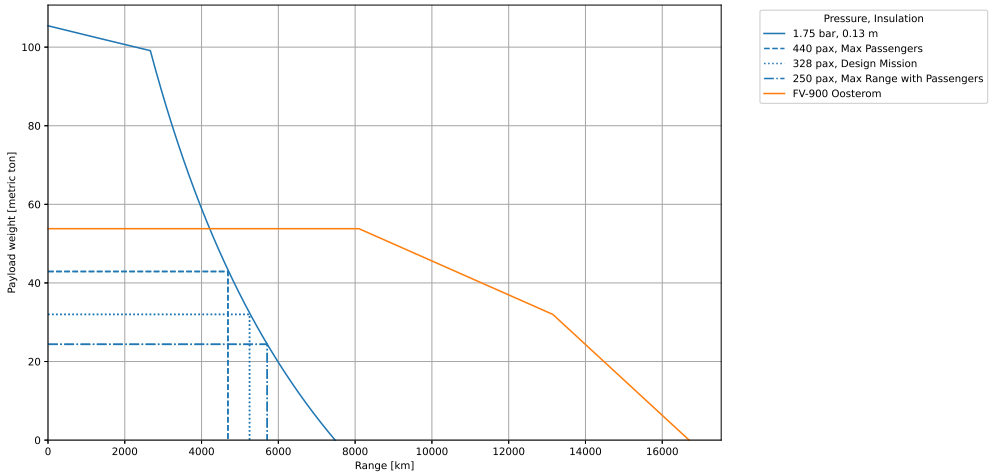

Figure 6.24: Payload-range diagram case 1, configuration 2

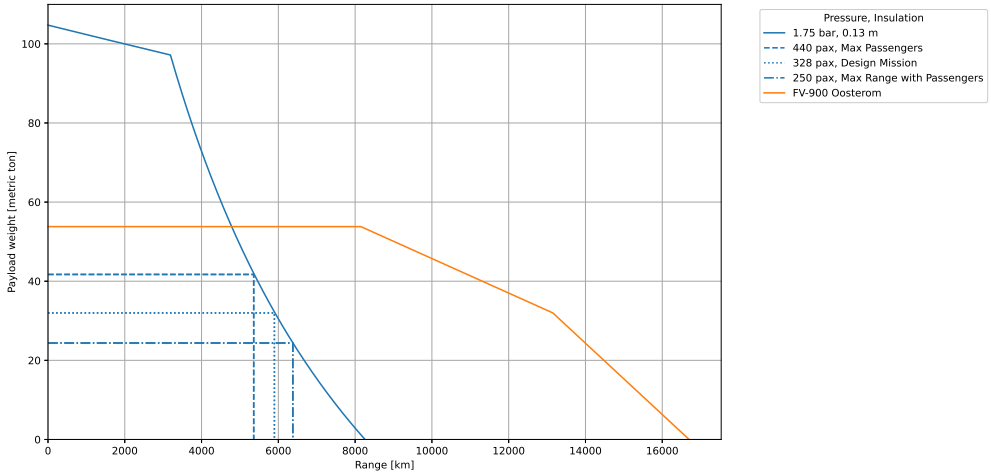

Figure 6.25: Payload-range diagram case 1, configuration 3

FLIGHT PERFORMANCE CASE 2: ITERATION

In case of the second case study, where the take-off weight will be lower compared to a kerosene based Flying-V, the wing loading is reduced. To be able to fly at the same cruise speed and lift-to-drag ratio the cruise altitude is increased to a cruise altitude of 13,000 meters, an increase of 2,000 meters compared to the kerosene based Flying-V.

Table 6.8: Flight performance analysis results for case 2: Iteration, plus the kerosene based FV-900

	Conf. 1	**Conf. 2**	**Conf. 3**	**FV-900**
MTOW [t]	159	147	148	234
OEW [t]	99	89	90	115
Range [km] with n_{pax} (PREE [-])				
440 pax	8900 (1.73)	6500 (1.87)	7300 (1.85)	10800 (1.31)
328 pax	10200 (1.52)	7900 (1.64)	8600 (1.64)	13200 (1.16)
250 pax	11400 (1.31)	9100 (1.44)	9800 (1.41)	16700 (0.98)

The second case study is regarding an iteration of the structure to take into account the aforementioned portion of the MTOW that is not used. Although the fuel system is heavier, the fuel itself is significantly lower in weight. Therefore the structure carries a lower load and can be lower in weight itself. A significant decrease can be noticed in the take-off weight. Compared to the MTOW of the FV-900 the take-off weight is reduced by 32%, 37% and 37% for configuration 1 to 3, respectively. The OEW is reduced by 14%, 23% and 22% for configuration 1 to 3, respectively.

Comparing the range there are a few options again, as discussed for case 1. Comparing the FV-900 to configuration 2, i.e. every number of passengers can carry the conventional luggage weight, the range is significantly lower again. However, compared to case 1 they are increased. Relative to the FV-900 the ranges are 40%, 40% and 46% lower for 440, 328 and 250 passengers, respectively. Again, looking at the design number of passengers in configuration 3, the range is increased with respect to configuration 2 and is only 35% lower compared to the FV-900. In case of the largest hydrogen fuel volume, configuration 1, the ranges are of course the closest to the FV-900. Comparing configuration 1 to the other configurations the range is increased significantly, but it is still less than the FV-900. That is, 18%, 23% and 32% lower for 440, 328 and 250 passengers, respectively. These ranges are close, but one has to take into account that the passengers cannot carry the normal luggage weight and the take-off weight is reduced by 32%, as a result of the structure weight iteration, for these ranges to happen.

The payload-range diagrams for configuration 1 to 3 are depicted in the following figures. The payload-range diagram of the FV-900 FO-F is imposed as well. Here one can again see the difference in range between the hydrogen and the kerosene aircraft, although this difference is less compared to case 1.

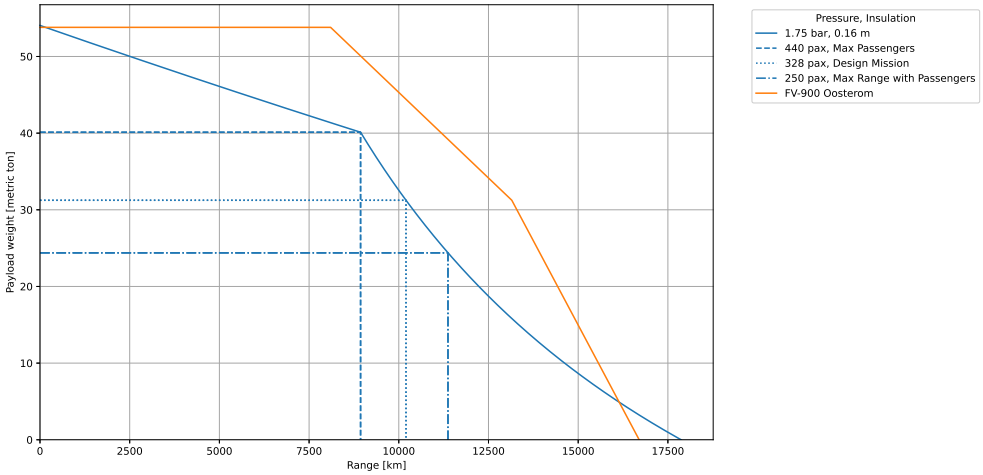

Figure 6.26: Payload-range diagram case 2, configuration 1

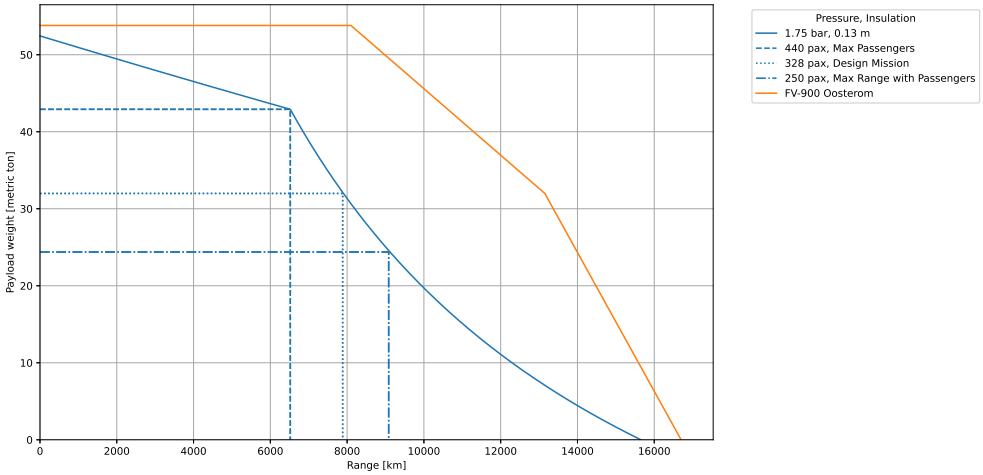

Figure 6.27: Payload-range diagram case 2, configuration 2

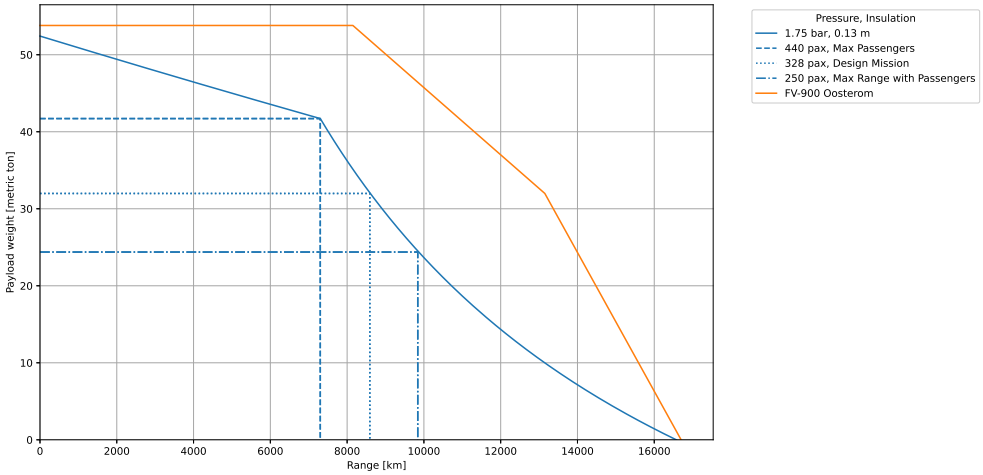

Figure 6.28: Payload-range diagram case 2, configuration 3

7

Conclusions and Recommendations

Aviation is growing and the amount of emissions resulting from the use of kerosene and its corresponding climate impact is raising concerns. Therefore, a main point of developments and research in the aviation sector is regarding the reduction of its climate impact. The climate impact of aviation can be reduced by making use of alternative fuels. Alternative fuels include cryogenic fuels such as liquid hydrogen. Liquid hydrogen has a higher energy content by weight and emits no CO_2 emissions compared to kerosene. Another way to reduce the climate impact of aviation is to design alternative aircraft concepts with lower fuel consumption. A popular configuration is the flying wing. An example of a flying wing is the Flying-V. This thesis project proposes to integrate liquid hydrogen fuel into the concept of the Flying-V. The main objective of the project is to contribute to the development of a design of a Flying-V with liquid hydrogen, by making an assessment of the implications on the fuel system and the effect on the mission performance from the change of fuel. This is done by making a geometry parametrization of the fuel tank, analyzing the mechanical and thermal design and compare its flight performance to a kerosene based Flying-V. Conclusions of this research are presented in Section 7.1. Recommendations for future work are discussed in Section 7.2.

7.1. Conclusions

The parametrization of the outer mold line is used as input for the parametrization of the fuel tank. The fuel tank is designed to have an oval cross-section. The same as used for the fuselage cabin. The fuel tank is located behind the passenger cabin in the tapered part of the wing. Just as with the fuselage cabin, the wing uses the shape of the fuel tank and the wall of the fuel tank doubles as the skin for the leading edge of the wing. By locating the fuel tank behind the passenger cabin part of the cargo volume is traded for fuel volume.

The cross-section of the fuel tank is defined by the part of the wing the fuel tank is located. In addition, the geometry of the fuel tank is defined by two parameters that specify the length and the starting point of the fuel tank. The parametrization of the fuel tank is only applicable to the tapered part of the wing.

The outer mold lines of the Flying-V are kept constant. Therefore an integral tank design is selected, as this is more volume efficient than an non-integral configuration in this case. Regarding the construction of the fuel tank internal insulation is selected. The fuel tank wall is aligned with the skin of the aircraft. The insulation is located on the inside of the fuel tank wall. To protect the insulation material from the liquid hydrogen an impermeable liner is required. In this research the fuel tank

wall material is selected to be aluminium and the insulation material is selected to be polyurethane foam.

For the mechanical design of the tank the fuel tank is designed to operate with a fluctuating pressure during flight. The insulation is required to keep the tank pressure below the venting pressure, minimizing the venting of fuel. However, with keeping the outer mold lines constant, the insulation layer will also consume the available fuel volume and it adds to the weight of the fuel tank. Therefore a trade-off between the boil-off rate, fuel volume and tank weight needs to be conducted. To determine these parameters with the corresponding insulation thickness a thermal model analyses the thermal performance of the fuel tank as a function of the insulation thickness. The thermal analysis is assumed to be steady-state. To make this assumption hold the boil-off rate is required to be less than 0.2% by weight per hour. This is to make sure the changes in fuel quality during flight are insignificant and the steady-state assumption holds in first approximation. Furthermore, the thermal analysis uses an electrical resistance analogy where the thermal resistances of the heat transfer processes are placed in series. The heat transfer processes include forced convection on the external surface, pure conduction through the tank wall and insulation layer, natural convection of gas and liquid on the internal surface and radiation and re-radiation of the skin. The modeled heat transfer rate for a reference nitrogen tank differs -1.2% and for a experimental liquid hydrogen tank it differs -3.1% and +4.4%.

The flight performance analysis uses the Breguet range equation and fuel fraction to determine the range from the available fuel volume. After adjusting the fuel fractions, the modeled range for a reference Boeing 747-400 differs between +0.2% and +3.6%. Regarding liquid hydrogen the fuel fractions are altered to provide a calorific equivalent fuel use for hydrogen with respect to kerosene.

The fuel tank performance and the flight performance are analyzed for three configuration with different fuel and cargo volumes. As expected, the larger the tank the higher the tank weight and the higher the heat leak. In this research the tank is increased in volume by expanding the fuel tank into the tapered part of the wing. This increases the tank volume, but also increase the tank structure weight even more. This is detrimental for the gravimetric storage density.

The flight performance analysis also takes into account two case studies. The first case study is regarding a retrofit of an existing Flying-V with a set of hydrogen fuel tanks. The operating empty weight is increased up to 8.7% while having the same take-off weight. All the configurations have a lower range compared to the FV-900. In case of the largest hydrogen fuel volume, configuration 1, the ranges are the closest to the FV-900. That is, 35%, 42% and 51% lower for 440, 328 and 250 passengers, respectively. The second case study is regarding an iteration of the structure to take into account the portion of the take-off weight that is not used by the savings in fuel weight. Compared to the take-off weight of the FV-900 the take-off weight is reduced by 32%, 37% and 37% for configuration 1 to 3, respectively. The operating empty weight is reduced by 14%, 23% and 22% for configuration 1 to 3, respectively. All the configurations still have a lower range compared to the FV-900. Comparing configuration 1 to the FV-900 the ranges are lower by 18%, 23% and 32% for 440, 328 and 250 passengers, respectively. These ranges are close, but one has to take into account that the payload weight is reduced. The configurations where the payload volume is sufficient have a significantly lower range compared to the kerosene based FV-900.

This research provides viable and usable designs of a Flying-V using liquid hydrogen if one is willing to compromise on the range and available payload weight for no CO_2 emissions. However, keeping the payload weight up, the available volume left is not enough volume for liquid hydrogen to have equivalent flight performance. The resulting ranges are significantly lower compared to a kerosene based Flying-V.

7.2. RECOMMENDATIONS

This research presents a first assessment of the integration of liquid hydrogen fuel into the concept of the Flying-V. From this research several recommendations can be made for future work regarding a liquid hydrogen based Flying-V.

Regarding the parametrization of the fuel tank, several aspects can be improved upon. First is the ability of the parametrization to create a fuel tank in the flying-V. At this point the model of the fuel tank is limited to the tapered part of the wing. The fuel tank model uses the geometrical relations of the tapered part of the wing. Outside of this tapered part these relations continue for the fuel tank, resulting a tank that intersects with and is located outside of the wing OML. If one wants to locate the fuel tank in a different part of the aircraft these relations need to be adjusted. Second is regarding the creation of the fuel tank domes. During the modelling of the fuel tank domes the oval cross-section is approximated with several ellipses to form a loft for the dome. However, when the difference between the crown arc and the keel arc becomes larger, this approximation becomes less accurate resulting in a possible error when trying to fuse the dome to the middle section of the fuel tank. The number of ellipses used can be increased to increase the accuracy, but this also increases the computation time, or a different method needs to be defined.

The thermal model uses several assumptions. The use of these assumptions deserves further attention. A significant assumption is the use of the "effective radius" for several of the calculations. Several of the equations used would normally be applied to cylinders. For future research the validity of this assumption should be investigated. Furthermore, several of the heat transfer processes are described by correlations, that is the convection of the external and the internal surface. Due to the lack of experimental data these aspects were not taken into account in the validation process. The accuracy of these correlations should be checked.

Regarding the structural design of the fuel tank several aspects need further attention. The first aspect is regarding the difference in temperature between the internal structure and the external wall. In this research a internal insulation concept is used. That is, the external wall is exposed to ambient conditions and is protected from the cryogenic conditions by the insulation. However, the internal structure is in contact with these cryogenic conditions. Therefore questions arise regarding the thermal expansion of the different structural part leading to possible stress locations where the internal structure is connected to the external wall. One could change the concept to external insulation, but then the wall no longer acts as the skin of the wing. That is, an additional wall is needed and the tank needs to be connected to the structure of the wing.
Furthermore, the analysis of the internal structure needs more attention. The current analysis of the internal structure provides a very conservative weight estimation of the structure. The design should be analysed by one with more knowledge on the subject, optimizing the structure and minimizing the weight. In this process one should also look into the use of different materials. In this research aluminium is selected as a safe and conservative choice. Aluminium is already used for cryogenic storage. However, other materials may result in a lower system weight. Verstraete [3] mentions the use of composites offer 25% weight savings compared to a monolithic aluminium tank.

Finally the overall hydrogen based aircraft needs more attention. The centre of gravity location and the static margin require a future investigation. Compared to a kerosene based aircraft the fuel system increases in weight, but the fuel itself is lower in weight. Also the fuel system cannot be spread out in the aircraft like a kerosene fuel system. A more detailed weight estimation can be used to improve the accuracy of the flight performance analysis.

Next to the possible improvements to this research, the scope can be increased to take into account the climate impact of a hydrogen aircraft. Even though the use of liquid hydrogen eliminates the emission of CO_2, there is still the emission of other climate agents such as nitrogen oxides and water vapour. The flight performance analysis of this research provides the amount of fuel used during cruise. This can be used to analyse the emissions of the aircraft and its climate impact.

BIBLIOGRAPHY

[1] H. Klug, *Cryoplane - Hydrogen Fuelled Aircraft*, Tech. Rep. (EADS Airbus GmbH, 2000).

[2] A. Rao, A. Sharma, and R. van Dijk, *A CFD Based Parametric Analysis of S - shaped Inlet for a Novel Blended Wing Body Aircraft,* in *International Conference on Advances in Thermal Systems, Materials and Design Engineering* (2017).

[3] D. Verstraete, *The Potential of Liquid Hydrogen for long range aircraft propulsion*, Ph.D. thesis, Cranfield University (2009).

[4] B. Khandelwal, A. Karakurt, P. R. Sekaran, V. Sethi, and R. Singh, *Hydrogen powered aircraft: The future of air transport,* Progress in Aerospace Sciences **60**, 45 (2013).

[5] M. Hillen, *Parametrisation of the Flying-V Outer Mould Line*, Master's thesis, TU Delft (2020).

[6] G. Brewer, *Hydrogen Aircraft Technology* (CRC Press, 1991).

[7] M. F. Hoogreef, *The Oval Fuselage*, Master's thesis, TU Delft (2012).

[8] S. Mital, J. Gyekenyesi, S. Arnold, R. Sullivan, J. Manderscheid, and P. Murthy, *Nasa-Tm-2006-214346*, Tech. Rep. (NASA, 2006).

[9] T. H. Megson, *Introduction to Aircraft Structural Analysis* (Butterworth-Heinemann, 2010).

[10] M. Shi, I. Chakraborty, J. Tai, and D. N. Mavris, *Integrated gas turbine and environmental control system pack sizing and analysis,* in *AIAA Aerospace Sciences Meeting, 2018* (AIAA SciTech Forum, 2018).

[11] D. Verstraete, P. Hendrick, P. Pilidis, and K. Ramsden, *Hydrogen fuel tanks for subsonic transport aircraft,* International Journal of Hydrogen Energy **35**, 11085 (2010).

[12] F. P. Incropera, D. P. Dewitt, T. L. Bergman, and A. S. Lavine, *Fundamentals of Heat and Mass Transfer*, sixth ed. (John Wiley & Sons, inc., 2007).

[13] J. P. Sass, J. E. Fesmire, Z. Nagy, S. Sojourner, D. Morris, and S. Augustynowicz, *Thermal Performance Comparison of Glass Microsphere and Perlite Insulation Systems for Liquid Hydrogen Storage Tanks,* in *Advance in Cryogenic Engineering: Transactions of the Cryogenic Engineering Conference - CEC*, Vol. 53 (American Institute of Physics, 2008).

[14] D. C. Maniaci, *Relative performance of a liquid hydrogen-fueled commercial transport,* in *46th AIAA Aerospace Sciences Meeting and Exhibit* (2008).

[15] J. Sun, J. Ellerbroek, and J. M. Hoekstra, *WRAP: An open-source kinematic aircraft performance model,* Transportation Research Part C: Emerging Technologies **98**, 118 (2019).

[16] L. Cadwallader and J. Herring, *Safety issues with hydrogen as a vehicle fuel*, Tech. Rep. (Lockheed Martin, 1999).

[17] M. Claeys, *Flying V and Reference Aircraft Structural Analysis and Mass Comparison*, Master's thesis, TU Delft (2018).

[18] J. Roskam, *Airplane Design Part V: Component Weight Estimation* (Design, Analysis and Research Corporation, 1985).

[19] W. J. Oosterom, *Flying-V Family Design*, Master's thesis, TU Delft (2021).

[20] International Energy Agency, *Transport, energy and CO2: Moving towards sustainability* (International Energy Agency, Paris, 2009).

[21] V. Grewe, L. Bock, U. Burkhardt, K. Dahlmann, K. Gierens, L. Hüttenhofer, S. Unterstrasser, A. G. Rao, A. Bhat, F. Yin, T. G. Reichel, O. Paschereit, and Y. Levy, *Assessing the climate impact of the AHEAD multi-fuel blended wing body,* Meteorologische Zeitschrift **26**, 711 (2016).

[22] D. S. Lee, G. Pitari, V. Grewe, K. Gierens, J. E. Penner, A. Petzold, M. J. Prather, U. Schumann, A. Bais, T. Berntsen, D. Iachetti, L. L. Lim, and R. Sausen, *Transport impacts on atmosphere and climate: Aviation,* Atmospheric Environment **44**, 4678 (2010).

[23] Airbus, *Cities, Airports & Aircraft 2019-2038 - Global Market Forecast*, Tech. Rep. (Airbus, 2019).

[24] J. Benad, *A New Aircraft Configuration for Commercial Passenger Transport,* in *Deutscher Luft- und Raumfahrtkongress* (2015) pp. 1–8.

[25] J. Benad, *Design of a commercial aircraft for high-subsonic speed as a flying wing configuration*, Tech. Rep. (Airbus, Berlin, 2015).

[26] F. Faggiano, *Aerodynamic design of a flying V aircraft*, Master's thesis, TU Delft (2016).

[27] F. Faggiano, R. Vos, M. Baan, and R. Van Dijk, *Aerodynamic design of a flying V aircraft,* 17th AIAA Aviation Technology, Integration, and Operations Conference (2017), 10.2514/6.2017-3589.

[28] L. A. Van Der Schaft, *Development, Model Generation and Analysis of a Flying V Structure Concept*, Master's thesis, TU Delft (2017).

[29] R. Vos, F. Geuskens, and M. Hoogreef, *A new structural design concept for blended wing body cabins,* in *53rd AIAA/ASME/ASCE/AHS/ASC Structures, Structural Dynamics and Materials Conference* (AIAA, 2012).

[30] B. Rubio Pascual, *Engine-Airframe Integration for the Flying V*, Master's thesis, TU Delft (2018).

[31] S. A. V. Empelen, *Engine Integration of the Flying V*, Master's thesis, TU Delft (2020).

[32] R. A. Viet, *Analysis of the flight characteristics of a highly swept cranked flying wing by means of an experimental test*, Master's thesis, TU Delft (2019).

[33] M. Palermo, *The Longitudinal Static Stability and Control Characteristics of a Flying V Scaled Model: An Experimental and Numerical Investigation*, Master's thesis, TU Delft (2019).

[34] E. Torenbeek, *Advanced Aircraft Design: Conceptual Design, Analysis and Optimization of Subsonic Civil Airplanes*, 1st ed. (John Wiley & Sons, Inc., 2013).

[35] H. Klug and R. Faass, *CRYOPLANE: hydrogen fuelled aircraft — status and challenges,* Air & Space Europe **3**, 252 (2001).

[36] A. Westenberger, *Hydrogen Fuelled Aircraft,* in *AIAA/ICAS International Air and Space Symposium and Exposition: The Next 100 Y* (AIAA, Dayton, 2003).

[37] Airbus Deutschland GmbH, *Liquid Hydrogen Fuelled Aircraft - System Analysis*, Tech. Rep. May (2003).

[38] W. P. P. Fischer, *Development of Cryogenic Insulations for Launcher Upper Stages,* in *44th International Conference on Environmental Systems*, July (ICES, 2014) pp. 1–14.

[39] C. Lin, N. van Dresar, and M. Hasan, *A pressure control analysis of cryogenic storage systems,* in *27th Joint Propulsion Conference* (1991).

[40] L. Allidieris and F. Janin, *Tanks (including insulation) - Task 3.6.2.1. Cryoplane project*, Tech. Rep. (2002).

[41] J. H. Lienhard IV and J. H. Lienhard V, *Heat Transfer Textbook*, 4th ed. (Dover Publications, 2011).

[42] M. P. Thekaekara, R. Kruger, and C. H. Duncan, *Solar Irradiance Measurements from a Research Aircraft,* Applied Optics **8**, 1713 (1969).

[43] R. de Vries, M. F. Hoogreef, and R. Vos, *Preliminary sizing of a hybrid-electric passenger aircraft featuring over-the-wing distributed-propulsion,* in *AIAA Scitech 2019 Forum* (AIAA, 2019).

[44] K. Schmidt and R. Vos, *A semi-analytical weight estimation method for oval fuselages in conventional and novel aircraft,* in *AIAA SciTech Forum - 52nd Aerospace Sciences Meeting*, Vol. 52 (AIAA, National Harbor, 2014).

[45] B. Scholtens, J. Fesmire, J. Sass, S. Augustynowicz, and K. Heckle, *Cryogenic thermal performance testing of bulk-fill and aerogel insulation materials,* in *AIP Conference Proceedings*, Vol. 152 (American Institute of Physics, 2008).

[46] E. Torenbeek, *Synthesis of subsonic airplane design* (Delft University Press, Delft, 1982).

[47] Y. M. Baan, *A Hybrid Method for the Interior and Exterior Design of Blended-Wing-Body Cabins*, Master's thesis, TU Delft (2015).

[48] A. Gomez and H. Smith, *Liquid hydrogen fuel tanks for commercial aviation : Structural sizing and stress analysis,* Aerospace Science and Technology **95** (2019), 10.1016/j.ast.2019.105438.

[49] O. Senkov, R. Bhat, and S. Senkova, *High Strength Aluminum Alloys for Cryogenic Applications,* Metallic Materials with High Structural Efficiency , 151 (2004).

[50] J. Aalders, E. Daugulis, S. van Dalen, T. Francotte, Y. Laar, L. Megill, M. Shi, S. de Vilder, F. Vossen, and Z. Wu, *The Cryo-V*, DSE 2020 (Tu Delft, 2020).

A

Inputs

Table A.1: Input parameters FV-900 FO-F [19]

Parameter	Symbol	Unit	Value
Cabin planform			
Untapered fuselage length	L_1	m	24.0
Tapered fuselage length	L_3	m	11.0
LE distance between section 1 and 2	l_2	m	0.0
Width at input height section 1	W_{H_1}	m	6.2
Width at input height section 3	W_{H_3}	m	5.8
Cargo containers			
Spanwise spacing between containers	y_{cargo}	m	0.01
Chordwise spacing between containers	x_{cargo}	m	0.01
Container type	-	-	'LD-9'
Container chordwise leading	-	-	[True, True, True, True]
Container chordwise trailing	-	-	[False, False, False]
Number of container	$n_{containers}$	-	none
Wing planform			
Outer wing span	b_{outer}	m	14.75
Planform chord at section 1 fraction	c'_1	-	1.11
LE sweep angle inboard wing	Λ_{in}	deg	64.5
LE sweep angle outboard wing	Λ_{out}	deg	40.7
Dihedral of wing trunk 4	Γ_4	deg	-0.1785
Dihedral of wing trunk 5	Γ_5	deg	5.825
Incidence angle section 4	i_4	deg	0.4
Incidence angle tip section	i_5	deg	-4.37
Taper ratio	λ	-	0.1
Length section 3 to 4	L_4	m	1.5
Planform chord at section 3 fraction	c'_3	-	1.13
Orientation ratio	-	-	1.0
Oval			
Cabin height section 1	H_{2_1}	m	2.25
Cabin height section 3	H_{2_3}	m	1.22
Height at input width section 1	H_{w_1}	m	0.6
Height at input width section 3	H_{w_3}	m	0.6
Crown height section 1	H_{1_1}	m	0.68
Crown height section 3	H_{1_3}	m	0.45
Keel height section 1	H_{3_1}	m	0.68
Keel height section 3	H_{1_1}	m	0.45
TE fairing			
Upper coefficients section 1	c_{up_1}	m^{-3}	$1e^{-5}$
Upper coefficients section 3	c_{up_3}	m^{-3}	$1e^{-5}$
Lower coefficients section 1	c_{low_1}	m^{-3}	0.002
Lower coefficients section 3	c_{low_3}	m^{-3}	0.0001
Vertical position of the TE section 1	z_{TE_1}	m	-0.3
Vertical position of the TE section 3	z_{TE_3}	m	-0.04
Start position of upper rear wing curve 1	$\bar{x}_{s_{up_1}}$	-	0.4
Start position of upper rear wing curve 3	$\bar{x}_{s_{up_3}}$	-	0.3
Start position of lower rear wing curve 1	$\bar{x}_{s_{low_1}}$	-	0.4
Start position of lower rear wing curve 3	$\bar{x}_{s_{low_3}}$	-	0.3
Outboard aerofoils			
Upper Bernstein coefficients of section 4	A_{up_4}	-	[0.088, 0.066, 0.21, 0.079, 0.24, 0.23]
Lower Bernstein coefficients of section 4	A_{low_4}	-	[-0.13, -0.084, -0.031, -0.31, 0.069, 0.20]
Upper Bernstein coefficients of section 5	A_{up_5}	-	[0.14, 0.068, 0.20, 0.078, 0.14, 0.29]
Upper Bernstein coefficients of section 5	A_{low_5}	-	[-0.099, -0.084, -0.025, -0.39, 0.061, 0.17]
Flight conditions			
Cruise Mach number	Ma_{cruise}	-	0.85
Cruise altitude	Alt_{cruise}	m	11000

Table A.2: Input parameters fuel tank geometry, mechanical design. thermal design and flight performance analysis

Parameter	**Symbol**	**Unit**	**Value**
Fuel tank			
Length tank	L_{01}	m	11.0
Length offset	L_{offset}	m	0.0
Dome ellipse ratio	-	-	1.6
Venting pressure	P_{vent}	bar	1.75
Insulation thickness	t_{ins}	m	0.16
Fuel tank Material			
Aluminium density [48]	ρ_{alu}	kg/m^3	2795.7
Fatigue stress aluminium [49]	σ_θ	MPa	424.03
Fatigue stress aluminium cryogenic conditions [49]	σ_θ	MPa	472.38
Young's modulus aluminium cryogenic conditions [50]	E	GPa	59.42
Polyurethane foam density [3]	ρ_{foam}	kg/m^3	32.0
Weld efficiency [3]	e_w	-	0.8
Safety factor	j	-	1.5
Thermal design			
Thermal conductivity air at cruise [12]	k_{air}	W/m K	1.952e^{-2}
Specific heat at constant pressure air at cruise [12]	$c_{\text{p}_{\text{air}}}$	J/kg K	
Thermal conductivity aluminium [12]	k_{alu}	W/m K	130.0
Temperature liquid hydrogen [16]	T_{H2}	K	20.268
Dynamic viscosity liquid hydrogen [16]	μ_{lh}	Pa s	1.3e^{-5}
Thermal conductivity liquid hydrogen [16]	k_{lh}	W/m K	0.103
Thermal conductivity gaseous hydrogen [16]	k_{gh}	W/m K	0.1897
Specific heat at constant pressure liquid hydrogen [16]	$c_{\text{p}_{\text{lh}}}$	J/kg K	9.69e^3
Density liquid hydrogen [16]	ρ_{lh}	kg/m^3	70.8
Density gaseous hydrogen [16]	ρ_{gh}	kg/m^3	1.34
CTE liquid hydrogen [16]	β	1/K	0.01658
Latent heat of vaporization [16]	λ	J/kg	445590
Lower heating value liquid hydrogen [16]	LHV_{H2}	J/kg	119.93e^6
Lower heating value kerosene [16]	LHV_{k}	J/kg	44.5e^6
Emittance aircraft skin [41]	ϵ	-	0.9
Solar absorptance aircraft skin [41]	α	-	0.26
Solar irradiance [42]	q_{solar}	W/m^2	1351.0
Flight performance analysis			
Maximum take-off weight FV-900 FO-F [19]	MTOW	t	234
Lift-to-drag ratio FV-900 FO-F [19]	L/D	-	21.6
Specific fuel consumption [37]	c_{j}	kg/Ns	5.755e^{-6}
Loiter period	E	min	30
Diversion distance	R	nm	200

B

Roskam Weight Fractions

Table B.1: Roskam weight fractions [18]

Aircraft	**struc/TO**	**pwr/TO**	**feq/TO**	**emp/TO**
DC-9-30	0.286	0.076	0.175	0.538
MD-80	0.304	0.079	0.182	0.564
DC-10-10	0.316	0.077	0.169	0.561
DC-10-30	0.281	0.067	0.137	0.485
B 737-200	0.27	0.071	0.129	0.521
B 727-100	0.317	0.078	0.133	0.552
B 747-100	0.298	0.062	0.089	0.498
A300-B2	0.353	0.076	0.116	0.559
B 707-121	0.259	0.081	0.103	0.444
B 707-320C	0.249	0.073	0.074	0.396
B 720-022	0.294	0.078	0.122	0.494
B 707-321	0.242	0.074	0.09	0.406
DC-8	0.31	0.129	0.119	0.562
DC-9-10	0.31	0.085	0.164	0.495
F 614	0.359	0.107	0.161	0.586
F28-1000	0.302	0.083	0.145	0.48
Caravelle	0.317	0.079	0.145	0.59
Average	0.2981	0.0809	0.1325	0.5136

C

Fuel tank Performance Conf. 3

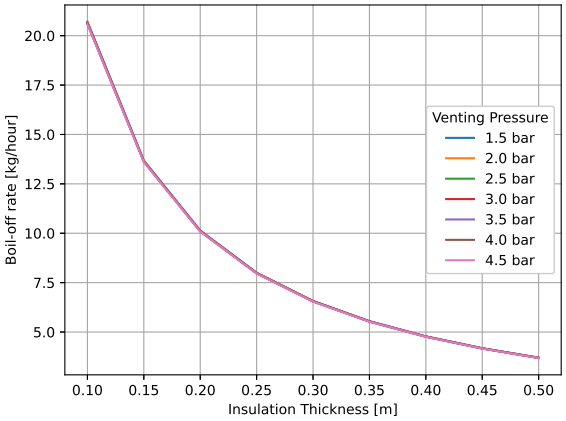

Figure C.1: Boil-off rate

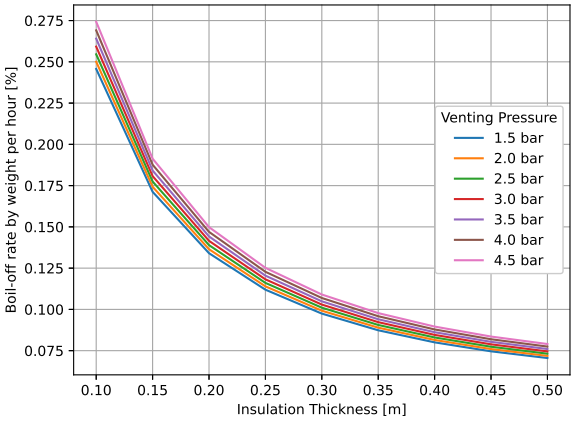

Figure C.3: Boil-off rate by weight per hour

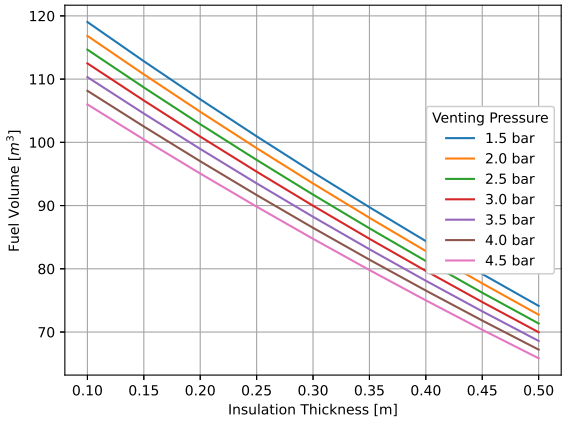

Figure C.2: Available fuel volume

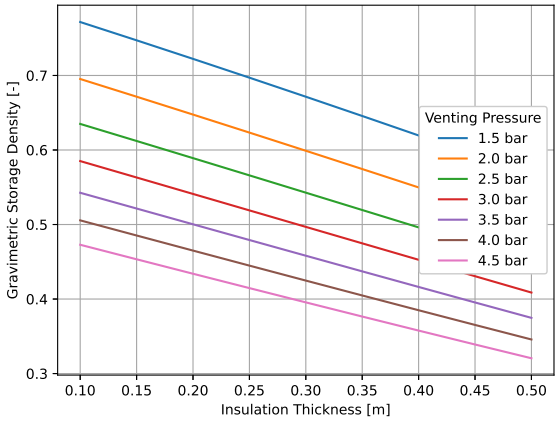

Figure C.4: Gravimetric storage density

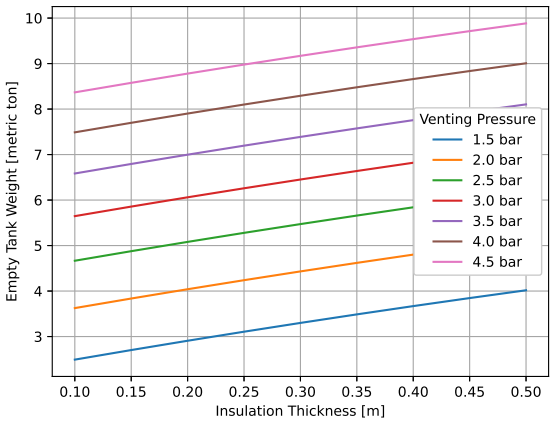

Figure C.5: Empty tank weight

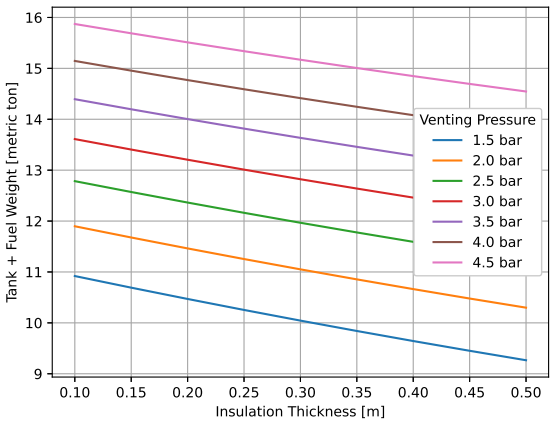

Figure C.6: Filled tank weight

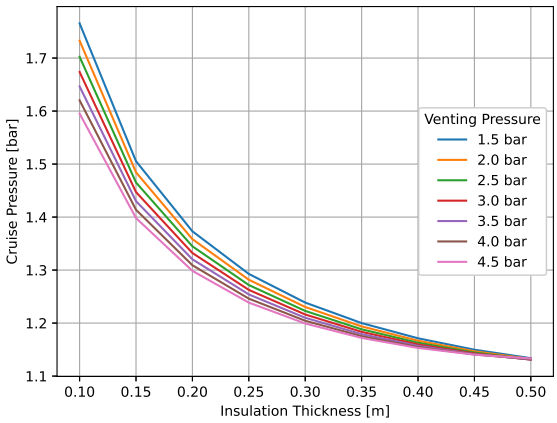

Figure C.7: Tank pressure end of cruise phase

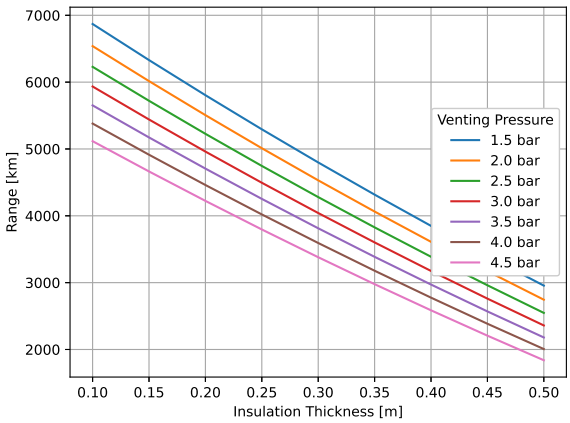

Figure C.8: Cruise range